

Development of an autonomous diesel power generation system for a high-altitude, remote astronomical facility for Antarctica

Author:

Hengst, Shane

Publication Date:

2011

DOI:

<https://doi.org/10.26190/unsworks/14976>

License:

<https://creativecommons.org/licenses/by-nc-nd/3.0/au/>

Link to license to see what you are allowed to do with this resource.

Downloaded from <http://hdl.handle.net/1959.4/51329> in <https://unsworks.unsw.edu.au> on 2024-03-28

Development of an autonomous diesel power generation system for a high-altitude, remote astronomical facility for Antarctica

by
Shane Hengst



UNSW
THE UNIVERSITY OF NEW SOUTH WALES
SYDNEY • AUSTRALIA

School of Physics
University of New South Wales

A thesis submitted in satisfaction of
the requirements for the degree of

Master of Science

in the Faculty of Science

PLEASE TYPE

THE UNIVERSITY OF NEW SOUTH WALES
Thesis/Dissertation Sheet

Surname or Family name: Hengst

First name: Shane

Other name/s:

Abbreviation for degree as given in the University calendar: MSc

School: Physics

Faculty: Science

Title: Development of an autonomous diesel power generation system for a high-altitude, remote astronomical facility for Antarctica

Abstract 350 words maximum: (PLEASE TYPE)

Antarctic astronomy is becoming ever more popular due to the astronomical potential that the Antarctic plateau has to offer. An analysis of potential Antarctic dome sites is essential before the construction of large telescope facilities. Reliable power generation systems for isolated locations on the Antarctic plateau are optimal for remote site-testing facilities. There has been little published work, however, on remote power generation in Antarctica. This thesis reviews potential in-situ power generation sources, with emphasis on the diesel engine that was chosen for the University of New South Wales site-testing facility: PLATO (PLATEau Observatory). PLATO currently operates on the highest point on the Antarctic plateau, Dome A (4093m). A single-cylinder, naturally aspirated diesel engine (Hatz 1B30) was chosen to be the primary power source for PLATO throughout the winter months. A description of the design of an environmental chamber to simulate high altitudes on the Antarctic plateau is presented. An experimental investigation of the engine operation at high altitude on Jet A-1 with comparison to the engine's performance at sea level is also presented. It was found that, although attention must be paid to provide adequate cooling, no modification to the engine itself was required. The selected engine power system provides very high reliability and produces 1500W of electrical power with a fuel consumption of 280g/kWh.

Declaration relating to disposition of project thesis/dissertation

I hereby grant to the University of New South Wales or its agents the right to archive and to make available my thesis or dissertation in whole or in part in the University libraries in all forms of media, now or here after known, subject to the provisions of the Copyright Act 1968. I retain all property rights, such as patent rights. I also retain the right to use in future works (such as articles or books) all or part of this thesis or dissertation.

I also authorise University Microfilms to use the 350 word abstract of my thesis in Dissertation Abstracts International (this is applicable to doctoral theses only).


Signature


Witness

20/9/2011
Date

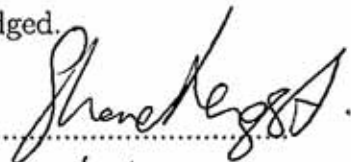
The University recognises that there may be exceptional circumstances requiring restrictions on copying or conditions on use. Requests for restriction for a period of up to 2 years must be made in writing. Requests for a longer period of restriction may be considered in exceptional circumstances and require the approval of the Dean of Graduate Research.

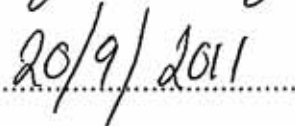
FOR OFFICE USE ONLY

Date of completion of requirements for Award:

ORIGINALITY STATEMENT

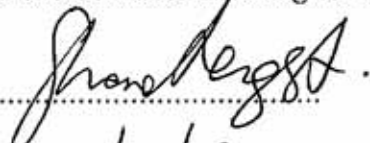
I hereby declare that this submission is my own work and to the best of my knowledge it contains no materials previously published or written by another person, or substantial proportions of material which have been accepted for the award of any other degree or diploma at UNSW or any other educational institution, except where due acknowledgement is made in the thesis. Any contribution made to the research by others, with whom I have worked at UNSW or elsewhere, is explicitly acknowledged in the thesis. I also declare that the intellectual content of this thesis is the product of my own work, except to the extent that assistance from others in the project's design and conception or in style, presentation and linguistic expression is acknowledged.


Signed 

Date 

AUTHENTICITY STATEMENT

I certify that the Library deposit digital copy is a direct equivalent of the final officially approved version of my thesis. No emendation of content has occurred and if there are any minor variations in formatting, they are the result of the conversion to digital format.

Signed 

Date 

ABSTRACT

Antarctic astronomy is becoming ever more popular due to the astronomical potential that the Antarctic plateau has to offer. An analysis of potential Antarctic dome sites is essential before the construction of large telescope facilities. Reliable power generation systems for isolated locations on the Antarctic plateau are optimal for remote site-testing facilities. There has been little published work, however, on remote power generation in Antarctica. This thesis reviews potential in-situ power generation sources, with emphasis on the diesel engine that was chosen for the University of New South Wales site-testing facility: PLATO (PLATeau Observatory). PLATO currently operates on the highest point on the Antarctic plateau, Dome A (4093m). A single-cylinder, naturally aspirated diesel engine (Hatz 1B30) was chosen to be the primary power source for PLATO throughout the winter months. A description of the design of an environmental chamber to simulate high altitudes on the Antarctic plateau is presented. An experimental investigation of the engine operation at high altitude on Jet A-1 with comparison to the engine's performance at sea level is also presented. It was found that, although attention must be paid to provide adequate cooling, no modification to the engine itself was required. The selected engine power system provides very high reliability and produces 1500W of electrical power with a fuel consumption of 280g/kWh.

ACKNOWLEDGEMENTS

I would like to thank my supervisors from the Antarctic astronomy group, Prof. John Storey and Dr. Jon Lawrence. Thanks also goes out to the PLATO team: Daniel Luong-Van, the ‘brains’ behind the project; Jon Everett for his mammoth achievement of getting the Nigel instrument off the ground; and Prof. Michael Ashley for his support and advice. Also to Graham Allen for his assistance with the engine test rig. Many thanks to Dr. Nick Tothill for his assistance in proof reading and giving the thesis a better direction. Special thanks for the support from the Department of Manufacturing and Mechanical Engineering, in particular Vince Carnevale of the Internal Combustion (I.C.) lab supervisor; Russell Hall, the Laboratory Manager; and Dr. John Olsen the then academic in charge of the I.C. combustion lab. In addition, a special thanks to the team out at Hatz Australia, in particular Ian O’Callaghan, Tissa Pathiratna and Sami Almogoawish.

Thanks also to Dr. Peter Reece for use of his optics lab for optimising our Nigel Instrument and Tamara Reztsova of the upper year laboratory for her assistance with the understanding of the Stirling engine. To Hualin Chen for assisting me with initial testing of the Nigel instrument at Siding Spring Observatory. In addition to Dr. Suze Kenyon for her input for the operation of Nigel.

A very special thanks to Chinese expedition teams of the Polar Research Institute of China and the Chinese Academy of Sciences for deploying PLATO to Dome A.

I would also like to thank Prof. Richard Newbury, Prof. Mike Gal, Sue Hagon (our “Physics Friend”) and Patricia Furst for their support.

I would like to thank all my friends, in particular Chris Atakilyan and Ankur Chaudhary for some proof reading.

And finally, to my family and Mikayla Keen, and her family, for their love and support.

Contents

1	Antarctica: The Last Frontier	3
1.1	Astronomy in Antarctica	6
1.2	Atmospheric Properties	6
1.3	Autonomous remote site-testing	9
1.4	Remote Power Generation	10
1.4.1	Solar Panels	11
1.4.2	Wind Turbines	12
1.4.3	Lead-Acid Batteries	12
1.4.4	Lithium Batteries	13
1.4.5	Fuel Cells	14
1.4.6	Thermoelectric Generators	15
1.4.7	Heat Engines	16
1.5	UNSW Autonomous Facilities	20
1.5.1	Site testing at the South Pole	21
1.5.2	Site testing at Dome C	23
1.5.3	Site testing at Dome A	25
1.6	Thesis Summary	26
2	PLATO	27
2.1	Dome A	27
2.1.1	PLATO design considerations	28
2.2	Instrument Suite	30

2.3	PLATO Design	32
2.3.1	Modular Design	32
2.3.2	Engine Module	33
2.3.3	Instrument Module	37
2.3.4	Control Systems	37
2.4	PLATO Performance	38
3	The Diesel Engine	41
3.1	The Diesel Cycle	41
3.1.1	Induction Stroke (a)	43
3.1.2	Compression stroke (b)	44
3.1.3	Ignition stroke (c)	44
3.1.4	Exhaust stroke (d)	45
3.2	Mechanical Processes	46
3.2.1	Mechanical system	46
3.2.2	Fuel Delivery System	46
3.2.3	Direct Injection	48
3.3	Fuel	49
3.3.1	Fuel Properties	49
3.3.2	Jet Fuel use in Diesel Engines	53
3.4	Diesel Engines in Antarctica	55
3.5	Hatz 1B30 for PLATO	56
3.5.1	Hatz 1B30	56
3.5.2	Fuel Selection	56
3.5.3	High-altitude Testing	57
4	Engine Test Rig	59
4.1	Mechanical Arrangement	60
4.2	Data Acquisition	63
4.3	Initial Test Results	64

4.4	Engine Test Results	67
4.4.1	Test Conditions	67
4.5	Implementation for PLATO	75
4.5.1	Field Results	76
4.6	Conclusions	80
5	Conclusions	83
5.1	Future Work	85
A	Nigel: The Aurora Hunter	89
A.1	Introduction	89
A.2	Wavelength Specification	90
A.3	Nigel's Hardware	91
A.3.1	Design and Assembly	92
A.4	Nigel Control	93
A.5	Nigel Testing	96
A.5.1	Focusing the CCD	96
A.5.2	Initial Results from Siding Spring Observatory	98
A.6	Preliminary Results from Dome A	100
B	Engine Raw Data	107
C	Published Papers	121

List of Figures

1.1	Contour map of Antarctica (courtesy of AAD)	4
1.2	Theoretical Stirling Cycle	17
1.3	Practical Stirling Cycle	19
1.4	AASTO at the South Pole.	21
1.5	AASTINO at Dome C.	23
2.1	Chinese at Dome A	29
2.2	PLATO at Dome A	34
2.3	Diesel Engines	35
2.4	Solar Panels at Dome A	36
3.1	Four-stroke Mechanical Diesel Cycle	42
3.2	Theoretical and Realistic Thermodynamic Work Cycles	43
3.3	Pump Element	47
3.4	Geared Control Rack	48
3.5	Direct Injection System	49
3.6	Hatz 1B30 Single-Cylinder Diesel Engine	57
4.1	Engine Test Rig	61
4.2	Engine Base Plate	62
4.3	Engine Test Measurements	66
4.4	Sea Level Map	68
4.5	Altitude Map	69
4.6	Fuel Consumption at 2200rpm	70

4.7	Fuel Consumption	71
4.8	Fuel Consumption at different pressures	73
4.9	Exhaust Gas Temperatures at different pressures	74
4.10	Generator Voltage	77
4.11	DC/DC Current Output	77
4.12	Cylinder Head Temperatures	78
4.13	Exhaust Gas Temperatures	79
4.14	Fuel Level	80
A.1	Aurora Spectra with respect to UBVRI passbands.	91
A.2	Nigel Spectra	92
A.3	Nigel's BOB	94
A.4	Nigel Instrumentation Rack	95
A.5	CCD Focus	97
A.6	Daytime Image and Spectra at SSO (unaligned filters)	101
A.7	Daytime Image and Spectra at SSO (aligned filters)	102
A.8	Light Bulb Spectra Image and Spectra	103
A.9	Mercury Gas Vapour Image and Spectra	104
A.10	Dome A Twilight Spectra	105
A.11	Dome A Nighttime Spectra	105
A.12	Convolved spectra response for all fibres.	106

List of Tables

2.1	Power Budget for PLATO	32
3.1	Fuel properties of Jet A-1, Automotive Diesel and Special Antarctic Blend (SAB)	54
B.1	Legend for Table Values	107
B.2	Engine Data - 1600rpm	108
B.3	Engine Data - 1800rpm	109
B.4	Engine Data - 2000rpm	110
B.5	Engine Data - 2100rpm	111
B.6	Engine Data - 2200rpm (First Test)	112
B.7	Engine Data - 2200rpm (Second Test)	113
B.8	Engine Data - 2400rpm	114
B.9	Engine Data - 2600rpm	115
B.10	Engine Data - 2800rpm	116
B.11	Engine Data - 3000rpm	117
B.12	Engine Data - 3200rpm (First Test)	118
B.13	Engine Data - 3200rpm (Second Test)	119

Chapter 1

Antarctica: The Last Frontier

“We must always remember with gratitude and admiration the first sailors who steered their vessels through storms and mists, and increased our knowledge of the lands of ice in the South”

- Roald Amundsen, Norwegian explorer of polar regions (1872-1928)

Antarctic dome sites have been revealed through site testing to have favourable atmospheric conditions for observational astronomy. To carry out site testing at high-altitude remote dome sites, it is optimal to have an unmanned and autonomous facility. The power generation system for this facility must be robust to endure the winter months.

Antarctica, on average, is the highest, coldest, windiest and driest continent on Earth (Quilty 1992). The Antarctic plateau is a vast, largely unexplored region in East Antarctica. Most of it is at an elevation of over 3000 metres as shown in Figure 1.1. Dome A is the highest point, at a physical altitude of 4093 metres.

When the Sun is well below the horizon, the average temperature in Antarctica is about -60°C . The lowest recorded temperature was -89.6°C measured at the Russian Vostok station in 1983 (Desonie 2008). The low temperatures in Antarctica (relative to temperate locations) lead to:

- A reduced atmospheric scale height (i.e. the atmospheric pressure de-

creases more rapidly with altitude);

- A lower atmospheric water vapour content; and
- A lower thermal emission from the atmosphere.

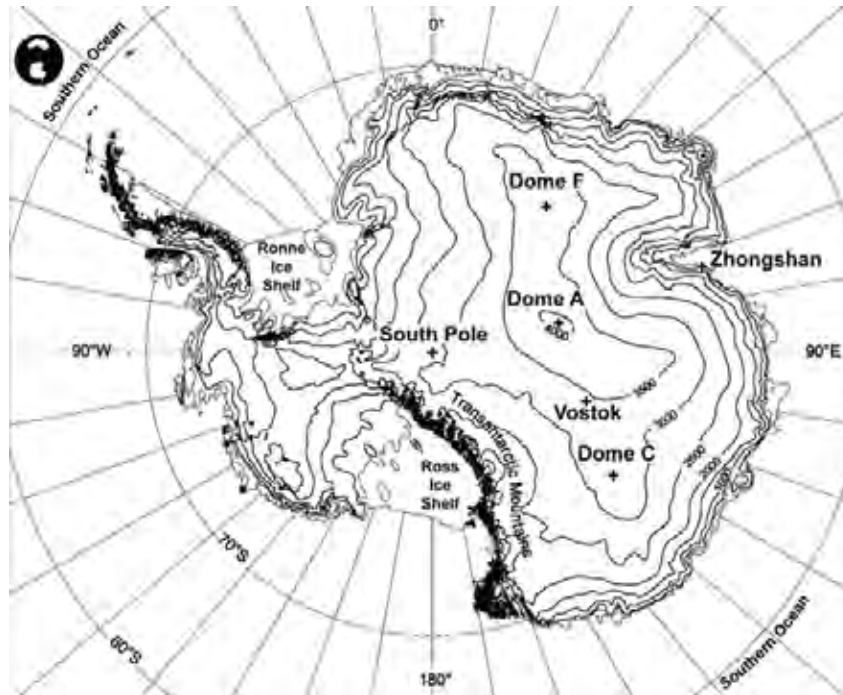


Figure 1.1: Contour map of Antarctica (courtesy of AAD)

The wind flows in Antarctica are mainly katabatic, i.e. stable, cool air flows, under gravity, radially from the highest point on the plateau towards the coast (Parish & Cassano 2003; and references therein). Because the gradient of the plateau is small, the corresponding wind speeds are slow. As the air approaches the coast, the gradient sharply increases resulting in much higher wind speeds.

The plateau of Antarctica receives very little precipitation, typically 50mm per year, making it the largest desert in the world. In Antarctica, 70% of the world's fresh water is stored as ice, which can influence the world's sea level

(Quilty 1992). The air above Antarctica is sensitive to distant human activity, specifically in the changing of the atmospheric gas composition (Francey 1992). Precipitation in Antarctica falls as ice and adds to the icesheet above the land mass. As a result, past atmospheric composition can be traced via Antarctic ice cores. Antarctica, therefore, probably holds the oldest record of Earth's climatic history (Lüthi *et al.* 2008; and references therein). Antarctica is considered to be one of the last remaining wildernesses (Gell 1989) and one of the last scientific frontiers on Earth.

The low temperatures, the dry conditions, and high altitudes on the Antarctic plateau are thought to provide the optimal environment for astronomical observation; which potentially makes Antarctica the best astronomical platform on the planet (Storey 2005; and references therein).

Permanent research facilities currently exist at the United States' South Pole station (on the edge of the plateau), the Russian Vostok station and the French/Italian station at Dome C. There are new stations under construction at Dome A and Dome F being led by the Chinese and the Japanese respectively. All of these stations are conducting part of their scientific research in astronomy and astrophysics.

This chapter will outline key properties of the atmosphere and why the Antarctic plateau is perhaps the best terrestrial site to perform observational astronomy. This chapter will also discuss the importance of autonomous site-testing facilities with robust power generation systems. A review of alternative power sources that could be used to power a remote facility is presented; with special emphasis on heat engines. Finally, an overview on previous site-testing facilities that have been designed and constructed by the Antarctic astronomy team from the University of New South Wales (UNSW) is presented.

This central aim of this thesis is to test a single-cylinder diesel engine that was selected to power the latest UNSW remote facility before being deployed to Dome A, Antarctica.

1.1 Astronomy in Antarctica

The study of astronomy in Antarctica is not just a modern endeavour. Astrogeology started with the first discovery of a meteorite by the Mawson team during their 1911-1914 expedition. Astrophysics in Antarctica began with the first cosmic ray observatory that was built at Mawson Station in 1955. Today, there are a number of telescopes that are taking advantage of this prime real estate. These range from high energy detectors observing neutrino and cosmic ray activity, to small optical and infrared telescopes. See Indermuehle *et al.* (2005) and Burton (2010) for reviews of the history of astronomy in Antarctica.

PILOT (Pathfinder for an International Large Optical Telescope) is a proposed 2 metre class telescope to be sited at Dome C (Burton *et al.* 2005). Although PILOT has a relatively modest aperture, it should be competitive with current 8 metre class telescopes because of the excellent site conditions at Dome C (Saunders *et al.* 2008). There are also conceptual ideas for bigger telescopes such as LAPCAT (Large Antarctic Plateau Clear-Aperture Telescope), an 8.4 metre off-axis optical/IR telescope (Storey *et al.* 2006), to be built on the Antarctic plateau.

Before taking on the challenge of building larger telescope facilities at Antarctic plateau sites, it is essential to survey site conditions in order to evaluate the real benefits of such an endeavour. Essentially, the atmospheric conditions must be superior to those found at prime mid-latitude sites, such as those on Mauna Kea and Cerro Paranal.

1.2 Atmospheric Properties

The astronomical potential of ground-based telescopes is limited by various atmospheric properties. The atmosphere above the Antarctic plateau creates conditions that are more favourable than the atmosphere above the best

terrestrial telescopes. The key atmospheric properties that can inhibit our vision of the night sky are turbulence, thermal emission, absorption and light contamination.

The phenomenon of the diffraction of light places a fundamental limit on the resolution of any telescope system. The diffraction limit is inversely proportional to the telescope's aperture, i.e. larger telescopes have higher spatial resolution. Most optical telescopes, however, do not reach the diffraction limited case but become 'seeing-limited' due to atmospheric turbulence. Thus, an important constraint on the image quality produced by the telescope is the atmosphere, as all terrestrial telescopes must see through it. In the atmosphere, there are parcels of air of different temperatures each traveling at different speeds. This phenomenon is called turbulence. Starlight, that originates from astronomical sources, travels through the Earth's atmosphere and the light's wavefronts will be distorted before reaching the telescope; as temperature differences result in refractive index changes and hence phase shifts occur in the light's wavefronts. The light from a point source (e.g. a distant star) is smeared out into a 'seeing disc'. This is quantified by its angular size measured in arcseconds. As the seeing limit is dependent on the atmosphere, the observed seeing disk will be same for all telescopes, regardless of the size of the telescope's aperture (Smith 1995).

In order to reduce the effect of turbulence, telescopes have been built at sites of higher elevation where the atmosphere is thinner and calmer. In addition, Adaptive Optics (AO) can be implemented in order to repair the distorted wavefront (Ealey 1992). Successful terrestrial platforms for large telescopes are currently situated in the high altitude sites of Mauna Kea (on the Island of Hawaii) and the Atacama Desert in South America.

To further improve the chances of an unhindered view, telescopes have been launched into space. The most successful examples were the NASA Great Observatories that were designed to cover four broad bands of the electromagnetic spectrum: the Hubble Space Telescope (optical/infrared,

Dalcanton 2009); the Compton Gamma Ray Observatory (safely decommissioned in June 2000, Kniffen 2003); the Spitzer Space Telescope (infrared, Patel & Spath 2004); and the Chandra X-ray observatory (Weisskopf 2006).

The temperature influences light transmission. Colder atmospheric temperatures lead to lower water vapour content, which results in higher transmission around water vapour absorption bands. This is particularly important for the mid-infrared and the sub-millimetre ranges. The temperature also affects the atmospheric thermal emission in the infrared. Thermal emission becomes the dominant source of the background for wavelengths longer than $\sim 2\mu\text{m}$. Atmospheric thermal emission becomes less dominant at regions of high altitude because of the reduced air density and lower temperatures.

Stray light contamination from natural and human sources can also affect image quality. Natural light contamination can arise from a number of sources (e.g. scattered sunlight, moonlight, aurora, airglow, etc). In addition, light pollution can also be produced from artificial sources (e.g. local city lights). See Kenyon & Storey (2006) for a discussion on sources of sky brightness.

Space is the most desirable location to place a telescope because of a continuous observational capability with no atmospheric thermal emission, absorption or light pollution. However, there are high transportation costs and challenging maintenance operations associated with space missions. As a compromise, a carefully selected ground-based location would be more economically viable. A ground-based observatory site will have the following atmospheric properties:

- Weak turbulence at high altitudes
- Low thermal emission
- Excellent seeing conditions
- Low light pollution

- High atmospheric transparency due to lower temperatures and the lower water vapour content
- Minimal cloud cover

The atmosphere above the Antarctic plateau offers the above-mentioned conditions. In addition, transportation costs for Antarctica are much lower than those needed for launching payloads into space. The Antarctic plateau is therefore a suitable compromise to undertake observational astronomy to that of space.

Experiments over the past decade have already suggested that the Antarctic plateau would provide a suitable platform for undertaking precise astronomy (Storey 2005; Swain & Hubert 2006). Atmospheric measurements at Dome C have suggested that the site is potentially one of the best astronomical sites on the Antarctic plateau and possibly the world (Sadibekova *et al.* 2007; Arnaud *et al.* 2006; Lawrence *et al.* 2007). Dome A and other isolated plateau sites may yet still provide the best platform for observational astronomy; however, these sites are more remote than Dome C. Therefore, an autonomous remote facility would be ideal in order to test the atmospheric conditions at these sites.

1.3 Autonomous remote site-testing

Remote sites that have no infrastructure to support humans throughout the year require site-testing facilities to be unmanned and fully autonomous. Power for the instruments must be generated on site. A stable temperature environment and continuous electrical power are required elements for an autonomously driven small observatory in Antarctica.

The National Science Foundation's Office of Polar Programs has placed automatic weather stations (AWSs) in a number of remote locations in Antarctica. The stations, as part of the United States Antarctic Program (USAP),

have measured continuous meteorological information such as air temperature, air pressure and wind velocities over the last few decades (Holmes *et al.* 1997; Stearns *et al.* 1997). During the summer and winter operations the stations are powered by solar panels and wind turbines respectively, which charge sealed lead-acid batteries in order to operate continuously throughout the year (White *et al.* 2006).

The United States also have an operational network of unmanned Automatic Geophysical Observatories (AGOs) that have been deployed to remote locations on the Antarctic plateau. These observatories have made measurements of the high-altitude ionosphere and magnetosphere. The AGOs were powered by propane fueled thermoelectric generators that can each produce up to 60W of electricity (Doolittle 1992; Doolittle *et al.* 1993). The thermoelectric generators were problematic and have now been replaced with solar panels and wind generators to power the AGOs. These AGOs are now part of the Polar Experiment Network for Geospace Upper-atmosphere INvestigations (PENQUIn) project (Lessard *et al.* 2009).

The British Antarctic Survey (BAS) has a similar network of AGOs that have small remote autonomous instruments to measure meteorological parameters at various locations in Antarctica. These systems are powered by lead-acid batteries that are charged by solar and wind generation systems that provide a nominal output of 100W (Dudneny *et al.* 1998).

Remote astronomical site-testing on the Antarctic plateau for higher power instrumentation suites necessitates the development of a more sophisticated power system than the AGO and AWS systems.

1.4 Remote Power Generation

The primary requirement for the observatory described in this thesis is to provide more than a kilowatt of electrical power for a remote instrumentation suite. The optimal power system for such an application would have:

- high reliability;
- minimal environmental impact;
- survivability in extremely low temperatures (from -30°C down to -90°C);
- operation at high altitude;
- fuel with a high energy density in order to reduce transportation costs across Antarctica.

The following sections present a review of possible remote power sources for use on the Antarctic plateau.

1.4.1 Solar Panels

Solar panels are a mature technology. Solar panels have silicon photovoltaic cells that generate power by converting solar radiation into a DC output (e.g. Jacobson 2009). The advantage of using solar panels in Antarctica is the opportunity to harness continuous power throughout the summer months. During the course of the year there will be periods where the Sun is: continuously above the horizon (summer season); rising and setting (autumn and spring seasons); and continuously below the horizon (winter season).

A one square metre solar panel can typically produce a maximum power output of 135W with conditions of 1000Wm^{-2} irradiance and 1.5 airmasses at 25°C (e.g. *Datasheet: "Solar Panel Pod", JCE Group 2010*). In practice in Antarctica, the silicon solar cell's electrical power output, compared to mid-latitude locations, can increase by 25% because of the lower temperatures and from the high reflectivity of the Sun's rays by the snow. The solar panel can still produce several watts of power when the Sun is directly behind it because of the snow's reflection of sunlight (Lawrence *et al.* 2005). An alternative power supply, however, is required when the Sun is below the horizon.

1.4.2 Wind Turbines

A wind turbine is a rotary device that extracts energy from the wind and converts it to an electrical output.

The mechanisms of katabatic winds have led to the fastest winds on Earth's surface being measured along the coast of Antarctica (Parish & Casano 2003). The ground level wind speed experienced at the coast is typically 20ms^{-1} but during a snow storm it can reach up to 80ms^{-1} . While it is very windy along the coastline, the average wind speeds on the Antarctic plateau are among the slowest in the world. The ground wind speeds that have been measured, averaged over one day, from both Dome C (Aristidi *et al.* 2005; Travouillon *et al.* 2008) and Dome A (Xiao *et al.* 2008) are always lower than 5ms^{-1} , with ground wind speeds peaking at $\sim 20\text{ms}^{-1}$. Although there is a strong gradient of wind in the surface layer, the wind speeds are still not strong even at a height of 30m.

When the wind speed is 5ms^{-1} and considering the mean air pressure at Dome A ($\sim 575\text{hPa}$), a wind turbine with its fan blades spanning 3m can theoretically extract up to $\sim 140\text{W}$ of recoverable power (Hickok 1975). This calculation indicates that the Antarctic plateau is not ideal for the construction of wind turbines.

1.4.3 Lead-Acid Batteries

A lead-acid battery is a reversible electrochemical device (Cowlshaw 1974). For use in Antarctica, the lead-acid battery is not an ideal choice because of the possibility of the liquid chemicals leaking if the battery is not stored properly (Pavlov 2006), although this risk is reduced for sealed lead-acid (SLA) batteries (see below). Batteries are subjected to self-discharging, which is the losing of stored charge without being connected to a load. A lead-acid battery has a poor volumetric energy density at $\sim 0.25\text{MJ/L}$ and has a high self-discharge rate of between 8-40% per month (Goswami & Kreith 2008).

The main difference between the SLA and lead-acid batteries is how the electrolyte is managed. There are two types of SLA batteries; gel-cell and absorbed glass mat (AGM). A gel-cell battery uses a gel, rather than a liquid, as the electrolyte. An AGM battery has a very fine fibreglass mat that absorbs and immobilises the electrolyte. The fibreglass matting is fixed between the electrodes allowing electrons to flow between them. These designs reduce the risk of spillage, corrosion and fumes that may cause environmental damage that are more prevalent in a standard lead-acid battery. In addition, the SLA battery typically has a self-discharge rate between 2-10% per month. Therefore, SLA batteries are better suited for long term use on the Antarctic plateau than lead-acid batteries (Holmes *et al.* 1997; Dudneny *et al.* 1998). SLA batteries, however, would not be suited to continuously power a remote facility but rather store electrical power whilst being charged by another source of power generation that has a higher volumetric efficiency (e.g. fossil-fuel).

1.4.4 Lithium Batteries

A lithium battery is another type of reversible electrochemical device (Scrosati & Garche 2010). The lithium battery type can be both used for small (e.g. lithium-ion) and large (e.g. lithium iron phosphate) power demands (Whittingham 2004). The advantage of using lithium batteries is that they have a higher power-to-weight and power-to-volume ratio than lead-acid batteries.

The lithium-ion battery typically has a volumetric energy density of $\sim 1.1\text{MJ/L}$, which is more than four times than that of lead-acid batteries. This makes lithium-ion batteries a suitable power supply for portable devices such as laptops and mobile phones (Takumra 2002). The self-discharge rate of a lithium-ion battery is 5% per month, which is comparable to that of a SLA battery. In addition, lithium-ion batteries, like lead-acid batteries, can handle hundreds of cycles of charging and discharging with minimal losses in

their specific capacities (Scrosati & Garche 2010). A major disadvantage for use in Antarctica is that lithium-ion batteries do not operate effectively at the extremely low temperatures that would be experienced at Dome A. However, as the technology matures in modifying the types of metals and chemicals used, operation at these temperatures may yet be feasible (Ai *et al.* 2004; Scrosati & Garche 2010).

The lithium iron phosphate (LiFePO_4) battery offers a better choice for the Antarctic plateau. One disadvantage, however, is that the LiFePO_4 battery can only operate down to a temperature of -25°C . Nevertheless, the LiFePO_4 battery has a longer cycling period of charging and discharging than the lithium-ion battery. The LiFePO_4 battery, along with the SLA battery, is better suited for long term use at a remote Antarctic dome site (Ashley *et al.* 2010).

1.4.5 Fuel Cells

A fuel cell is a device that directly changes chemical energy (derived from combining hydrogen and oxygen) into electrical energy and produces heat and water as by-products. The fuel cell works principally the same as a battery but it is used as a source, rather than storage, of electrical energy (Viswanathan & Schibioh 2007).

Fuel cells have a low environmental impact. One disadvantage, however, is that the volumetric energy density of the fuels (e.g. hydrogen) used in fuel cells is lower than that of fossil-fuels. For example, the volumetric energy densities of liquid hydrogen and diesel are $\sim 10\text{MJ/L}$ and $\sim 37\text{MJ/L}$ respectively. However, the energy per unit mass of the hydrogen fuel (i.e. specific energy) is potentially 2.5 times greater than diesel. Nevertheless, when the weight of the container is taken into account, hydrogen is no longer competitive with fossil-fuels (Kolb 2008). For operation on the Antarctic plateau, fuel cells still need to mature in cost-effectiveness and reliability.

1.4.6 Thermoelectric Generators

A thermoelectric generator (TEG) is a device that directly converts heat into electricity. The various types of TEGs depend on the source of heat.

Propane fueled TEGs rely on the burning (or catalytic oxidation) of propane gas in order to produce electricity. TEGs are a mature technology and have no moving parts; however, TEGs can consume up to 3.5kg of propane per kWhr (Pietras 1993). For continuous operation at greater than a kilowatt in a remote location, TEGs would not be cost effective for the Antarctic plateau because of the requirement for delivery of large quantities of propane (Herdman 1994).

Radioisotope thermoelectric generators (RITEGs) provide a reliable, steady flow of power derived from radioactive decay. RITEGs are recommended for use in low power applications. For example, RITEGs provided 10W of electrical power and 200W of heat for remote magnetometers placed at sites in East Antarctica from 1975 to 1984 (Papitashvili 1999; references therein). To increase the power output of an RITEG to 1kW would increase the amount of radioactive material, which increases the risk of environmental damage.

A solar-driven thermoelectric generator (STG) relies on heat from the Sun to produce electricity. In its simplest form, a STG consists of a solar (thermal) collector connected to a thermoelectric generator. The electricity produced is proportional to the change in temperature. STGs are reliable because they operate silently, have a long shelf-life and are constructed with no moving parts. In practice, however, STGs have low efficiencies and are usually combined with photovoltaic cells to increase the power output (Chen 1996; Hongxia *et al.* 2007). In addition, the STG system would not be an alternative power source during the winter months on the Antarctic plateau.

1.4.7 Heat Engines

A heat engine is a machine that converts thermal energy into a mechanical output. A generator can then couple to the heat engine in order to produce an electrical output. The types of heat engines that can be used as portable generators are external combustion engines (e.g. Closed Cycle Vapour Turbogenerators and Stirling engines) and internal combustion engines (e.g. diesel and petrol engines).

Closed Cycle Vapour Turbogenerators

A Closed Cycle Vapour Turbogenerator (CCVT) follows the Rankine cycle. The CCVT produces electricity from a turbine that is driven by the vapour pressure obtained from boiling an organic fluid. A CCVT will continuously operate as long as heat is always applied to the vapour generator (Bareli 2004).

CCVTs have been specifically designed and have successfully operated remotely in the Arctic region for microwave repeater stations for telecommunications (Belousenko 1997). CCVTs can produce power between 400W and 2400W, and operate as low as -60°C ; standard units can operate at 2000m altitude but with a modification they can operate as high as 5000m (Gropper 2000).

The disadvantages of a CCVT are poor thermal efficiency and high unit cost ($\sim \$100,000$). For an unit fueled by propane, the fuel-to-electricity conversion can be as low as 6%, but a typical thermal efficiency is approximately 15% (Miller 1983).

Stirling Engines

The Stirling engine operates on a closed thermodynamic cycle (Harrod et al. 2009; Thombare & Verna 2006). The Stirling cycle is closed because there is no mass exchange of the working fluid to the environment.

The Stirling engine comprises of a cold space and a hot space. The cold space is maintained at a low temperature (T_{min}) and the hot space is maintained at a high temperature (T_{max}). The Stirling engine system also encloses a working fluid that can flow between the hot and cold spaces.

An ideal Stirling engine is configured with the cold and hot spaces separated by a regenerator. A regenerator is a device that acts like a “thermal sponge” by absorbing and releasing heat (Thombare & Verma 2006). The phases of the Stirling cycle are shown in the P-V diagram of Figure 1.2 and are described as follows:

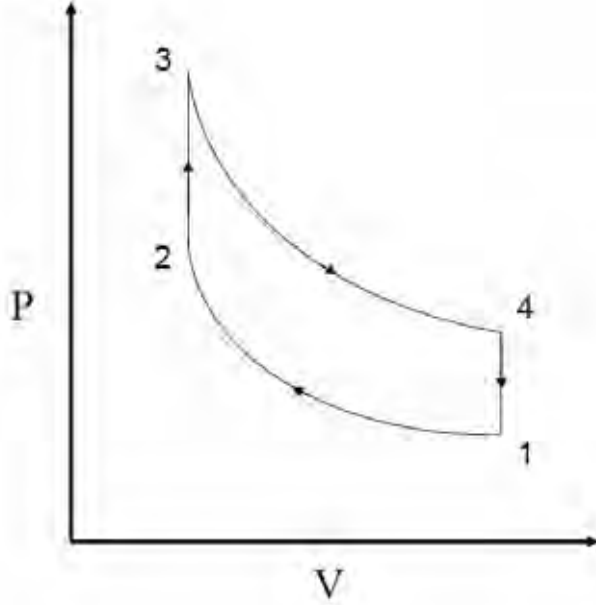


Figure 1.2: Theoretical Stirling Cycle

Simple P-V Diagram showing the two isothermal (1-2 and 3-4) phases and the two constant volume phases (2-3 and 4-1) in an idealised Stirling cycle.

1-2 As the volume of the cold space decreases, heat is transferred from the working fluid to the external heat dump maintaining the temperature of the system at T_{min} .

2-3 The regenerator releases heat into the working fluid as it passes into the hot space. This increases the temperature of the working fluid from T_{min}

to T_{max} .

3-4 Once the volume of the cold space stops decreasing, the volume of the hot space increases. Heat is transferred from an external source to the working fluid. The working fluid remains at T_{max} as its pressure decreases.

4-1 Once the volume of the hot space reaches maximum capacity it starts to decrease and the volume of the cold space starts to increase. The working fluid then transfers heat back into the regenerator as it shuffles back into the cold space, reducing the temperature of the working fluid back to T_{min} . The cycle begins again when the cold and hot spaces return to their original volumes.

Therefore, the Stirling cycle performs a series of compressions and expansions of the working fluid due to the temperature difference between the hot and cold spaces. The constant-temperature hot and cold regions surrounding the Stirling engine supply and reject the heat, as required by the second law of thermodynamics to produce a net output of work (Walker & Senft 1985).

Typical gases for the working fluid are air, hydrogen and helium (Mago *et al.* 2009). The Stirling engine is a type of external combustion engine; however, this can be misleading because the external heat can not only be produced from burning combustible fuels but also from solar or geothermal energy (Mago *et al.* 2009; and references therein).

In practice, the four phases of the P-V cycle are not sharply distinct because a practical engine suffers from frictional losses and the working fluid is not completely sealed from its environment (Walker & Senft 1985). A more realistic P-V cycle is shown in Figure 1.3, where there are nearly two isothermal processes and nearly two constant volume phases.

Stirling engines are mechanically very simple devices, which leads to low maintenance. Other advantages include quiet operation, clean burning, having multiple fuel capability and are reasonable efficiency. In addition, the

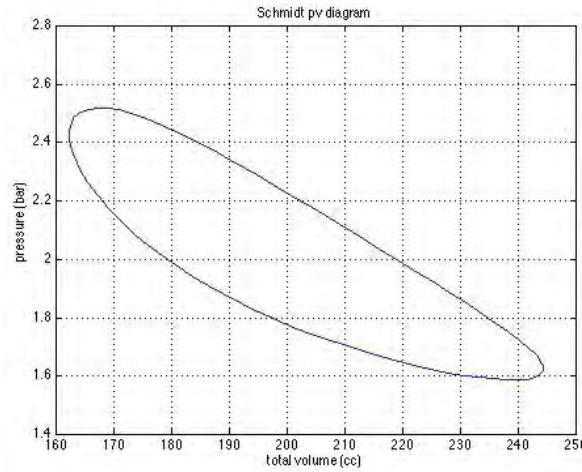


Figure 1.3: Practical Stirling Cycle

A more realistic P - V cycle derived from the Schmidt Analysis of the Stirling engine (Urieli & Berchowitz 1984).

waste heat produced can be easily recovered. Unfortunately, Stirling engines do have some disadvantages. As the heat source is external it takes a while to acquire the desired temperature difference. As a result, the power output cannot readily be changed.

The WhisperGen is a commercially available Stirling engine that is ideal for remote operation. The WhisperGen is an “alpha” design consisting of four double acting pistons arranged in a square configuration (Clucas & Raine 1994b). It uses a “wobble yoke” mechanism to produce a smooth reciprocating motion of the pistons (Clucas & Raine 1994a). The WhisperGen Stirling engine has successfully powered a remote facility in Antarctica; see section 1.5.2.

Diesel and Petrol Engines

Diesel and petrol engines are a mature technology with reasonable efficiency and are relatively inexpensive. At maximum compression, combustion will be initiated under high pressure inside a diesel engine; whilst combustion starts with a flame (e.g. a spark plug) inside a petrol engine. Petrol engines

have a lower efficiency than diesel engines because:

1. diesel engines have a greater thermal efficiency due to their higher compression ratios; and
2. diesel engines maintain a constant air-flow with the power being proportional to the amount of fuel used. In petrol engines, air-flow is not constant as the power is proportional to the amount of air that is being pumped into the engine that is controlled by a butterfly valve. This is to maintain the stoichiometric ratio between air and fuel (see section 3.3.1). As a result, petrol engines experience greater pumping losses at partial or no load than diesel engines.

In addition, diesel fuel ($\sim 37\text{MJ/L}$) has a larger volumetric energy density than petrol ($\sim 34\text{MJ/L}$).

A diesel generation system operating autonomously in Antarctica would operate effectively by having multiple engines in order to gain a high level of redundancy. For example, there are six independent diesel engines that are in use at the Terra Nova Bay site to supply power to the instruments during the winter months (Meloni *et al.* 1992). Similarly, six independent diesel engines are in use at Dome A to power PLATO.

The diesel engine was selected for the PLATO facility because it has a quick-start and variable-load capability. The diesel engine was chosen instead of the Stirling engine because of the capability of producing the required higher power output with a better efficiency (see Chapter 2 for an overview of the PLATO facility).

1.5 UNSW Autonomous Facilities

The Antarctic Astronomy group at the UNSW has developed three remote site-testing observatories at three separate locations on the Antarctic plateau. These site-testing facilities are AASTO and AASTINO that operated at the

South Pole and at Dome C respectively; and the latest site-testing facility, PLATO, which is currently in operation at Dome A.

1.5.1 Site testing at the South Pole



Figure 1.4: AASTO at the South Pole.

The Amundsen-Scott South Pole station is located on the edge of the plateau at an altitude of 2800m. The United States operate the base all year round. A remote facility called the Automated Astrophysical Site-Testing Observatory (AASTO), shown in Figure 1.4, was designed and supported by both the Australian National University and UNSW. The AASTO was deployed at South Pole in the summer of 1997.

AASTO was built by Lockheed and was based on the US Automated Geophysical Observatory. AASTO's power generation system consisted of a propane-fueled thermoelectric generator that produced some 50W of electrical power and 2.5kW of heat (Doolittle 1992; 1986; Doolittle *et al.* 1993).

AASTO housed a suite of instruments that included:

- AFOS (Antarctic Fibre Optic Spectrometer), the light captured by a telescope was coupled to a bundle of optic fibres that was fed into a spectrograph. The purpose of AFOS was to measure the transmission of optical and ultraviolet wavelengths (Boccas *et al.* 1998; Dempsey *et al.* 2004).
- SODAR (SOund Detection And Ranging) was a sonic radar that measured the turbulence in the atmosphere as a function of height (Travouillon *et al.* 2003b).
- NISM (Near-Infrared Sky Monitor) measured the emission in the atmosphere at $2.35\mu m$ (Storey *et al.* 1999).
- MISM (Mid-Infrared Sky Monitor), a similar instrument to NISM but measured the emission in the atmosphere in the mid-infrared up to $15\mu m$ (Chamberlain *et al.* 2000).
- SUMMIT (Sub-millimetre Tipper), a similar instrument to both NISM and MISM but took measurements in the sub-millimetre regime at $350\mu m$ (Calisse *et al.* 2004).
- ADIMM (Antarctic Differential Image Motion Monitor) was an instrument that measured the ‘seeing’ conditions at visible wavelengths (Dopita *et al.* 1996).

AASTO obtained data from all of these instruments. The South Pole site was shown to have a poor median seeing of 1.8arcsec at 500nm (Travouillon *et al.* 2003a; Marks *et al.* 1999). However, thermal-emission observations in the near- and mid-infrared ranges have shown lower sky brightness than at any prime mid-latitude sites: MISM, during the winter of 1998, measured up to an order of magnitude lower sky brightness in the mid-infrared (Chamberlain *et al.* 2000); and NISM, during the winter of 2001, measured up to two orders of magnitude lower sky brightness in the near-infrared (Lawrence

et al. 2001). The South Pole was also shown to have excellent potential for sub-mm astronomy because of a dry and stable atmosphere (e.g. Rathborne & Burton 2003).

Over several years of operation, the TEG power generation was shown to be inefficient and unreliable, which eventually led to the AASTO being switched over to the South Pole station power for operation. AASTO was decommissioned in December 2005.

1.5.2 Site testing at Dome C

Dome C is located at a physical elevation of 3250m above sea level. There is currently a French/Italian scientific research station named Concordia at the site (Fossat 2005). It has long been believed that Dome C would be an exceptional site for optical observations (Gillingham 1991).



Figure 1.5: AASTINO at Dome C.

AASTINO (Automated Astronomical Site-Testing InterNational Observatory), shown in Figure 1.5, was designed by the UNSW Antarctic astronomy group and deployed to the Dome C station in January 2003 where it was able to operate autonomously from February 5th to July 1st, 2003 and again in 2004 (Lawrence *et al.* 2005).

AASTINO was powered by two WhisperGen PPS16 24VDC Stirling Engines burning Jet A-1 fuel. This was the first implementation of the hybrid system consisting of solar panels and Stirling engines (Lawrence *et al.* 2005). The two engines were cooled with a glycol loop that fed into large heat exchangers, which kept AASTINO warm via the waste engine heat. At sea level the WhisperGen engines produced 750W of electrical power. At the higher altitude of Dome C, each engine was able to produce up to 500W. Waste heat equivalent to 3.5kW was recovered from the Stirling engines. AASTINO also used two solar panels to provide additional power during the summer months. A standard 167W solar panel was able to produce up to 220W because of the lower temperatures and from the bright reflection off the snow. This was sufficient power and heat for the instrumentation suite on AASTINO.

The following instruments were powered by AASTINO (Lawrence *et al.* 2005):

- SODAR and SUMMIT, the same instruments that were used with the AASTO to measure the atmospheric conditions at Dome C.
- ICECAM, a CCD camera that took sky images of a 30 degree field-of-view to determine cloud-cover statistics above Dome C (Ashley *et al.* 2005).
- COBBER, another instrument that determined the cloud-cover statistics above Dome C by measuring the thermal emission (Dempsey *et al.* 2004).

- Nigel, a fibre-fed optical spectrograph that was cannibalised from AFOS (Kenyon *et al.* 2006). Nigel is currently operating with PLATO at Dome A (see Appendix A for an overview, Sims *et al.* 2010).
- MASS (Multi-Aperture Scintillation Sensor) was the most successful instrument. It was designed to measure the scintillation index of the atmospheric turbulence in four concentric apertures with photo-multiplier tubes. From this, the vertical turbulence profile can be determined (Tokovinin *et al.* 2003). MASS was mounted inside AASTINO and peered through a thick glass window in AASTINO's roof. MASS reported a median seeing value of 0.27 arcsec and below 0.15 arcsec 25% of time, which is better than the best ground-based sites in the world. The exceptional seeing value for Dome C is one justification for the construction of the PILOT observatory (Lawrence *et al.* 2004).

AASTINO was decommissioned in February 2005.

1.5.3 Site testing at Dome A

PLATO (PLATeau Observatory) is the latest facility produced by the UNSW Antarctic astronomy group, which has been deployed by the Polar Research Institute of China (PRIC) and the Chinese Academy of Sciences to Dome A. PLATO successfully collected data from January to August 2008 and since the servicing mission in January 2009 has recommenced operation. Since then, as of March 23rd 2011, PLATO has been operating continuously for 800 days. A description of the PLATO power system and its suite of instruments are discussed in Chapter 2.

PLATO was designed to operate a larger and more sophisticated instrument suite than its predecessor AASTINO. Therefore, this required a more powerful system than the Stirling engines could provide. As a result, the PLATO power system is composed of a hybrid system of diesel engines and solar panels. The engine was chosen to be a commercially available Hatz 1B30

single-cylinder diesel engine. A review of the diesel engine, mechanical processes, chemical and physical properties of diesel fuel and diesel-compatible fuels, and a description of the Hatz 1B30 are given in Chapter 3.

1.6 Thesis Summary

Before deployment, there were a number of tests on the Hatz 1B30 diesel engine at simulated high altitude. This thesis reports measurements of efficiency and reliability of the Hatz 1B30 engine at simulated atmospheric pressures that are expected for Dome A. This work forms the bulk of this thesis, as there had been little or no published work on autonomous, remote power generation systems for high altitude operation. In particular, there had been no formal research into the operation of single-cylinder diesel engines operating on jet fuel in low pressure environments. The main goals for this thesis are to estimate the fuel efficiency at high altitude; monitor temperatures at different points on and around the engine; and finally, to experiment with the fuel injection timing. Chapter 4 describes the methodology of testing the Hatz engine at high altitude, which is followed by an analysis and discussion of engine tests.

The thesis also aims to emphasise the important relationship between engineering and instrumentation in application for Antarctic astronomy. During the course of this work, some development and testing of the Nigel spectrometer was also carried out. The results of these (unpublished) tests are described in Appendix A. The raw engine test data are presented in Appendix B.

The author has been first author on two papers resulting from the work presented in this thesis, and co-author on a further two refereed and six conference papers. These are listed in Appendix C, and the two first-author papers are presented in their entirety.

Chapter 2

PLATO

“Astronomy compels the soul to look upwards and leads us from this world to another.”

Plato, The Republic Greek author & philosopher in Athens
(427 - 347 BC)

PLATO (PLATeau Observatory) is an autonomous facility that was successfully deployed to Dome A, Antarctica in January 2008. PLATO is designed to provide power, heat, communication and control for site-testing and science instruments at Dome A (Yang *et al.* 2009). The primary goal of the instruments is to measure atmospheric conditions above Dome A in order to determine if it is worthwhile to build large astronomical facilities.

2.1 Dome A

Dome A is located at a high altitude. The corresponding thin atmosphere makes it a promising site for astrophysics. The seeing conditions at Dome A are thought to be unprecedented for any ground-based observational platform. It is also believed that the atmospheric transparency is greater at Dome A, especially in the sub-millimetre wavelengths (or terahertz frequencies) than other temperate sites (Lawrence 2004; Kulesa *et al.* 2008). Though

recent work has indicated that an even better site for terahertz astronomy is Ridge A, which lies some distance from Dome A (see Saunders *et al.* (2009) for details).

The Polar Research Institute of China (PRIC) intend to place a permanently manned station at Dome A within the next decade. They have research goals in the scientific fields of astronomy, glaciology, subglacial geology, climatology, and upper atmospheric physics. For climatology, the Chinese hope to obtain the longest climate history by drilling the deepest ice cores (Chen 2008).

Dome A is located about 1200km from the nearest coastal stations of Davis and Zhongshan; and is about 1100km from the geographic South Pole (Yang *et al.* 2009). The summit of Dome A was first reached by a team from PRIC in January 2005 via an inland traverse from the Chinese coastal station, Zhongshan (see Figure 2.1). A second team involving the PRIC and the Chinese Academy of Sciences reached the summit again in January 2008 as part of the International Polar Year PANDA (Prydz Bay, Amery Ice Shelf and Dome A Observatories) expedition. It was on this expedition that the Chinese transported and deployed the PLATO facility at the Dome A site.

2.1.1 PLATO design considerations

In developing PLATO, several new factors had to be considered in addition to the experiences from the earlier facilities of AASTO and AASTINO (see section 1.5). The new challenges faced at Dome A were:

- **No preferred wind direction**

Unlike at Dome C and the South Pole, the wind at Dome A has almost no preferred direction.

- **Higher altitude**

Dome A has a physical altitude of 4093m that corresponds to a pressure altitude that is typically 4600m.

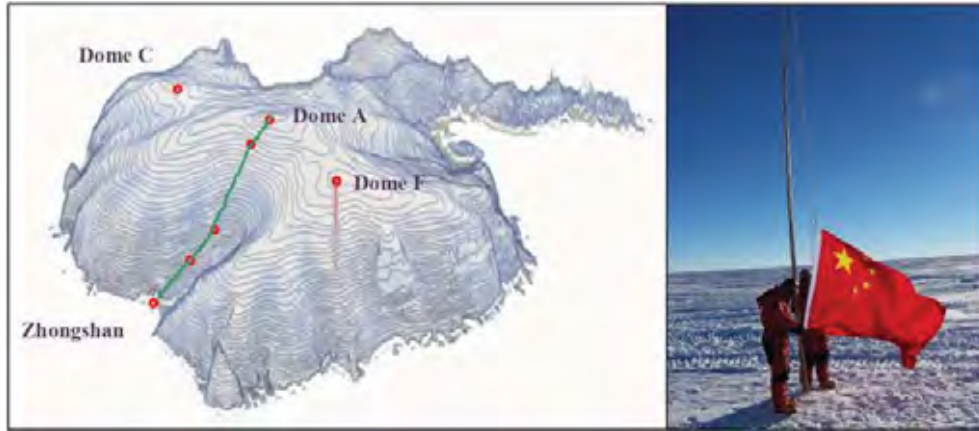


Figure 2.1: Chinese at Dome A

*Left Panel: 3D Topographical feature map of Antarctica showing PRIC's inland traverse from Zhongshan station to Dome A (courtesy of PRIC).
Right Panel: Chinese astronomers placing their national flag at the Dome A site in 2005 (courtesy of PRIC).*

- **Colder**

Dome A is probably one of the coldest places on Earth, although this is not yet firmly established as meteorological records are only recognised if they are made by a human observer. Nevertheless, temperatures as low as -90°C appear possible. This is well below the “dry ice” temperature, emphasizing the need for extremely well-insulated structures and very efficient use of energy.

- **More remote**

The greater difficulty of bringing materials to Dome A makes it even more important that the power solution be optimised in terms of fuel type, fuel efficiency, and power management. Dome A is a new site and has currently no infrastructure to support humans throughout the winter months. Thus, PLATO needed to be unmanned and fully autonomous throughout the year.

- **Shorter installation time**

The Chinese are currently the only people who have successfully reached the summit of Dome A. Their current method is an ice-breaker ship to Zhongshan coastal station and then undertaking a ~ 1200 km tractor traverse to Dome A. This results in limited supplies (e.g. food and equipment) being transported. As Dome A currently has no permanent infrastructure, working in a low temperature environment becomes extremely hazardous the longer humans remain on site. A remote facility at Dome A requires a shorter timescale to assemble. Due to the time constraints and logistics that the Chinese have for traveling to and from Dome A, they typically have 2-4 weeks on site for installation compared to several months that are possible at South Pole and Dome C.

- **Higher power requirements**

Increasingly sophisticated astronomical instruments require more electrical power output from PLATO than its predecessors of AASTO and AASTINO. The power requirements for the AASTO and the AASTINO were up to 50W and 500W respectively, whilst PLATO requires up to 1kW. In addition, about 1kW of heat is needed to keep the instruments warm (see section 2.2).

2.2 Instrument Suite

PLATO's instrumentation suite is larger and more diverse than either of its predecessors, AASTO and AASTINO. The following describes each PLATO instrument:

- **CSTAR**

CSTAR (Chinese Telescope ARray) is composed of four optical telescopes to observe variable stars, the atmospheric extinction, the sky background, and cloud coverage at Dome A (Yuan *et al.* 2008).

- **Snodar**

Snodar (sonic non-Doppler acoustic radar) is used to measure the height of the atmospheric boundary layer at Dome A (Bonner *et al.* 2008).

- **Pre-Heat**

Pre-HEAT is the precursor to HEAT (High Elevation Antarctic Terahertz telescope), which is a submillimeter-wave telescope to measure the 450-micron sky opacity above Dome A. This is both a site-testing and scientific instrument (Kulesa *et al.* 2008).

- **Gattini-II**

Gattini-II is a sequel to Gattini that was deployed to Dome C, is composed of two cameras designed to measure the optical sky brightness, cloud cover, and to detect auroral emission (Moore *et al.* 2008).

- **Nigel**

Nigel is a optical/UV fibre fed spectrograph designed to measure optical sky brightness and auroral lines (Kenyon *et al.* 2006; Sims *et al.* 2010), and was deployed on PLATO's servicing mission in January 2009. Nigel is both a site-testing and scientific instrument (see Appendix A for an overview of the Nigel instrument).

- **Dasle**

Dasle is a 15m tower fitted with sensors to evaluate the meteorological conditions within the boundary layer (Yang *et al.* 2009).

- **Webcams**

Web-cameras are installed for the daily monitoring of the PLATO facility (Lawrence *et al.* 2008).

- **HRCAM**

A high-resolution optical camera was installed in the summer of January 2010 in order to take all-sky photos from the Dome A site.

Table 2.1 presents the approximate peak power requirements of each instrument for the operation of PLATO during the winter months in terms of electrical power and heat.

Instrument	Electrical (W)	Heat (W)
CSTAR	200	400
Pre-HEAT	80	60
SNODAR	200	50
Nigel	70	20
Gattini-II	110	100
Dasle	30	250
Computers/Webcams	150	150
Heaters	150	N/A
HRCAM	2	30
Total	$\sim 1\text{kW}$	$\sim 1\text{kW}$

Table 2.1: Power Budget for PLATO

Table shows the power requirements for each instrument separated into their electrical and heat components. The approximate peak power values presented are for the operation of the PLATO instruments during the winter months.

2.3 PLATO Design

The new constraints for PLATO at Dome A forced the UNSW Antarctic team to change the design strategy from their previous facilities of AASTO and AASTINO. The major change was in the primary power generation system, from Stirling engines used on the AASTINO to a bank of diesel engines.

2.3.1 Modular Design

The absence of a preferred wind direction makes it impossible to protect the astronomical instruments from the exhaust stream by simply placing them upwind of the engines, as was done with the AASTINO. Instead, a separate engine and instrument module are required, spaced at a sufficient distance that the exhaust stream is less likely to intrude into the atmosphere through

which the instruments are observing. Having two modules also allows for the instruments to be isolated from engine noise and vibrations. The disadvantage of this approach is that it is then no longer possible to use waste engine heat to keep the instruments warm, unless the engine coolant is plumbed between the two units. This option, however, was considered to be impractical, leading to a solution in which the instruments and control computers are heated purely by electrical power. As a result, PLATO consists of two modules, an instrument module and an engine module, each built into a standard ten-foot shipping container.

The two modules were constructed and tested at UNSW before deployment, which permitted the Chinese to have a shorter installation time of PLATO at Dome A. The modules were designed to be attached to each other and transported as an ISO standard 20 foot container for ease of transport by road, rail, sea, and ice sled in order to reach Dome A. Once at Dome A, the engine module could then provide power to the instrument module via a 50m electrical umbilical connected between the containers (See Figure 2.2).

To protect the instruments and the engines from the cold, each module has insulation that is 150-200mm thick and composed of polyurethane foam layered with Colourbond steel. The insulation was designed with a thermal conductivity of 12 W K^{-1} (Luong-Van *et al.* 2010).

2.3.2 Engine Module

It is desirable to have the engines start reliably at the altitude of Dome A with a sufficient power output despite the thinner air they will be breathing. In practice, this means choosing an engine of a significantly larger displacement than would be required at sea level (or even for places such as the South Pole or Dome C).

The engine module houses two banks of three Hatz 1B30 engines (see



Figure 2.2: PLATO at Dome A

The instrument module is the yellow container in the centre. The engine module is the green container located in the background to the right.

(Image Credit: Zhenxi Zhu).

Chapter 3 for an overview of the diesel engine) that sit on top of a 4000 litre fuel tank. Usually, one engine is operating at any given time but more engines can operate simultaneously in order to gain more power. Having six engines creates a high level of redundancy with the ability to increase the base load generating capacity (Hengst *et al.* 2008). In order to start the engines reliably in the cold, an ultracapacitor bank replaces the usual lead-acid battery to electro-mechanically crank the engine (Hengst *et al.* 2009).

The engines have a standard service interval of 200 hours; however, maintenance cannot be achieved until the following summer. Each engine was outfitted with its own bulk oil filtration and recirculation system in order to increase the service interval to about 2000 hours (Lawrence *et al.* 2009).

During PLATO's inaugural mission, it was decided to deploy two different types of generators in order to maximise the chances of success. The



Figure 2.3: Diesel Engines

A bank of three Hatz 1B30 diesel engines inside the engine module during construction at UNSW. The eCycles alternators are mounted on the left and middle engines and the Mavilor generator is mounted on the right engine (Image Credit: Michael Ashley).

generators chosen were:

- A three-phase brushless bearing-less alternator made by eCycle. These units are lightweight and compact, with the NdFeB permanent magnet rotor mounted directly onto the crankshaft. The output of the alternator is rectified with an IR 70MTKB diode bridge. The manufacturer quotes an efficiency of about 90% under the operating conditions for PLATO, which does not include the losses in the diode bridge. For PLATO's first season of operation, the eCycles' windings were custom wound to achieve a voltage constant of 50V/krpm.
- A DC servo motor MSS-22 made by Mavilor (MG-1-48). This disc motor has very high efficiency (both as a motor and generator) as it does not suffer from iron loss.

See Figure 2.3 for a picture of a bank of diesel engines (with their respective generators) mounted inside the engine module during the construction phase at UNSW.

Solar Power

Whilst not physically attached to the engine module, solar panels provide the primary power during the summer months. The solar panels are arranged in two arrays of three paralleled panels (see Figure 2.4). Each panel is polycrystalline silicon Conergy C167P, with a nominal power output of 167W at 25°C for 1.5 air-masses. Each array of three panels is fed to an Apollo Solar T80 maximum-power-point tracker (MPPT).

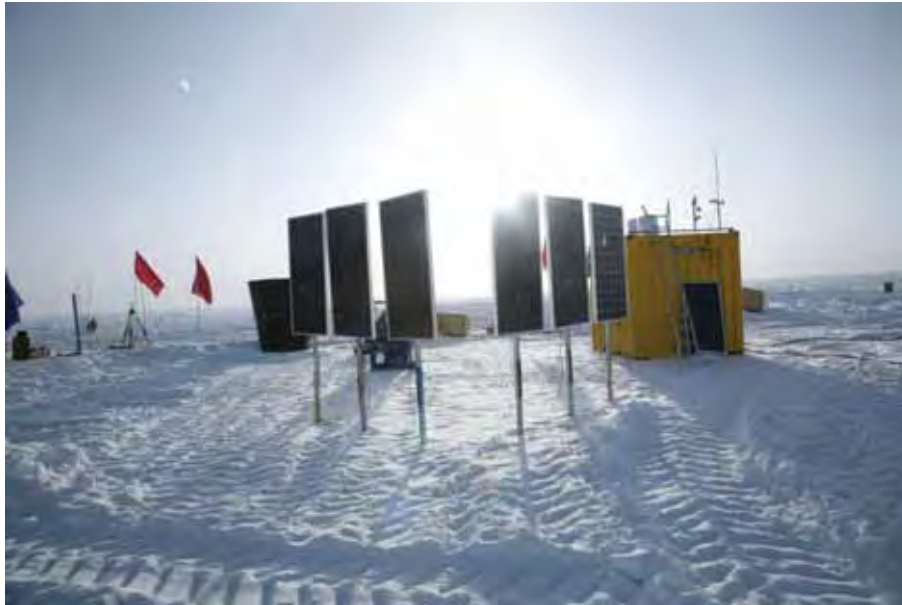


Figure 2.4: Solar Panels at Dome A
*Solar Panels for PLATO installed in front of the instrument module
 (Image Credit: Zhenxi Zhu).*

2.3.3 Instrument Module

The instrument module is a modular system that allows for the installation of multiple instruments that are independent and autonomous. The instrument module houses all the instrument computers and control electronics and the PLATO control “supervisor” computers. Outside communications to each supervisor computer are made possible via the Iridium satellite network. SLA batteries are used for power storage (see Section 1.4.3) and are also kept inside the instrument module. The PLATO instruments are either mounted to the roof of the module or are placed externally on the snow surface (Luong-Van *et al.* 2008; Lawrence *et al.* 2009).

2.3.4 Control Systems

In order to run PLATO continuously at high reliability, the hardware and software systems must be able to operate with little human intervention.

The hardware consists of two linux-based supervisor computers for dual redundancy. Each supervisor unit has its own management electronics and an Iridium modem. The supervisor computers control and monitor instrument power sharing, thermal-management and engine sub-systems. A wired LAN is used to communicate between the supervisor computers and instruments. External communications from remote operations at UNSW are achieved via the Iridium Satellite Network.

A script is executed from the supervisor computers in order to carry out high-level functions. These include the instrument scheduling, heat allocation, engine power regulation, battery charge management, and communications (Luong-Van *et al.* 2008).

2.4 PLATO Performance

PLATO, on its first mission, managed to operate successfully for a period of 204 days after it was deployed in January 2008. This fell short of the original goal of reaching the following year but still was a significant achievement. At this time, this was the longest continuous operation (without direct human intervention) of any of the facilities designed by the UNSW Antarctic astronomy group.

The January 2009 servicing mission was a success and with the updated system, the engine module survived the Antarctic winter to the following summer for the next re-servicing. At the time of this thesis submission (end of March 2011), the PLATO engine system has continuously operated for over 800 days (see: <http://mcba11.phys.unsw.edu.au/~plato/> for latest operational time). See section 4.8 for plots corresponding to engine operation throughout the year.

The insulation used for the modules was shown to be very effective. The mean thermal conductivity of the instrumentation module through the winter season of 2009 was measured to be 11.9 W K^{-1} , which was consistent with design requirements (Luong-Van *et al.* 2010).

The power generation system also performed effectively. The two generators that were selected performed well with similar efficiencies during PLATO's first year of operation. It was decided for the servicing mission in January 2009 to only use the eCycle alternators because of their light and compact design for ease of installation. All existing eCycles were replaced with new units that had their windings custom wound to 60V/krpm in order to increase the voltage output.

During the summer months, the two arrays of solar panels were able to produce a power output of up to 1000W. An individual solar panel was able to produce up to 220W in direct sunlight; about 50W higher than their nominal power output. Unfortunately, when the Sun's rays are behind the

solar panels, they produce little power; and so the engines provided the required additional power.

The PLATO instruments have taken invaluable measurements of atmospheric properties above Dome A. CSTAR, during its 2008 operation, has shown that for about 67% of the time when the Sun is well below the horizon, there is little or no cloud cover. In addition, only $\sim 2\%$ of the CSTAR images were affected by strong aurorae (Zou *et al.* 2010). Snodar, throughout the winter season of 2009, measured a median height of the boundary layer to be 13.9 ± 0.7 m, and to be as low as 9.7 ± 0.5 m 25% of the time (Bonner *et al.* 2010). Pre-HEAT observations measured a very low water vapour content in the atmosphere above Dome A, which offers higher transmission in the far-infrared spectral ranges than for any other ground-based site. Observing through these windows will gain stronger statistics on star formation, the life cycle of the interstellar medium and the evolution of galaxies (Yang *et al.* 2010). Nigel also confirmed an extremely low water vapour content. Nigel has also showed that Dome A, during the winter months, has a large amount of available dark time (Sims *et al.* 2010).

Yang *et al.* (2009) present a detailed description of PLATO and the results from the instruments that were deployed in 2008. Lawrence *et al.* (2009) present a detailed description of PLATO's power generation and control systems with an overview of the system performance for 2008.

Chapter 3

The Diesel Engine

“The use of plant oil as fuel may seem insignificant today. But such products can in time become just as important as kerosene and these coal-tar-products of today.”

Rudolf Diesel, German Inventor and Mechanical Engineer
(1858-1913)

The diesel engine was designed and patented by Rudolf Diesel in 1892. Since then, the diesel engine has matured with over 100 years of development. In 1922, the development of Robert Bosch’s high-pressure fuel pump considerably improved the diesel engine performance (Bosch GmbH 2005). The Hatz 1B30, which was selected for the PLATO programme, is a naturally aspirated, directly injected single-cylinder diesel engine. This chapter will review the diesel engine’s mechanical processes, fuel usage and properties.

3.1 The Diesel Cycle

All engine systems undergo a cyclic motion that starts and ends at the same position. The Hatz 1B30 engine follows a four-stroke diesel cycle:

1. Induction (a)
2. Compression (b)

3. Ignition (c)

4. Exhaust (d)

Figure 3.1 shows a pictorial representation of the four strokes (a-b-c-d) performed in a single-cylinder direct injection diesel engine. The diesel engine takes in air into its cylinder (a). The air is then highly compressed by a piston (b). A small quantity of fuel is then squirted into the volume of compressed air and after a short delay, the air-fuel mixture spontaneously ignites. The explosion forces the piston downwards producing mechanical power (c). The cycle then finishes with the expulsion of the residue gas from the cylinder (d).

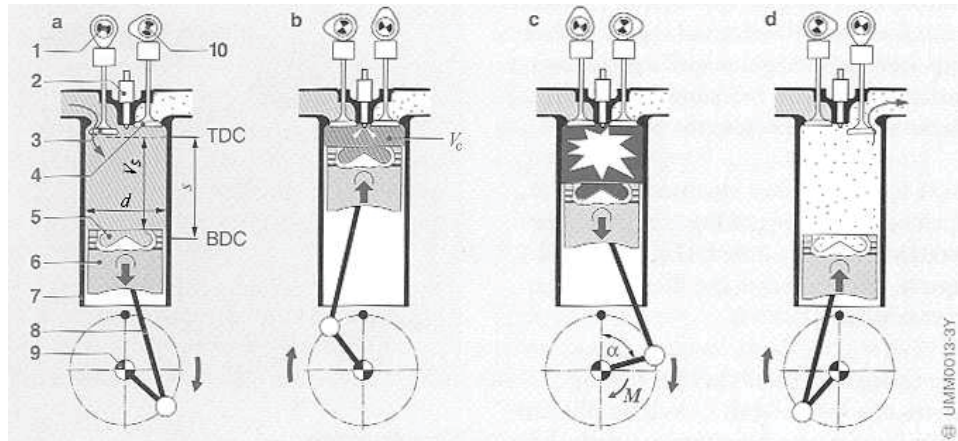


Figure 3.1: Four-stroke Mechanical Diesel Cycle

a. Induction stroke b. Compression Stroke c. Ignition Stroke d. Exhaust Stroke
 1. Inlet-valve Cam 2. Fuel Injector 3. Inlet Valve 4. Exhaust Valve
 5. Combustion Chamber 6. Piston 7. Cylinder Wall
 8. Connecting Rod 9. Crankshaft 10. Exhaust-valve Cam
 α : Crankshaft angle of rotation; d : Bore; M : Turning Force s : Piston Stroke; V_c = Compression Volume V_s = Swept Volume (Bosch GmbH 2005).

The four-stroke cycle can be described by a pressure-volume (P-V) diagram. The theoretical P-V cycle (or Seilinger process) (Mahon 1992; Bosch GmbH 2005; see Figure 3.2 - Left Panel), however, cannot fully describe

the diesel four-stroke cycle. The induction and exhaust strokes, in particular, cannot be represented as the Seilinger process because the theoretical process assumes a closed system. The induction and exhaust strokes could instead be represented by the F-A and A-F sequences respectively shown in Figure 3.2 (Left Panel) in performing no overall net work. Figure 3.2 (Right Panel) shows a more realistic P-V cycle of the four-stroke diesel cycle and is described in the following sections.

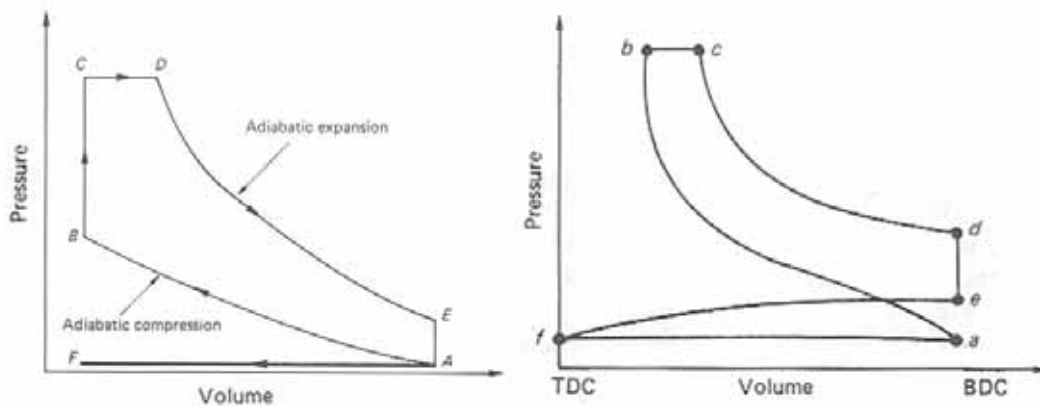


Figure 3.2: Theoretical and Realistic Thermodynamic Work Cycles
Left Panel: shows the theoretical P-V cycle of combustion process in a Diesel engine. Right Panel: shows a more realistic P-V cycle of the four-stroke diesel cycle: Induction (f-a); Combustion (f-a); Ignition (b-c-d-e); and Exhaust (e-f) (Mahon 1992).

3.1.1 Induction Stroke (a)

The induction stroke, also known as the intake stroke, starts when the piston is at Top Dead Centre (TDC, see Figure 3.1a) with the inlet valve closed and the outlet valve still open. At TDC, the piston recess and the remaining volume inside the cylinder are together defined as the clearance volume (V_c). As the piston moves down the inlet valve is open to allow air to be sucked inside the cylinder with the outlet valve closed to ensure no air escapes. When the piston reaches Bottom Dead Centre (BDC, see Figure 3.2a), the

cylinder has reached maximum capacity. The piston has swept through a specific volume of the cylinder capacity (V_s). Therefore at BDC the total volume is ($V_s + V_c$). The induction stroke corresponds to the f-a sequence on the realistic thermodynamic work cycle in Figure 3.2 (Right Panel).

3.1.2 Compression stroke (b)

In the compression stroke both the inlet and outlet valves are now closed. The piston moves upwards compressing the trapped air inside the cylinder until it reaches TDC. Hence, the compressed air is now contained inside the clearance volume (V_c). The air can heat up to 900°C during the compression phase because the compression is essentially adiabatic. The compression ratio (ϵ) is defined as:

$$\epsilon = 1 + \frac{V_s}{V_c}. \quad (3.1)$$

Typical compression ratios (ϵ) for diesel engines range from 6:1 in large-scale engines to 24:1 in automobiles. At a specific time before reaching TDC in the compression stroke the fuel is injected at high pressure into the hot, compressed air (see ignition stroke).

The compression stroke corresponds to the a-b sequence in Figure 3.2 (Right Panel). Theoretically, the compression stroke corresponds to the adiabatic compression of the working fluid during the A-B sequence in the Seilinger process of Figure 3.2 (Left Panel).

3.1.3 Ignition stroke (c)

This stroke is also known as a combustion stroke or a power stroke. There is lag between when the fuel is injected to when it is ignited. The ignition delay is timed so that the fuel is spontaneously ignited when the piston reaches TDC. It is at this moment is when the ignition stroke begins. During the first phase of combustion, the injection nozzle atomises the fuel at very

high pressure. The mass of fuel that is injected essentially determines how much energy is released during the combustion. The increase in pressure experienced inside the cylinder forces the piston downwards. The piston and the crankshaft are connected via the connecting rod, resulting in a torque at the crankshaft.

The ignition stroke corresponds to the b-c-d sequence on the realistic thermodynamic work cycle in Figure 3.2 (Right Panel). When the combustion is initiated, there is constant pressure and the volume increases (b-c). As the volume continues to increase, the pressure decreases (c-d).

Theoretically, this stroke corresponds to the B-C-D-E sequence in the Seilinger process in Figure 3.2 (Left Panel). The B-C sequence is an isochoric heat transfer whereby the working fluid rises in pressure, with an increase in heat but with no change in the gas volume. Next, there is an isobaric heat transfer (C-D), which is when the volume of the working fluid initially increases at a constant pressure. An isentropic expansion (D-E) sequence is then followed, i.e. an adiabatic expansion whereby the volume of the working fluid increases and the pressure drops.

3.1.4 Exhaust stroke (d)

Just before reaching BDC, the exhaust valve is opened allowing for the hot outflow of pressurised gas. The exhaust stroke corresponds to the d-e sequence on the realistic thermodynamic work cycle. Theoretically, when the exhaust valve opens the heat is dissipated at constant volume (E-A).

The piston then moves up disposing of any remaining exhaust gases (e-f), and the cycle begins again with the induction stroke. At the end of the exhaust stroke the crankshaft has completed two revolutions.

3.2 Mechanical Processes

A diesel engine has one or more cylinders. The diesel engine, also known as a compression-ignition engine, requires high temperatures in order to ignite the fuel.

This section will describe the mechanical system, the process of the fuel delivery system and how direct injection operates in a single-cylinder diesel engine.

3.2.1 Mechanical system

The main mechanical parts of a typical single-cylinder diesel engine include: cylinder, connecting rod (con-rod), piston, valves, flywheel, crankshaft, cams, camshaft, injection nozzle (fuel injector), fuel and barrel assembly (pump element) and governors. The cylinder houses the piston and the con-rod. The reciprocal movement of the piston aids in the rotation of the crankshaft via the con-rod, i.e. producing torque. A cam is an irregular-shaped disc, mounted on the crankshaft, which rotates at half the speed of the crankshaft. The cam's function upon rotation is to open and close valves, and to create the required reciprocal motion of the pump element.

3.2.2 Fuel Delivery System

To produce power in a diesel engine, a tiny amount of fuel is injected via a nozzle at the top end of the cylinder towards the end of compression. The pump element is composed of a plunger that is an exact fit inside a barrel. The amount of fuel injected is determined by the plunger. The cam determines the injection timing that activates the pump element for fuel injection.

The plunger has a helical channel (known as a 'helix') that is machined-cut into its surface. The position and shape of this helix determines the fuel quantity being pumped into the injection nozzle (see Figure 3.3). The ro-

tation of the plunger is controlled by the ‘geared control rack’, which varies the fuel quantity (see Figure 3.4). A variable-governor (or governor lever) mechanically controls the control rack. The plunger’s reciprocal motion is determined by a cam. The timing of the fuel injection is therefore a function of crankshaft rotation (or ‘crank angle’) and is measured in degrees. Modifying the fuel injection timing by a few degrees of crank angle is achieved by inserting or removing shims from underneath the plunger assembly. This will result in the advancing or retarding of the time of fuel injection.

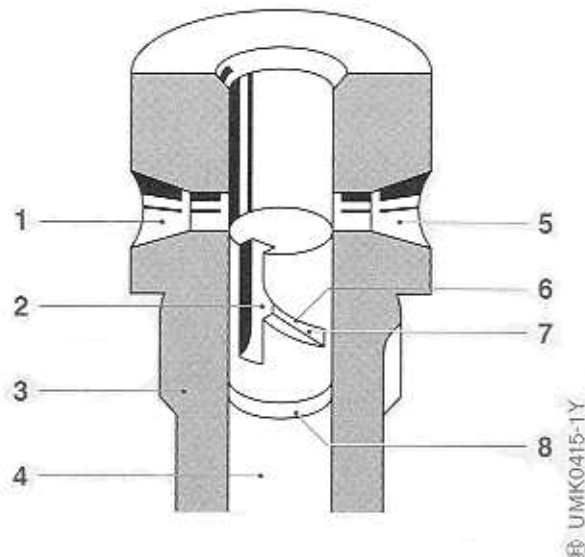


Figure 3.3: Pump Element

1. Inlet Passage 2. Vertical Groove 3. Pump Barrel 4. Pump Plunger 5. Control Port 6. Helix 7. Helical Channel 8. Ring groove for lubrication (Bosch GmbH 2005).

If the fuel quantity is increased, then there is more fuel to burn with the air. This increases the downward force on the piston and effectively increases torque. Engine speed is the rotational speed of the crankshaft and has units of revolutions per minute (rpm). Diesel engines normally operate with excess air because the air intake flow is not restricted.

The engine would “overrev” if there were no means of limiting its max-

imum speed. The Hatz 1B30 has a centrifugal governor, which utilises the force from flyweights (mounted to the crankshaft) to increase the tension in a coiled spring that is connected to the geared-control rack, i.e. limiting the amount of fuel being delivered.

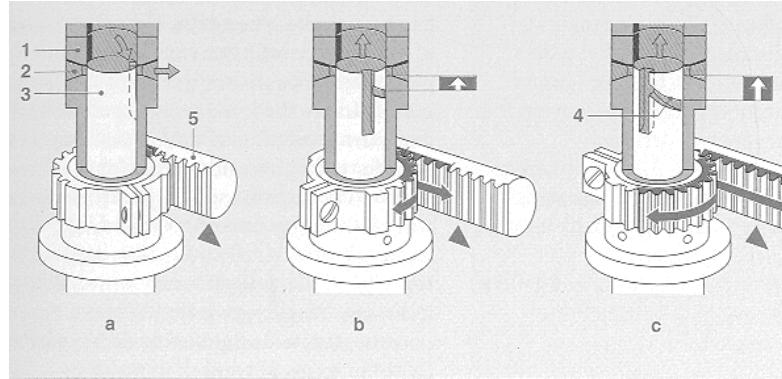


Figure 3.4: Geared Control Rack

a. Zero Delivery b. Partial Delivery c. Maximum Delivery 1. Pump Barrel 2. Inlet Passage 3. Pump Plunger 4. Helix 5. Geared Control Rack (Bosch GmbH 2005).

3.2.3 Direct Injection

The design of the combustion chamber is critical for diesel engine performance. A maximum amount of turbulence is desirable to thoroughly mix the high-pressure fuel into a volume of hot, compressed air in order to maximise combustion. Only a direct injection system will be described here as it is system used in the Hatz 1B30.

In a direct injection system, fuel is squirted at the top of the cylinder via multi-hole nozzle just before the piston fully compresses the air. The fuel, upon injection at very high pressure, is atomised and mixed in with the hot, compressed air. The piston top has a cavity (known as the piston recess) specifically designed to increase the turbulence of the air-fuel mixture to ensure complete combustion (See Figure 3.5). A glow plug (See Figure 3.5) may be used if the engine is too cold to start due to the air-fuel mixture

not reaching the required temperature to spontaneously ignite. However, the Hatz 1B30 does not use a glow plug but instead uses a resistive coil to heat the air before induction.

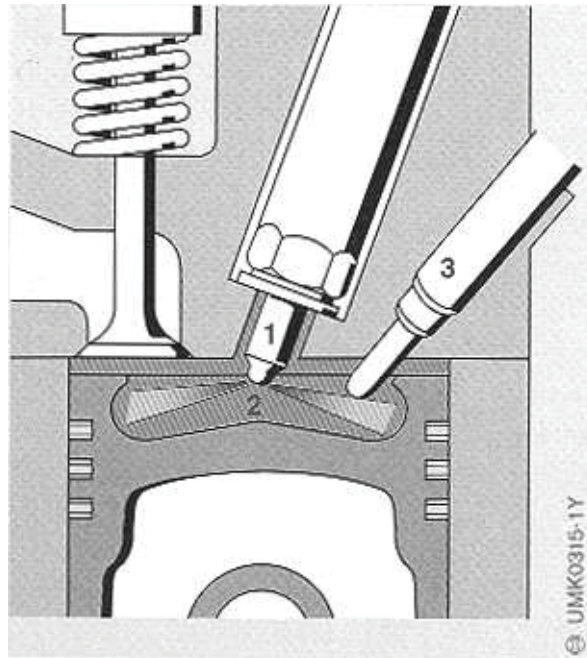


Figure 3.5: Direct Injection System

1. *Multi-hole Injector* 2. *Piston Recess* 3. *Glow Plug* (Bosch GmbH 2005).

3.3 Fuel

3.3.1 Fuel Properties

Understanding of the fuel's physical and chemical properties is essential to create the right conditions to operate an engine efficiently. Diesel engines are very versatile in their fuel use. The nominal and the most readily available fuel used is automotive diesel oil.

Automotive diesel oil can be mixed with additives in order improve fuel properties; for example, Special Antarctic Blend diesel (or SAB). Other types of diesel fuel are kerosene (or paraffin) based liquids such as jet fuels. These

fuel types are typically used for low-temperature operation. Theoretically, any hydrocarbon based fuel can be utilised in a diesel system including bio-diesel or other renewable fuels.

Diesel fuels are comprised of the heavier hydrocarbons that have 12 to 16 carbons per molecule. As a result, the evaporation temperature is much higher than that of petrol (with typically 5 to 8 carbons per molecule). The following sections discuss desirable diesel fuel properties.

Cetane Number

The cetane number (CN) describes the ignition quality of the diesel fuel. A higher number corresponds to a shorter ignition delay, or equivalently, a greater the tendency for the fuel to ignite. A lower number corresponds to a longer ignition delay. The CN of the fuel is a numbered between 0 and 100. A fuel which ignites readily, n-hexadecane (cetane), is assigned the cetane number of 100. A very slow igniting fuel, methyl naphthalene, is assigned the cetane number of 0. For a diesel engine, a fuel with a cetane number around 50 is most desirable in order to create the ideal ignition delay (Bosch GmbH 2005; Pulkrabek 2004). A cetane enhancer can be added to the fuel in order to decrease ignition delay.

Cetane Index

The cetane index is an approximation to the CN and is calculated on the basis of the fuel's density and distillation range. However, unlike the CN, the cetane index does not take into account the influence of cetane improvers on ignition quality (Bosch GmbH 2005; Pulkrabek 2004).

Flash point

The flash point is when the temperature at which the fuel vapour will ignite upon the application of a spark. This property does not affect the operation of the diesel engine. However, it is important for safety during transport and

storage of the diesel fuel as the ambient air temperature should be kept less than the flash point of the fuel.

Pour point

The pour point is the lowest fuel temperature at which the liquid can be poured with no waxy components (Batchelor *et al.* 1997).

Auto-ignition

The auto-ignition temperature is the temperature of the fuel when it spontaneously ignites.

Energy Density

The energy density is a measure of the energy content of the fuel. It is measured by how much energy can be extracted from one kilogram of fuel (i.e. joules per kilogram).

Viscosity

Too little viscosity increases leakage in the fuel-injection system, thus creating an overall decrease in engine performance. Too much viscosity results in high peak injection pressures and larger droplets being injected into the cylinder by the nozzle.

Sulphur

A high sulphur content could cause corrosion on the engine's exhaust systems, and sulphur-containing exhaust emissions can be harmful to the environment. In certain conditions, sulphur can burn to make sulphur dioxide and can react with water vapour to produce sulphurous acid. During the refinement process on the fuel, a hydrogenation process can be conducted at high pressure and temperature in order to reduce the amount of sulphur.

Water

A small quantity of water (up to 200mg/kg) absorbed by the diesel fuel will not impact highly on the combustion process. However, a small quantity of undissolved water can lead to major damage to fuel injection systems and corrosion on cylinder walls in just a few days of continuous operation.

Diesel additives

Additives are mixed with the diesel fuel in order to, amongst other things, reduce engine wear. Carbon residue can build up on the injection nozzle, which hinders the fuel injection process. Carbon-deposit, or ‘coking’, is influenced mainly by the components that diesel fuel has at the final boiling point.

The concentration of additives is usually kept to less than 0.1% in order to retain the physical properties of the fuel, such as density, viscosity and boiling points. Diesel additives include:

- Detergents that clean the system, especially to prevent coking on the injection nozzle.
- Flow improvers to enhance reliability of the fuel at low temperatures.
- Wax anti-setting agents to improve reliability and storage of the fuel at low temperatures.
- Lubricity enhancers to reduce fuel-injector wear.
- Anti-foaming additives to ensure no foam build-up during refueling.
- Anticorrosive additives (or corrosion inhibitors) to prevent surface deposit on metal parts caused by water.

In addition, the stoichiometric ratio (or ‘Stoich’) is also important, as it is the chemical ratio of air-mass to fuel-mass at the time of combustion. If

the air-fuel ratio is greater than Stoich, then there is more air than necessary to fully oxidise the fuel for complete combustion; the engine is said to be running ‘lean’. If the air-fuel ratio is less than Stoich, then there is too much fuel to have complete combustion; the engine is said to be running ‘rich’. In order to achieve a high efficiency, diesel engines operating at constant speed typically have a lean mixture that reduces the fuel being used. Operating with a rich mixture is used when the engine is accelerating or to achieve a cold-start because it will enable a better ignition (Pullkrabek 2004).

3.3.2 Jet Fuel use in Diesel Engines

There are many types of jet fuels available, with many developments over time for specific operational requirements (Maurice *et al.* 2001). The most common type of jet fuel is Jet A-1 (with its US counterpart Jet A and military counterpart JP-8), which is a kerosene grade that contains a complex mixture of higher-order hydrocarbons. Jet A-1 (and Jet A) is widely used for commercial aircraft with turbine engines, whilst JP-8 is used for military aircraft. In terms of physical properties, Jet A-1 and JP-8 are different from Jet A just in their pour points; that of Jet A is higher by about 7°C. Jet A, Jet A-1, and JP-8 have very similar chemical compositions; however, it does not necessarily mean that they will behave the same in any given situation. Furthermore, specific jet fuel properties will also vary from source to source (Colket *et al.* 2007). Table 3.1 present typical values of the basic properties of Jet A-1, automotive diesel and SAB. There is no specified value for the cetane index of Jet A-1, but it is assumed to be similar to that of JP-8.

As mentioned before, the Cetane Index (or Cetane Number) is an important fuel property for diesel engines. For example, diesel oil usually has a Cetane Index of about 55 and it corresponds to a shorter ignition delay than Jet A-1 (or JP-8). Thus, changing an engine’s designated fuel will affect the combustion pressures experienced inside the cylinder (Pullkrabek 2004). This

Fuel	Density @ 15°C (kg/L)	Energy density (MJ/kg)	Cetane Index (-)	Max. Viscosity @ 40°C (mm ² /sec)	Pour Point (°C)	Flash point (°C)	Auto- ignition point (°C)
Jet A-1	0.81	42.8 (min)	47*	2.0	< -47	> 38.0	280
Diesel	0.85 (max)	45.6	55	6.0	< -35	> 60.0	240
SAB Diesel	0.82	46.4	51	7.0	< -35	> 61.5	240

Table 3.1: Fuel properties of Jet A-1, Automotive Diesel and Special Antarctic Blend (SAB)

**Cetane Index (CI) quoted for Jet A-1 is actually the CI for JP-8 (Papagiannakis et al. 2006; BP Australia 2008; 2006; Shell 2005; BP Australia MSDS 2008).*

then necessitates research into the optimum fuel injection timing to allow for the slower burning of jet fuel (Kouremenos *et al.* 1997; Papagiannakis *et al.* 2006; Assanis *et al.* 2007).

As Jet A-1 is primarily used for turbine engines, it must be combined with additives in order to be compatible with diesel engines. NATO, for example, made a decision to switch to JP-8 (or NATO code: F-34) as the single fuel to be used for all of their land and air military transports; this is known as the Single Fuel Concept (SFC, Kouremenos *et al.* (1997)). JP-8 is simply Jet A-1 blended with three specific additives (Batchelor *et al.* 1997):

1. An icing inhibitor is added to prevent the growth of ice crystals that are derived from minute concentrations of water.
2. A corrosion inhibitor is added to reduce degrading of pipelines and storage tanks, and as a bonus, this additive also increases the lubricity of the fuel, removes the sulphur content, and reduces aromatics.
3. A conductivity additive is used to reduce the build up of static electric charge in order to avoid sparks upon refueling vessels.

3.4 Diesel Engines in Antarctica

In Antarctica there is a long tradition of using large turbocharged diesels for both power generation and for vehicles. At regions of high altitude the air density substantially reduces. The reduction of air intake into the cylinder of a diesel engine can lead to a decrease in power output. Turbocharging is sometimes used to provide some altitude compensation.

The Amundsen-Scott South Pole station is powered by a set of turbocharged diesel generators, with similar systems being used at the coastal Antarctic stations such as Casey, Davis, and Mawson. These stations typically have six-cylinder Caterpillar 3306 diesel engines that drive 125 kVA alternators. The fuel these stations use is mainly SAB and was chosen primarily for its cold temperature characteristics (Steel & Guichard 1993; Steel 1993).

For its low temperature characteristics, Jet A-1 was chosen as the primary fuel used for a bank of six diesel engines for the winter operation of the Italian Antarctic coastal station at Terra Nova Bay (Meloni *et al.* 1992).

The high cost (typically \$4 - \$10/kg) of transporting fuel to and across Antarctica implies that the optimum strategy for inland stations is to use a fuel of the highest possible energy density. Similarly, the environmental issues associated with transport logistics tend to outweigh the environmental effects of burning the fuel itself. This gave options for the PLATO observatory of using either SAB or jet fuel, which are the highest energy-density fuels readily available. The Chinese Expedition team uses Jet A-1 to power their tractors to Dome A. Jet fuel is cleaner burning and has a significantly lower pour point (see section 3.3.1) than even SAB.

3.5 Hatz 1B30 for PLATO

3.5.1 Hatz 1B30

The diesel engine selected was a Hatz 1B30: a commercially available single-cylinder, naturally aspirated four-stroke engine with a cylinder-capacity of 347ml (see Figure 3.6). It is a direct-injection, air-cooled engine with a cylinder-bore diameter of 80mm and stroke of 69mm, and has a compression ratio of $\epsilon = 21.5$. The Hatz engine utilises a single cam that controls both valves and the fuel injection timing. The nozzle injects fuel at a pressure of 400 bar. The normal speed range of operation is between 1500 and 3600rpm. The Hatz 1B30 engine was chosen for its low exhaust emission, compact design and ease of modification of fuel and oil systems.

At 2200rpm the Hatz 1B30 engine can produce up to 4kW of electrical power at sea level. It was then expected that the electrical power output would be reduced to about 2kW for the altitude at Dome A, because the air pressure is approximately half atmospheric. Therefore, for powering PLATO, turbocharging would be unnecessary because the goal was to produce power between 1-2kW. In addition, having no turbocharger made installation and maintenance of the Hatz 1B30 simpler.

3.5.2 Fuel Selection

Jet A-1 was chosen to be the primary fuel for the Hatz 1B30 to power PLATO because of its low-temperature characteristics and for its availability from the Chinese Expedition team. The Hatz 1B30 is specified for use with Jet A-1 and does not require a cetane enhancer. The fuel was mixed with $\sim 2\%$ fully synthetic “Racing 2T” 2-stroke oil to provide lubrication for the fuel pump and the injection system.

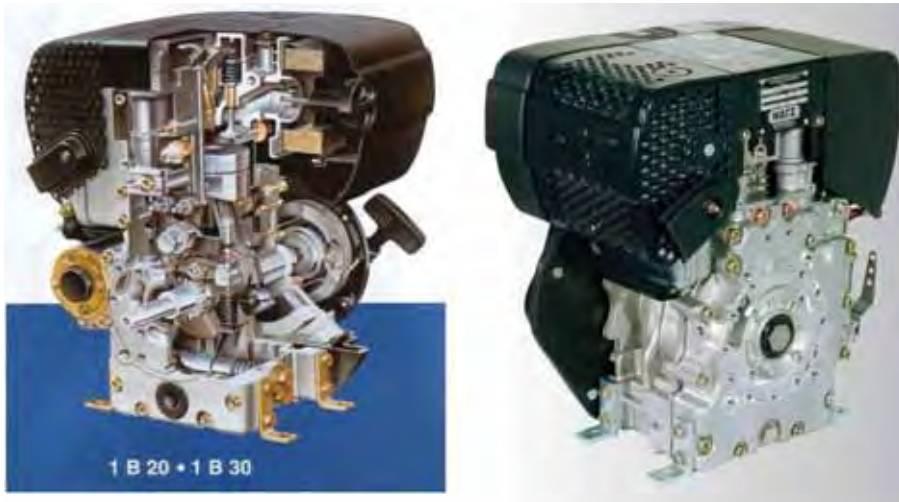


Figure 3.6: Hatz 1B30 Single-Cylinder Diesel Engine

The left image is a cutaway artist impression of the Hatz 1B30 diesel engine. The right image shows the Hatz 1B30 without the starter motor. (Courtesy of Hatz Australia).

3.5.3 High-altitude Testing

For engine testing (see Chapter 4), the Hatz engine was loaded with a three-phase brushless bearing-less alternator made by eCycle. The alternator was directly coupled to engine's crankshaft. To the author's knowledge, there are no published experiments on a single-cylinder diesel engine running on jet fuel operating in a low pressure environment.

Chapter 4

Engine Test Rig

“The formulation of a problem is often more essential than its solution, which may be merely of mathematical or experimental skill.”

- Albert Einstein, Theoretical Physicist, Philosopher and Author
(1879-1955)

Testing at high-altitude conditions of the Hatz 1B30 engine was conducted in order to determine the efficiency and reliability of the PLATO generation system operating on the Antarctic plateau. As the Hatz 1B30 is a naturally aspirated engine, the surrounding air pressure needed to be reduced in order to effectively test the engine at simulated high-altitude conditions. A system was therefore constructed consisting of a chamber, Roots blower and a butterfly valve. The Hatz 1B30 was then placed inside the chamber and several tests were conducted on the engine at various pressures. All engine tests presented in this chapter used PLATO’s designated fuel of Jet A-1 mixed in with $\sim 2\%$ “Racing 2T” 2-stroke oil.

4.1 Mechanical Arrangement

Environmental Chamber

To simulate the low atmospheric pressure of Dome A in the laboratory, an environmental chamber was constructed that was able to maintain a constant pressure down to half an atmosphere with the engine running at full power. The chamber consisted of a base plate and a bell-jar made from mild steel. The base plate was a circular disk, 30mm thick, with an outer diameter of 1100mm. The bell-jar had a wall thickness of 5mm, with a welded dome-shaped top and a welded bottom flange. Two lifting hooks were welded on either side of the bell-jar to accommodate a crane. The bell-jar was placed over the base plate and was sealed via an O-ring (see Figure 4.1). An 8 cubic metre/minute Longtech LTV-100 Roots blower, driven by a Teco CNS-C4088 15kW 3-phase electric motor, extracted air from the chamber and vented it outside the building. The flow rate was chosen to be an order of magnitude greater than the rate at which the engine consumes air, so that the engine exhaust was well diluted before reaching the Roots blower. Air was continuously introduced into the chamber via an air-filter box and butterfly valve. The butterfly valve was manually adjusted to set the desired pressure within the chamber.

Engine Mounting System

The engine was attached via rubber isolation dampeners to the base plate of the chamber (see Figure 4.2). The eCycle alternator was directly attached to the engine crankshaft, and the three-phase electrical output coupled via a diode bridge to a pair of resistor load banks. The engine breathed the reduced pressure air from inside the chamber, while the exhaust exited via a diffuser that allowed the exhaust gases to be well mixed with the main airflow before it reaches the Roots blower.

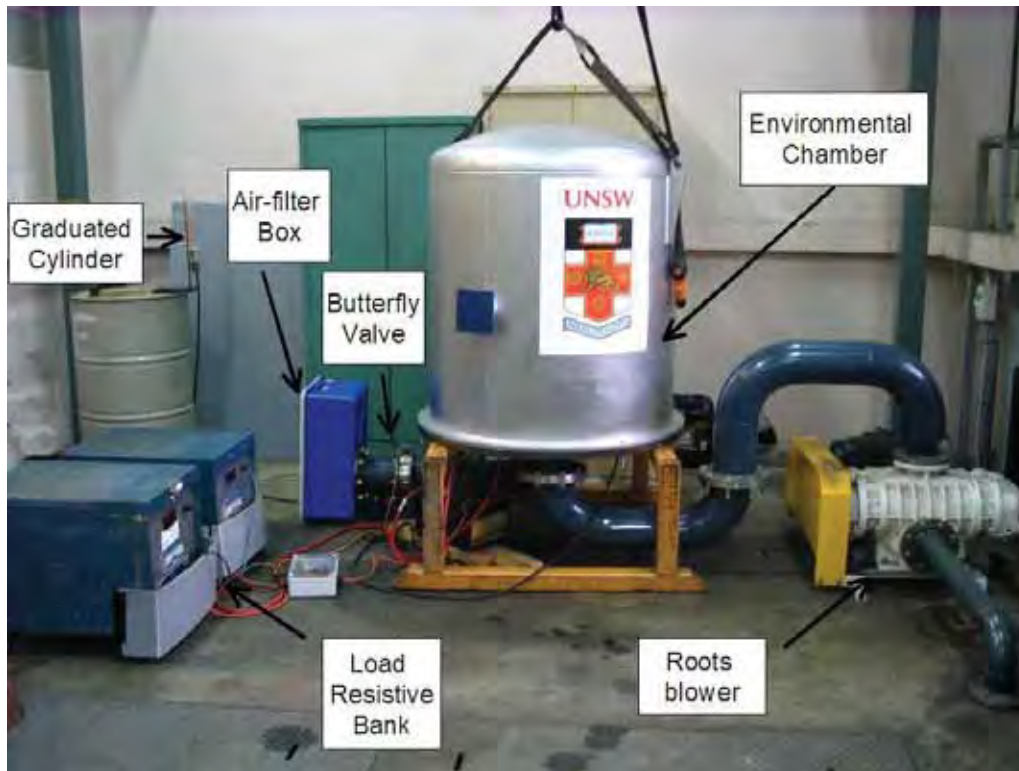


Figure 4.1: Engine Test Rig

The air flows through the air-filter box to the environmental chamber. The rate of airflow is controlled by the butterfly valve. The Roots blower runs at constant speed, pumping air from the environmental chamber.

Engine Control

To control the speed of the engine, a motor-driven lead screw was attached to the engine's governor lever. The actuator was mounted on the engine plate and was electrically controlled via a switch that was external to the chamber.

The engine was started by the key-start mechanism; however, the starter system was modified so that the key was able to be turned from outside the chamber.

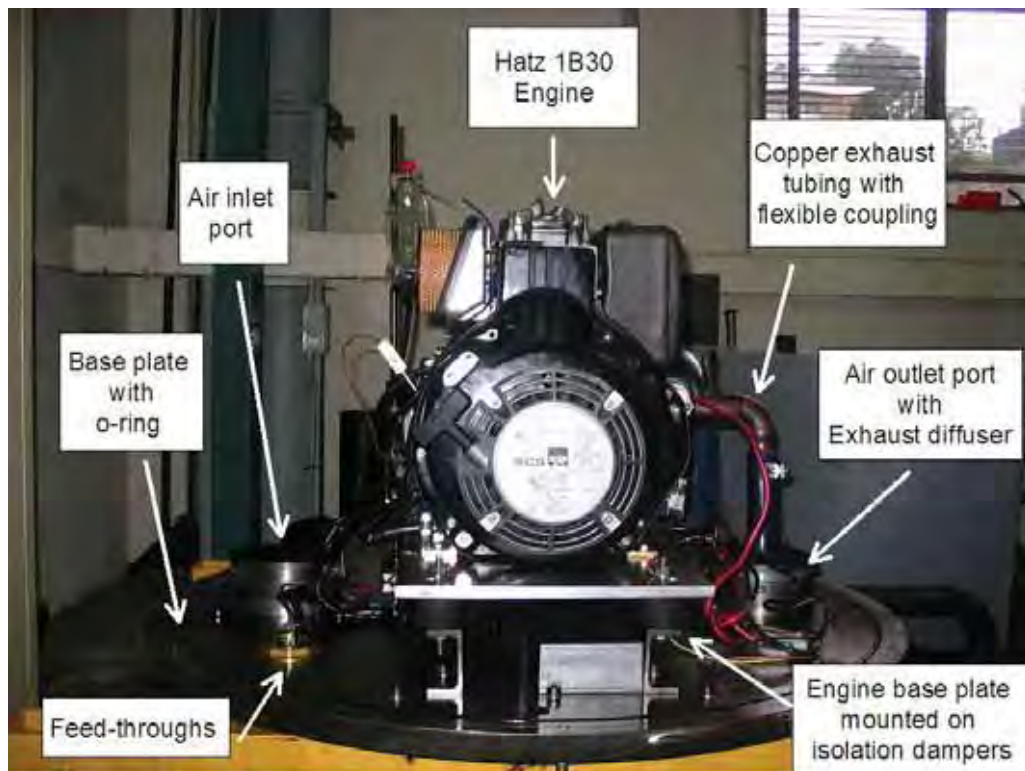


Figure 4.2: Engine Base Plate
Engine mounted on base-plate of the environmental chamber with peripherals.

Fuel System

Fuel consumption was measured using an externally mounted graduated cylinder, which delivered fuel via a fuel line that led through the base plate to the engine. By having the fuel-feed system mounted externally to the pressure chamber, less vibration was coupled to the graduated cylinder, which allowed a more accurate reading of the fuel level and constant operation without the need to remove the bell jar was possible.

4.2 Data Acquisition

To monitor the engine parameters, several sensors were placed on and around the engine. These sensors fed into a desktop PC that operated Windows XP. K-type thermocouples measured the temperatures of the ambient air, oil sump, cylinder head, exhaust gas, alternator and the intake air. Two Motorola MPX4115AP pressure sensors that have a maximum pressure rating of 400kPa and an operating temperature between -40°C and 125°C were placed inside the chamber. The alternator voltage and current through the resistor load bank were also monitored. Readings from the thermocouples, pressure sensors, and the load bank were all monitored via signal receiver modules (15 Ch Digital I/O Module: ADAM-4050) connected by an Ethernet cable to the Desktop PC via a serial device server (Moxa NPort 5410). The engine speed was also monitored by a tachometer and was directly connected to the serial device server.

All signals received from sensors were interpreted by the software package: LabVIEW. Data was displayed on the computer monitor in real time and also saved to an output file. Matlab and Microsoft Excel were used for the data analysis and plotting.

Test Run Procedure

The procedure for acquiring data for each test run was as follows:

1. Set the desired load on the resistive bank.
2. Turn on Roots Blower.
3. Set the desired pressure by adjusting the butterfly valve.
4. Measure the initial fuel level.
5. Start engine and set the desired speed via the external switch for the actuator.

6. Monitor and record the safety conditions and engine parameters for the duration of the test run.
7. Turn off engine.
8. Measure the final fuel level.

4.3 Initial Test Results

The engine managed to successfully start and stop at a variety of simulated altitudes, up to more than 5000m. The ambient air temperature was typically $\sim 25^{\circ}\text{C}$.

An initial test was conducted in order to see what to expect during a typical test run. This particular engine test run was conducted at a simulated pressure altitude of $\sim 5000\text{m}$ and at a speed of 2200rpm. The engine run-time was 390 seconds (5.5 minutes). The corresponding data set for this engine test run is presented in plots of Figure 4.3.

The ambient temperature (see Figure 4.3a) inside the chamber was observed to increase by about 10°C during the operation of the engine. This increase in intake air temperature resulted in a small loss of power from the engine as the run progressed, this was reflected by the slight decrease in generated voltage and current (see Figure 4.3b). The exhaust gas temperature (see Figure 4.3c) was monitored to indirectly gauge how efficiently the engine was running and also to see if the engine was overheating. The pressure was measured inside the chamber to ensure that the engine was operating at the desired simulated altitude; see Figure 4.3d for an example of a pressure altitude of $\sim 5000\text{m}$. The speed, measured in rpm, was monitored to ensure that the engine was running at the same speed throughout the course of a test; see Figure 4.3e for an engine speed being kept steady at 2200rpm. The temperatures of the cylinder head, the generator and the oil sump (see Figure 4.3f) were also monitored so that the observer could initiate an immediate

shutdown of the engine and the Roots blower in the event of a problem.

For an engine test run to operate for more than 10 minutes, it would appear to slightly overheat the chamber. Therefore, this would change the initial conditions for which the engine would start and stop for the next test run. As a result, short duration tests were needed in order for the chamber to cool down in preparation for the next test run.

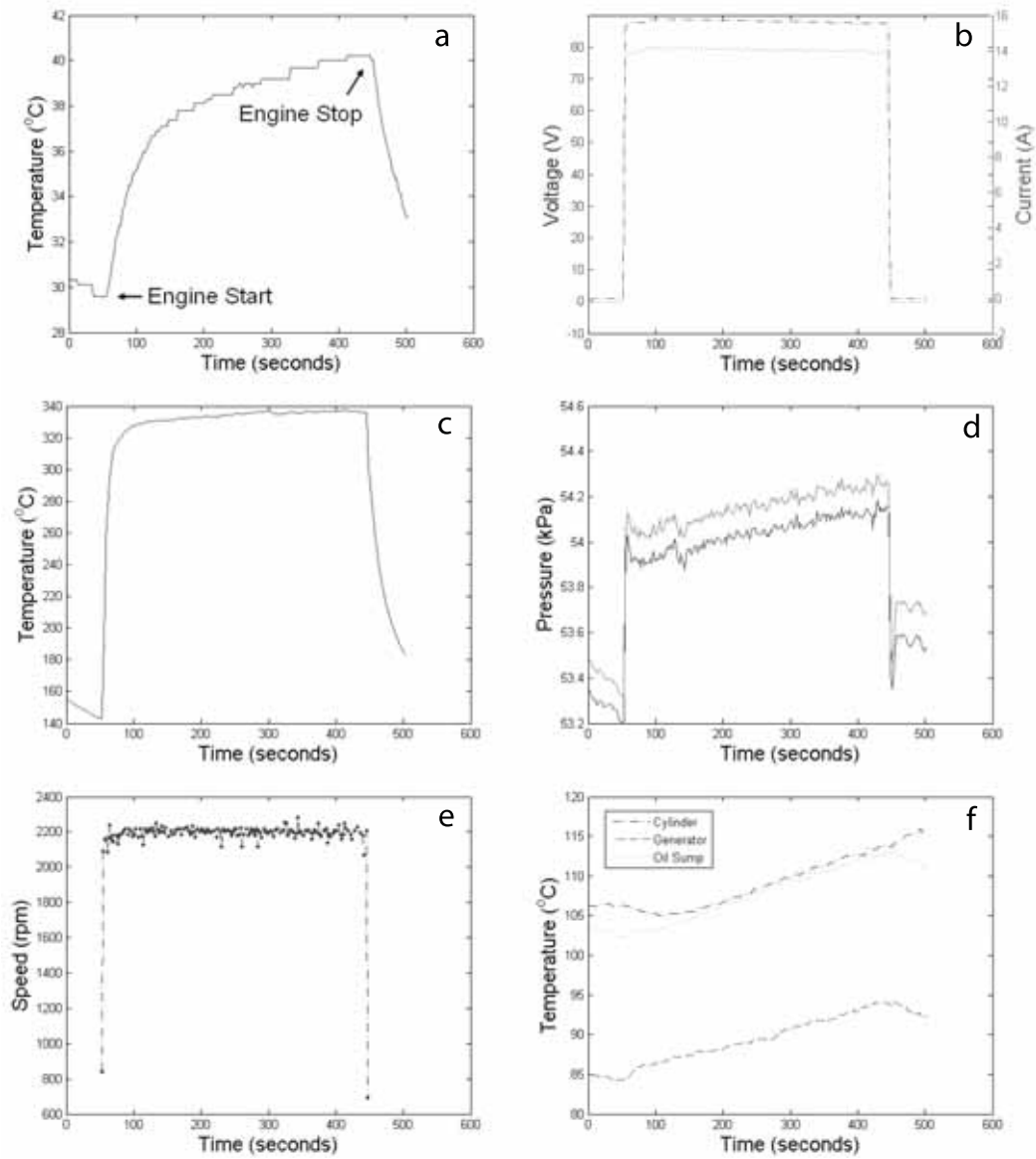


Figure 4.3: Engine Test Measurements

All data presented were measured as a function of time (seconds). (a) Ambient temperature inside the chamber. (b) Voltage (bottom dotted line) and current (top dotted line) for the resistor load bank. (c) The engine's exhaust gas temperature. (d) The two pressure sensors indicated an average pressure of ~ 54.1 kPa. (e) Engine speed indicating the stability of the engine governor. (f) The cylinder head, alternator and oil sump temperatures.

4.4 Engine Test Results

The following results and subsequent discussion have been presented in the published paper Hengst *et al.* (2009).

4.4.1 Test Conditions

To avoid possible overheating of the engine within the chamber, each test was allowed to go for no more than ten minutes. These tests were conducted at a fuel injection timing of 18° crank angle before top dead centre (CA BTDC). Tests were made under otherwise identical conditions at both sea-level atmospheric pressure (1000hPa) and at a pressure of about 540hPa (hereinafter described as “at altitude”). The corresponding pressure altitude is 5000m, which is well above that of Dome A. The engine speed was set at discrete intervals from 1600 to 3200rpm. At each setting, the following parameters were recorded:

- Fuel consumed
- Load-bank voltage and current
- Exhaust gas temperature

Another set of tests was conducted at altitude with the injection timing set to 13° CA BTDC. These tests were conducted at a fixed engine speed of 2200rpm.

Engine Map Data and Efficiency

Comparisons between the results of sea level and at-altitude conditions for the Hatz 1B30 were made; in particular comparing conditions of engine speed, load and pressure. This was achieved by comparing engine measurements of exhaust gas temperature for a given power output and by determining the overall efficiency.

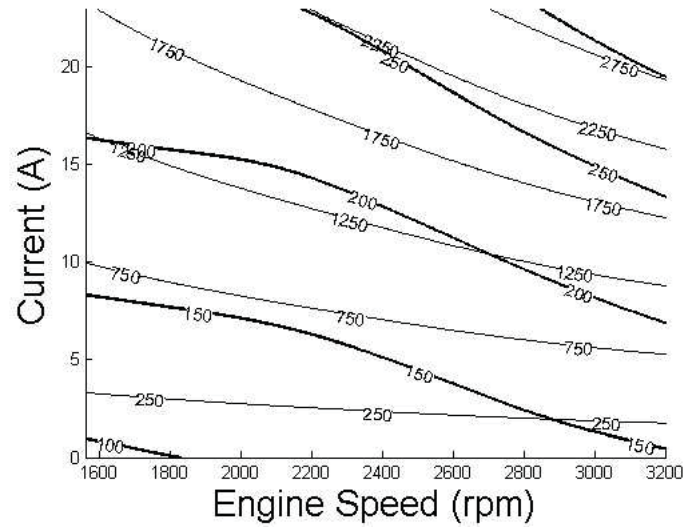


Figure 4.4: Sea Level Map

Figure showing the exhaust gas temperature ($^{\circ}\text{C}$, thick line) and power output (W, thin line) as a function of current and engine speed.

Two maps of data points corresponding to sea level and at altitude were constructed. An individual map required discrete data as a function of speed and load: a series of 10 different speeds ranging from 1600-3200rpm were selected and tested for a variety of loads between 0-25A. At a particular (engine and load) parameter, the exhaust gas temperature and the total power measurements were used to construct the map. This resulted in an approximately 10x10 grid of data points that was later smoothed to yield contours. Map data points were smoothed because of the expected scatter of the variables. It was challenging to obtain data points for high rpm and load for discrete tests at altitude due to the engine overheating, with exhaust temperatures reaching as high as $\sim 600^{\circ}\text{C}$. See Appendix B for raw results of engine parameters that were derived from the analysis of the output file produced in LabVIEW as a function of engine speed.

Figures 4.4 and 4.5 are the resulting smoothed engine contour maps at sea level and at altitude respectively. Each contour map shows exhaust gas temperature and the total power as a function of current and engine speed. The

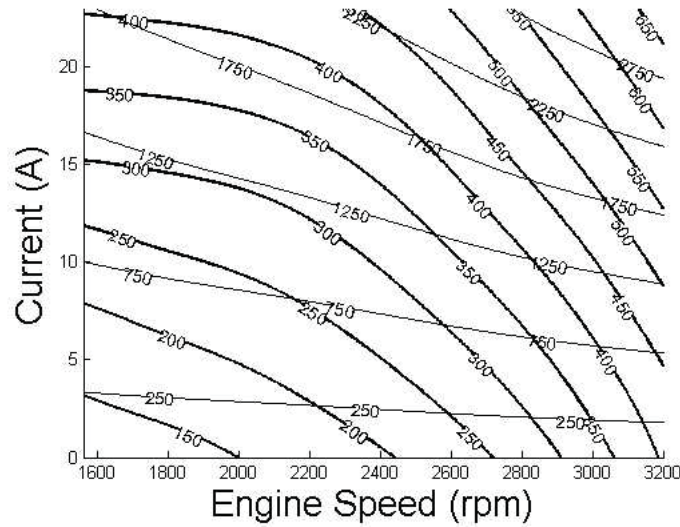


Figure 4.5: Altitude Map

Figure showing the exhaust gas temperature ($^{\circ}\text{C}$, thick line) and power output (W , thin line) as a function of current and engine speed.

current is directly proportional to the torque developed by the engine. The engine maps of Figure 4.4 and 4.5 show a greatly increased exhaust temperature at altitude for the same power output. This is to be expected because for a given power output and rpm, a specific amount of thermodynamic work has to be performed in each cycle. At altitude, only 54% of the mass of air is present in the cylinder compared to sea level, so this air must undergo a greater temperature excursion to perform the same work. In addition, the amount of air available for cooling is also reduced by nearly 50%.

The engine's efficiency was determined by calculating the brake specific fuel consumption (BSFC) measured in units g/kWh . The power that is recorded is the electrical output power from the alternator, and thus includes the alternator and rectifier losses. The stated manufacturer's alternator efficiency is 90% and the density of Jet A-1 is about 0.81g/ml . The BSFCs presented here are therefore an overall fuel-to-electricity efficiency. At an engine speed of 2200rpm, the engine efficiency changes remarkably little between sea level and at altitude (see Figure 4.6). However, as the engine speed

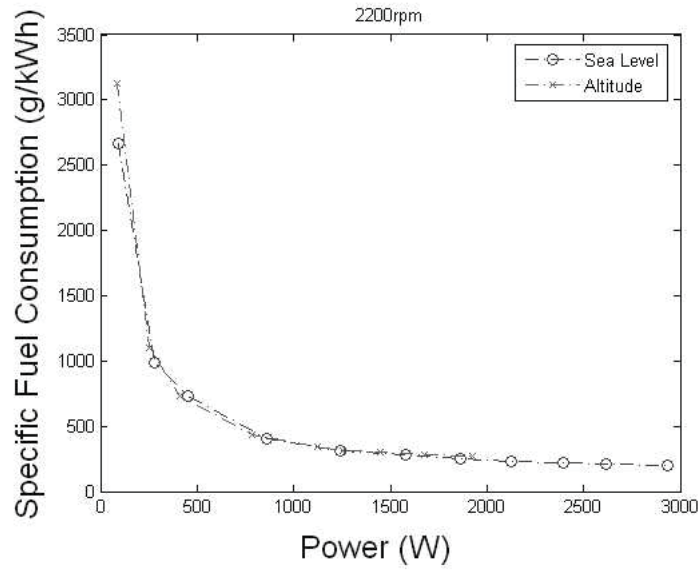


Figure 4.6: Fuel Consumption at 2200rpm

Brake specific fuel consumption (g/kWh) as a function of power at a fixed engine speed of 2200rpm.

is increased above 2600rpm the engine becomes progressively less efficient at altitude than it is at sea level (see Figure 4.7). At the preferred engine speed of 2200rpm and a power output of 1500W, the engine's BSFC at altitude was measured to be $\sim 280\text{g/kWh}$. For a power output of 800W (typical power usage for PLATO), the engine's BSFC at altitude was measured to be $\sim 450\text{g/kWh}$.

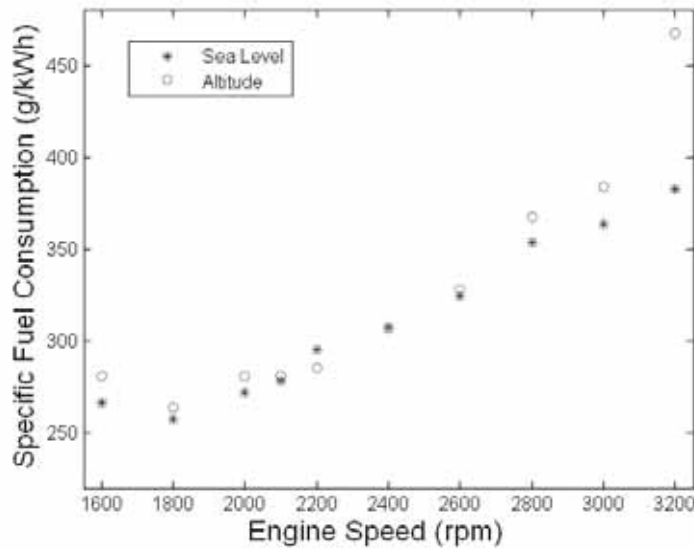


Figure 4.7: Fuel Consumption

Brake specific fuel consumption (g/kWh) for a fixed power output of 1500W as a function of engine speed.

Injection Timing

Tests involving the changing of the injection timing were carried out in order to observe if delaying the fuel injection had any affect on the overall engine performance.

In Figures 4.8 and 4.9 we present the results of tests at an injection timing of 18° CA BTDC (“Test A”), 13° CA BTDC, then again at 18° CA BTDC (“Test B”), the engine speed was fixed at 2200rpm. From Figure 4.8 it is clear that at 2200rpm the injection timing has little effect on the fuel consumption; however, as seen in Figure 4.9 the engine runs hotter at 13° CA BTDC than at 18° CA BTDC both at sea level and at altitude. At altitude, the exhaust gas temperature can be as much as 65°C hotter with the less advanced timing.

This increase in exhaust temperature was due to a slower combustion because of the reduced air density. Heat that is liberated towards the end of

the ignition stroke does no useful work and only serves to heat up the exhaust valve and pipe (Ricardo & Hempson 1968). Nevertheless, it is surprising that the injection timing has such a profound effect on the exhaust temperature, while having little or no effect on the fuel consumption.

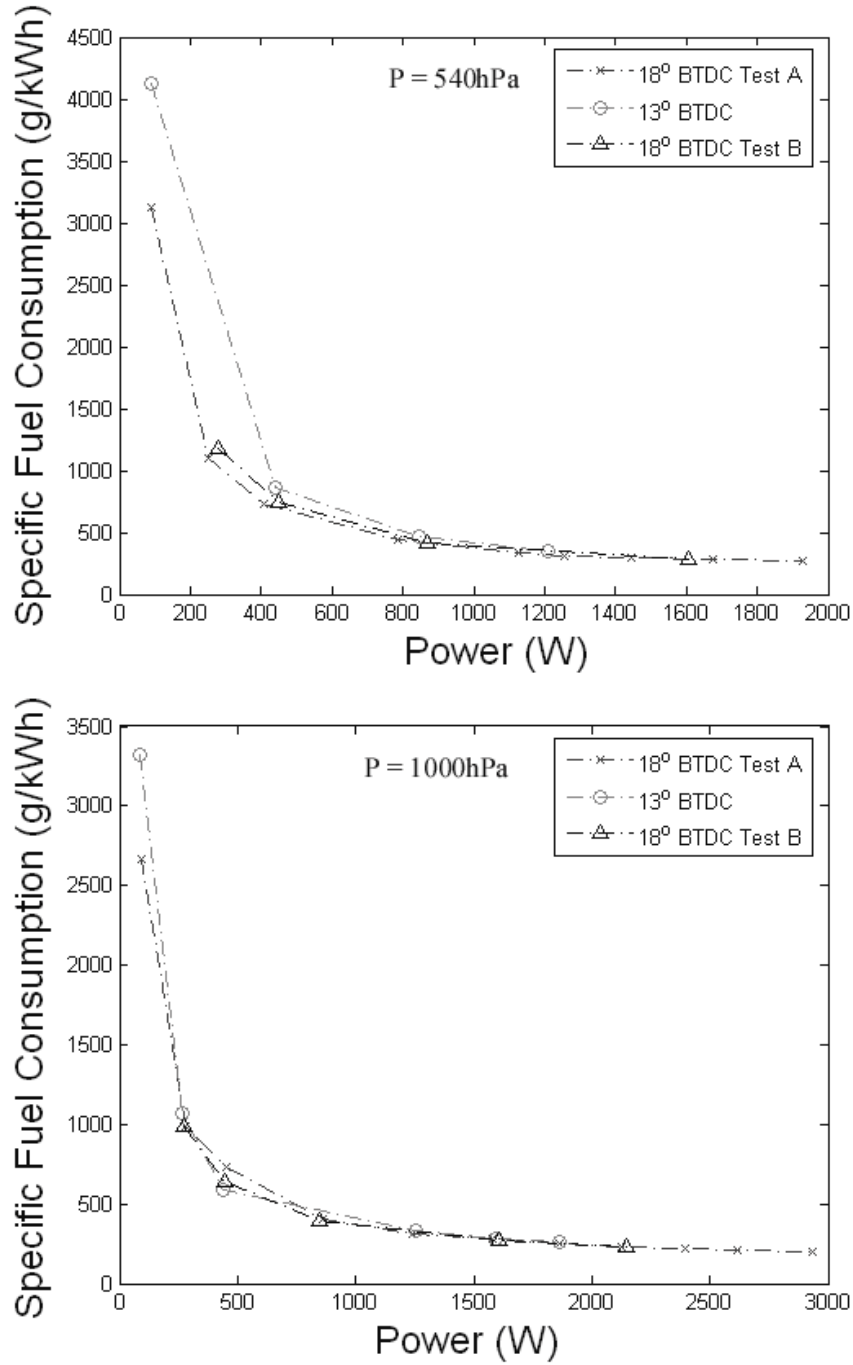


Figure 4.8: Fuel Consumption at different pressures
Brake specific fuel consumption at altitude (top panel) and at sea level (bottom panel) at fuel injection timings of 13° and 18° CA BTDC.

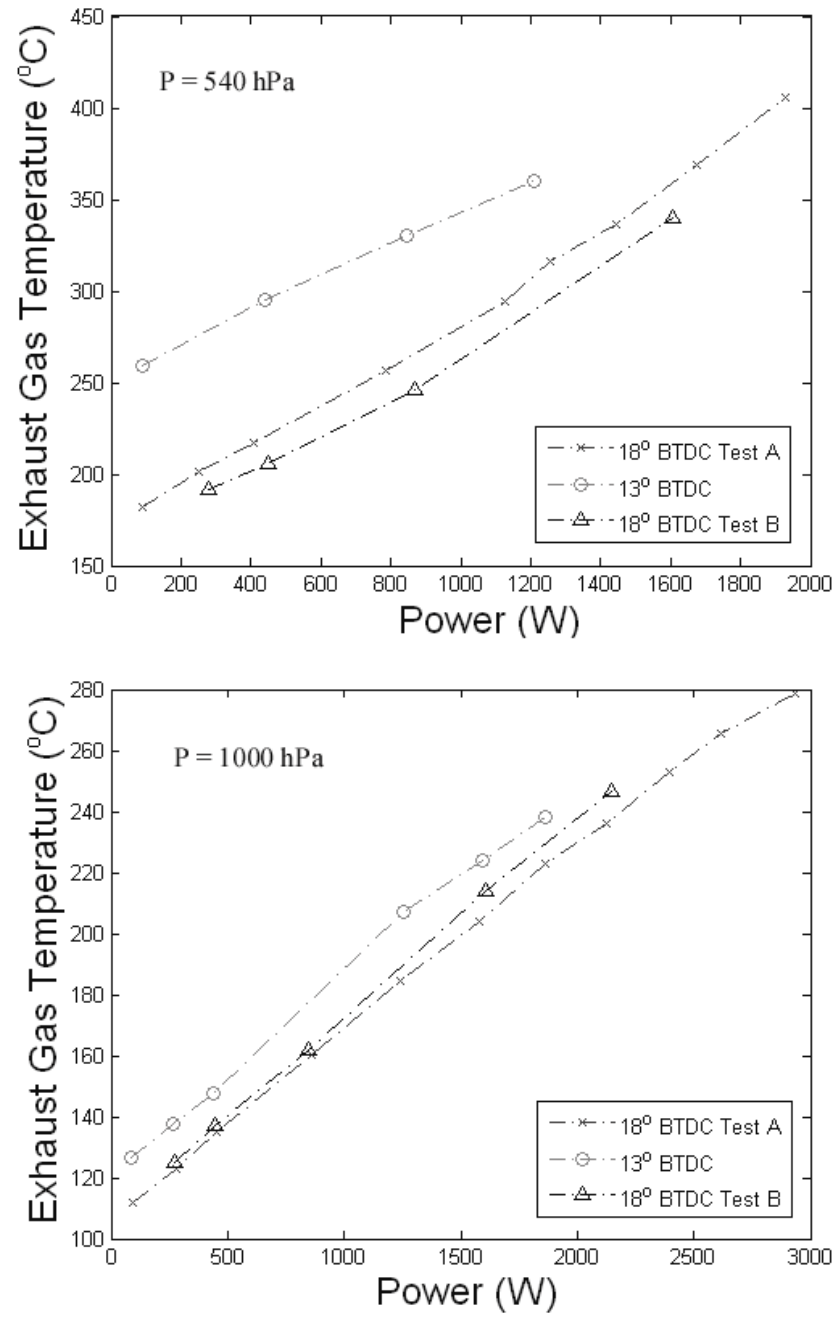


Figure 4.9: Exhaust Gas Temperatures at different pressures
Exhaust gas temperature at altitude (top panel) and at sea level (bottom panel) at fuel injection timings of 13° and 18° CA BTDC.

4.5 Implementation for PLATO

The conclusions drawn from these experiments influenced the decision making on the implementation of the PLATO engines for operation at Dome A. The Antarctic astronomy group decided to install six Hatz 1B30 engines into the engine module with only a few modifications.

The design speed of operation for the Hatz engine is between 1500 and 3600rpm. At 3600rpm the engine can produce 5000W at sea level. In order to minimise fuel consumption and maximise the longevity of the engines for PLATO, they were fixed to operate at 2200rpm. At this lower speed, and allowing for the lower atmospheric pressure at Dome A, we expect a maximum power output of $\sim 2\text{kW}$. In practice, the engine is run at lower power levels, partly to ensure complete combustion and partly to reduce pollution to an absolute minimum.

The injection time was set to 18° BTDC, as this timing appeared to reduce the exhaust gas temperatures under experimental conditions but with little change to the engine efficiency.

An oil was selected to prolong the nominal 200hr maintenance of changing the oil. The crankcase oil selected was Mobil 1 Delvac 5W-40, chosen for its low pour point of -45°C and for its recommended use in high performance applications of heavy-duty diesel engines.

For maintaining the ambient air temperature inside the engine module, the standard engine cooling fan was retained of each unit and the warm air passing over the cylinder head was allowed to circulate within the engine module. The overall internal temperature of the engine module is regulated by a separate thermal management system (Luong-Van *et al.* 2008).

Additional tests were also carried out on the engine for cold starting conditions. An ultracapacitor starting bank has been shown to provide ample cranking current at temperatures as low as -40°C . Both the engine and the starting bank survived temperature cycling to -90°C with no discernable ill

effect (Hengst *et al.* 2009).

4.5.1 Field Results

The Polar Research Institute of China and the Chinese Academy of Science deployed PLATO to Dome A, Antarctica in January 2008.

The Hatz engine has shown that it can operate efficiently in both simulated and in-situ high-altitude conditions. Figures 4.10-4.11 show performance plots for PLATO at Dome A over the course of a year. The constant monitoring of engine parameters enabled us to record possible points of failure in order to solve and to prevent issues arising again. Current PLATO data can be found at: <http://mcba11.phys.unsw.edu.au/~plato/>; the website is the work of Daniel Luong-Van and Prof. Michael Ashley. In PLATO's inaugural run during 2008, a large number unexpected engine stoppages occurred. This was attributed to air being trapped in the fuel lines. A re-design of the system undertaken during the 2009 servicing mission reduced the number of engine stoppages (Lawrence *et al.* 2009).

Figure 4.10 shows the generator voltage from all six engines. The alternators are designed so that they produce 120V AC for an engine speed of 2200rpm. This electrical power is then converted to a 28V DC (nominal) bus that charges the 320 A h SLA battery bank.

Figure 4.11 shows the DC/DC output from each engine bank. Continuous periods of high DC output indicates intense engine operation when the Sun was below the horizon. Hence, the dip in DC output during the summer months corresponds to when engine power was reduced to conserved fuel consumption. With a peak DC output of about 30A, the rectified 28V DC yielded a total electrical power of about 800W.

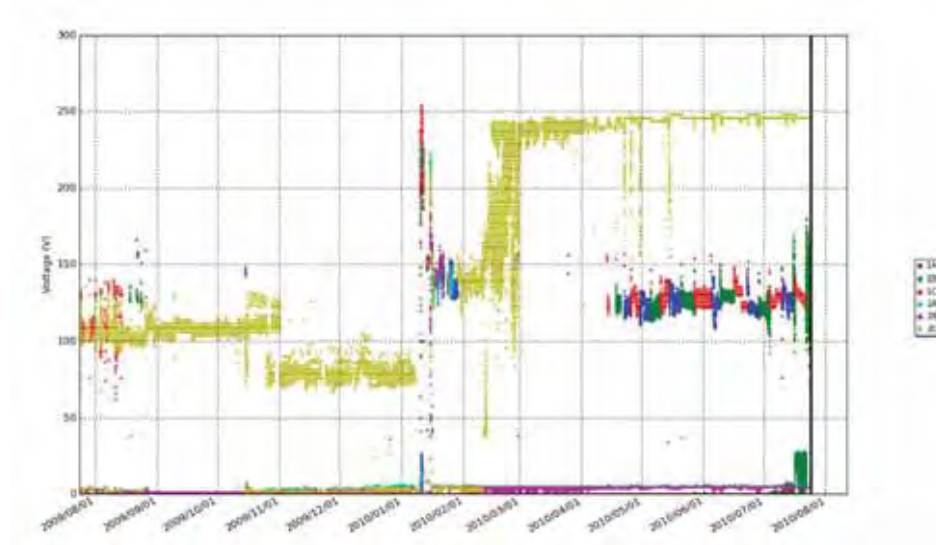


Figure 4.10: Generator Voltage

Generator Voltage for PLATO measured at Dome A from August 2009 to August 2010 (Data Credit: CCAA, PRIC, UNSW).

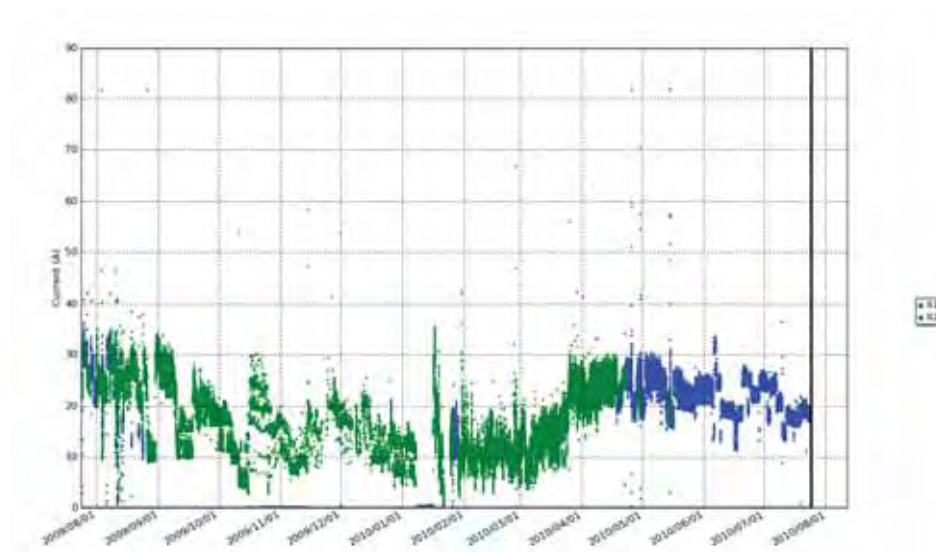


Figure 4.11: DC/DC Current Output

Current Output for PLATO measured at Dome A from August 2009 to August 2010 (Data Credit: CCAA, PRIC, UNSW).

Figure 4.12 shows the cylinder head temperatures of all six engines. The vertical lines shown in the plot during the summer months of 2009/10 were when the diesel engines periodically started and stopped because the solar panels were able to provide the majority of the power at times when engines were not operating.

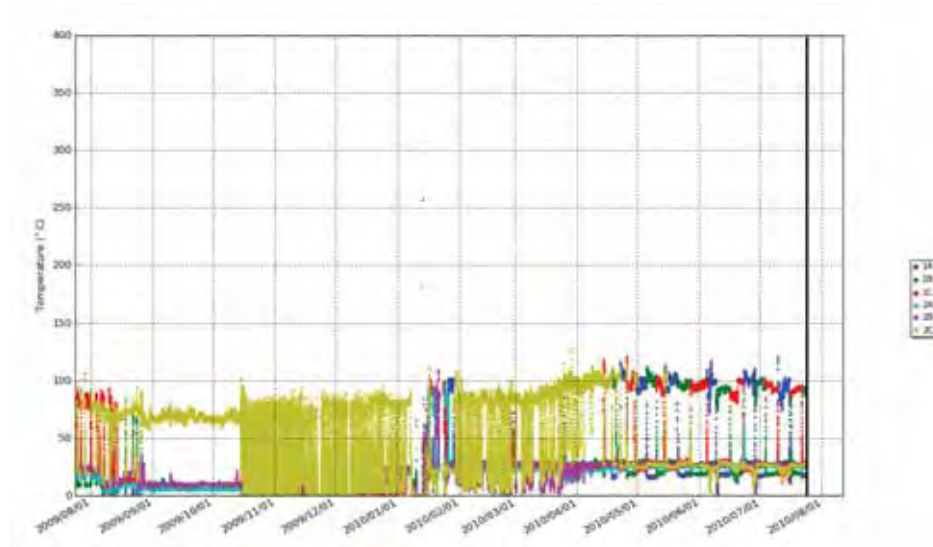


Figure 4.12: Cylinder Head Temperatures
Cylinder Head Temperatures for PLATO measured at Dome A from August 2009 to August 2010 (Data Credit: CCAA, PRIC, UNSW).

Figure 4.13 shows the exhaust gas temperatures of all six engines. Periods of high exhaust temperatures indicate when an engine was operating harder in order to produce a higher power output.

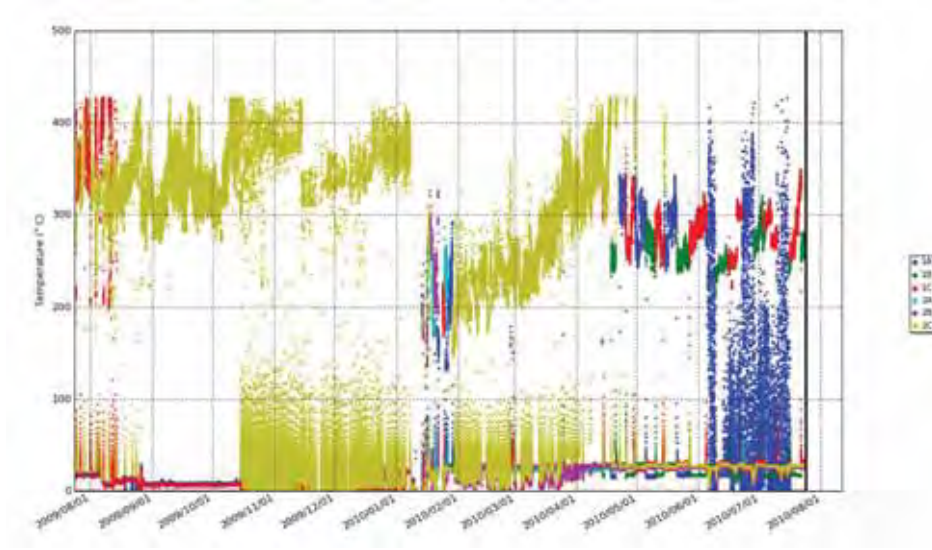


Figure 4.13: Exhaust Gas Temperatures

Exhaust temperatures for PLATO measured at Dome A from August 2009 to August 2010 (Data Credit: CCAA, PRIC, UNSW).

Figure 4.14 shows the approximate amount of fuel left in the 4000L tank as a percentage. The sudden rise in fuel level in January 2010 is due to the tank being refueled as part of the servicing mission. The clipped peak at the beginning of 2010 is a result of the fuel tank being filled just above the fuel sensor. The reduced amount of fuel consumption towards the end of 2009 corresponds to the conservation of fuel as all major dark observations has been completed. The fuel level here does not consider thermal expansion because there is no fuel temperature measurement. The average fuel consumption for operation in 2009 was 460g/kWh for an average power output of 800W (Luong-Van *et al.* 2010).

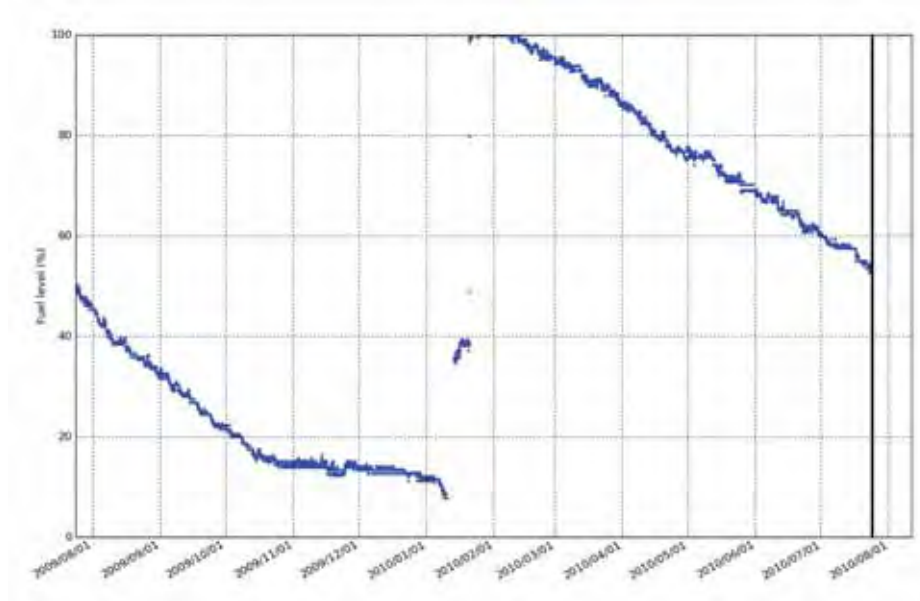


Figure 4.14: Fuel Level

Fuel level for PLATO measured at Dome A from August 2009 to August 2010 (Data Credit: CCAA, PRIC, UNSW).

4.6 Conclusions

The simulated altitude tests for the Hatz 1B30 engine demonstrated that little modification to the engine was required for it to start and run satisfactorily at an altitude of up to 5000m. Because the maximum power output at a given speed is reduced in direct proportion to the air pressure, the maximum fuel delivery must also be correspondingly reduced. However, because the air is less dense, there is less working fluid available to do the thermodynamic work and less cooling is available, and so the temperature rise (cylinder head, exhaust gas etc.) is greatly increased for a given power output. By advancing the start of the fuel delivery timing there is more time for combustion early in the ignition stroke, which liberates useful work and minimises this increase in exhaust gas temperature.

Allowing for an alternator efficiency of approximately 90%, we find that the brake specific fuel consumption (BSFC) of the engine at sea level is

consistent with the Hatz published data. Furthermore, little loss of efficiency, if any, was encountered when the engine is running at high altitude. For providing an approximate power output of 800W, the BSFC is estimated to be about 450g/kWh. This BSFC is therefore consistent with operating the Hatz 1B30 diesel engine at Dome A (460g/kWh; see section 4.5.1) for the same power output of 800W.

Chapter 5

Conclusions

“If you wish to make an apple pie from scratch, you must first invent the universe.”

- Carl Sagan, Astrophysicist, Author and Communicator
(1934-1996)

In order to perform atmospheric observations for astronomical site testing from isolated locations on the Antarctic plateau, an autonomous facility, PLATO, has been developed. PLATO is powered by a diesel engine bank and an array of solar panels.

PLATO is the latest facility designed by the University of New South Wales Antarctic team and has been deployed by Polar Research Institute of China and the Chinese Academy of Sciences to Dome A. The team had to overcome new challenges such as higher altitude, a more remote location, and colder temperatures in comparison to the other sites of South Pole and Dome C. PLATO's power generation system consist of solar panels for the summer months and Hatz 1B30 diesel engines when the Sun is either behind the panels or below the horizon. The power generation system provides both electrical power and heat for the instruments and control computers. Communications are made available using modems that link up with the Iridium

satellite network. The PLATO power generation system is an innovative and scalable system that can be implemented for remote sites anywhere on the Antarctic plateau and at other high-altitude locations.

The single-cylinder diesel engine is an efficient and reliable system providing power for PLATO during the Antarctic winter. The Hatz 1B30, a naturally-aspirated single-cylinder diesel engine, has been shown to be a good choice for providing 1-2kW of power. The engine's fuel, Jet A-1 mixed with 2-stroke motorcycle oil, has a high energy density and a low pour point that is ideally suited for operation in Antarctica.

Tests carried out in the laboratory allowed us to measure efficiency and determine performance of the Hatz 1B30 diesel engine prior to deployment at Dome A. Higher exhaust temperatures were observed at low pressure for a given power output. The brake specific fuel consumption (BSFC) at an engine speed of 2200rpm at sea level and at low pressure (~ 540 hPa) were similar. Having the injection timing set at 18° BTDC was shown to produce a lower exhaust gas temperature at an engine speed of 2200rpm but had little effect on the brake specific fuel consumption.

The conclusions drawn from the laboratory experiments influenced the decision making on the implementation of the PLATO engines for operation at Dome A. The engines were fixed at a speed of 2200rpm with a fuel injection timing of 18° BTDC. For an engine speed of 2200rpm and a power output of 800W, the BSFC measured in the laboratory (~ 450 g/kWh) was consistent with the BSFC calculated for the Hatz 1B30 operating at Dome A (~ 460 g/kWh).

The diesel engines, during the winter months, were able to provide adequate electrical power and heat to the PLATO instruments, which resulted in successful observations of the atmosphere above Dome A. Initial results of the PLATO instruments have shown that Dome A is a worthwhile site to conduct observational astronomy. CSTAR showed during the winter months about 67% of the time had little or no cloud cover and 2% of the time

had strong aurorae (Zou *et al.* 2010). Snodar observed that Dome A has a low turbulent boundary-layer with a median height of 13.9m (Bonner *et al.* 2010). Pre-HEAT has verified that Dome A is the best ground-based site yet measured to perform terahertz astronomy and hence giving opportunity to obtain important spectral information on the evolution of stars, the interstellar medium and galaxies (Yang *et al.* 2010). Nigel showed that Dome A has exceedingly low water vapour content and a large amount of available dark time, which is advantageous for astronomical observations, and also characterised the auroral activity (see Appendix A).

Antarctic astronomy is fast becoming a popular scientific field because of the potential of the Antarctic plateau to provide conditions for performing precise astronomy. Before the construction of large telescope facilities for a new site on the Antarctic plateau, an analysis of the site is essential. The engineering solutions for providing site-testing facilities in Antarctica has paved the way for performing astronomy from the Antarctic plateau.

This thesis is also an attempt to stress the importance of the relationships between engineers, instrument builders and observational astronomers. Modern astronomy requires these key relationships. The advancement of technology must also be included in the definition of astronomy; as modern day astronomy can not move forward without overcoming the engineering challenges that exist for both terrestrial and space platforms for astronomical observations.

5.1 Future Work

Future experiments in the laboratory would be to perform long endurance tests on the Hatz 1B30; however, this would require a way to keep the chamber cool to avoid overheating. More tests involving different injection timings will determine the optimal point of fuel injection. A check to see what is produced in the exhaust emission would determine if complete combustion takes

place and determine the conditions required to have the minimal amount of pollutants. In addition, it would be good to check how rich or lean the air-fuel mixture is during combustion.

Future installments of PLATO are also on their way. A PLATO facility is planned to be deployed to the Japanese site of Dome F. Additionally, another power module is scheduled to go to Dome A with improvements made to the battery and electrical systems with a new engine starting mechanism; see (Ashley *et al.* 2010) for details.

Appendix A

Nigel: The Aurora Hunter

“With the northern lights a-running wild in the land of the midnight sun”

North to Alaska (Song, 1960)

Johnny Horton, Singer and Writer (1925-1960)

A.1 Introduction

Nigel, a fibre-fed UV/Visible spectrometer coupled to a thermo-electrically cooled 256 x 1024 CCD camera, is both a site-testing and scientific instrument designed to take sky spectra from the Antarctic plateau.

Among the early instruments of AASTO (see Section 1.5.1) was AFOS (Antarctic Fibre-Optic Spectrometer), which was in operation from 2002 to 2003 (Storey 1998; Dempsey *et al.* 2004). The spectrograph and CCD camera were cannibalised from AFOS to create Nigel. At Dome C, the Autonomous Astronomical Site-Testing InterNational Observatory (AASTINO) commenced operation in 2003. Kenyon *et al.* (2006) originally started work on Nigel to undertake observations of the optical sky background during the Dome C winter session of 2005. Unfortunately, Nigel ended its operation at Dome C when the AASTINO was decommissioned in February 2005. Nigel

was selected to join the PLATO instrument suite.

Due to technical difficulties with Nigel, it was unable to be deployed with PLATO in the summer of 2007/08. Nigel, however, joined the 2008/09 summer mission to Dome A. Nigel's purpose is to take measurements of twilight, air-glow, cloud-cover and aurorae above Dome A. Nigel will not only be a site-testing instrument for the optical sky background but also a scientific instrument analysing the intensity and frequency of aurorae.

This appendix will describe Nigel's hardware and software, how it was modified for Dome A, and preliminary results from initial testing at Siding Spring Observatory and from observations at Dome A, Antarctica.

A.2 Wavelength Specification

As observing aurorae is the main science driver for Nigel, we need to use the entire available spectrum (350nm to 820nm) in order to cover the strongest emission lines in the optical. Figure A.1 shows a particular auroral spectrum that was observed during a bright auroral event overlaid with the UBVRI pass-bands (Dempsey *et al.* 2005). Swenson *et al.* (1998) have used the 427.8nm, 557.7nm and the 630.0nm lines to study the temporal and spatial behaviour of auroral emission. It is aim of the Nigel project to perform a similar task for observations of the Dome A sky.

The wavelength coverage of the spectrograph used for Nigel is from 190nm to 900nm. Since the atmosphere is a natural absorber for wavelengths below ~ 300 nm due to ozone and molecular oxygen (McEwen *et al.* 1983), second order contamination will effect wavelengths greater than ~ 600 nm. A glass-filter was used to absorb light below 515nm. Thus, for a given observed position of the sky, two optical optical fibres will be used with one fibre being coupled with the glass-filter. For use on Nigel, there are two defined wavelength regimes; Blue (300 to 515nm) and Red (515 to 850nm).

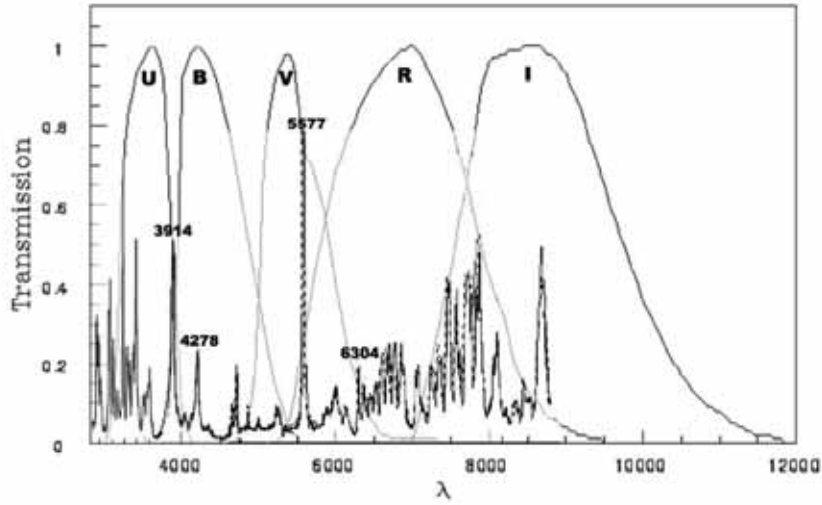


Figure A.1: Aurora Spectra with respect to UBVRI passbands.
The auroral spectrum, transmission as function of wavelength, spans 300 to 890nm (Swenson et al. 1998; Paxton & Meng 1999).

A.3 Nigel's Hardware

The chosen spectrograph and CCD camera were originally components from the AFOS telescope at the South Pole. The commercial imaging spectrometer (Jobin Yvon model CP200, 1989) houses a concave holographic diffraction grating that has 200 grooves per millimetre. The grating linearly disperses the optical radiation from 24.6nm/mm for blue light to 25.7nm/mm for red light onto a CCD (Kenyon *et al.* 2006). The CCD camera is an Andor unit selected from Oriel Instruments (model Instaspec IV, open electrode) with an exposure area of 1024 x 256 pixels that is sensitive from 200nm to 1000nm. The physical size of each pixel is $27\mu\text{ m} \times 27\mu\text{ m}$, giving a total physical area of 27.6 x 6.9mm (Dempsey *et al.* 2004; Kenyon *et al.* 2006). An example of an (false-colour) CCD image taken by the Nigel instrument during the daytime at Dome A can be seen in Figure A.2.



Figure A.2: Nigel Spectra

A false-colour CCD image showing the individual spectra corresponding to each of the six optical fibres. The wavelength decreases from left to right ($\sim 820\text{nm}$ to $\sim 300\text{nm}$). The top pair, middle pair, and bottom pair of spectra correspond to the zenith fibres, the west fibres, and the north fibres respectively.

A.3.1 Design and Assembly

Nigel's Bob

The fibre housing unit aligns each of the red/blue fibre pairs in the three designated elevations (North (40° Elv.), West (71.5° Elv.) and Zenith) towards the Dome A sky. It is crucial to the success of the Nigel instrument that the fibres are resistant to ice formation on their exposed faces. To achieve this, the fibres were mounted flush with the surface of a hollow stainless steel sphere. This has two important advantages: the sphere, being highly reflective, can be heated with a small amount of electrical power; and the spherical shape is resistant to the build-up of snow. The stainless steel sphere, also known as the “Bob” (see Figure A.3), is 120mm in diameter and constructed from two polished stainless steel hemispheres. The lower hemisphere is attached by an internal demountable collar which in turn is supported by a hollow stainless steel stalk. The upper hemisphere contains three dual fibre windows each consisting of an SMA connector stub drilled to fit two optical fibres and retained in a modified SMA bulkhead connector housing. The end of each fibre pair was inserted from the inside and oriented via pre-drilled holes at the three fixed positions on the sky. The fibres were then optically polished flush with the outer surface of the upper hemisphere. The three assemblies are also attached to internal copper plates which can be electrically

heated via current flowing through two 25Ω 10W resistors. This arrangement ensures the fibre windows are kept clear of frost or ice. The Bob is supported by a hollow stalk through which the six fibre patch cords pass into the instrument module (Sims *et al.* 2010).

The Bob design is credited to J. R. Everett (School of Physics, University of New South Wales) and the author (Shane Hengst). The Bob was manufactured by Pritipal Baweja and Paul Hallahan from the Science Faculty Workshop of the University of NSW.

Nigel's Box

The author modified an instrumentation rack in order to house the Spectrograph, CCD camera, filter rack and associated computer components of Nigel (See Figure A.3.1).

The filter rack is held in place on the front panel of the instrumentation rack. Each optical fibre being streamed from the Bob is terminated on the front panel that supports the six collimating filter assemblies.

Pseudo-Slit connector

The fibre terminator end, a brass connector, is attached to the spectrograph. All six fibres are evenly aligned and bonded on a machined 'v-grooved' mount, which was polished flush. The linear array of fibres creates a pseudo-slit that allows the collected light to propagate into the housing of the spectrograph.

A.4 Nigel Control

Sole control of Nigel's operation is by the PLATO "supervisor" computers, running Debian Linux. The supervisor computers are monitored off-site via the Iridium Satellite network. A separate PC104 computer, running MS-DOS 6.22, controls the CCD camera. Nigel's computer and the PLATO supervisor computer communicate with each other via an ERIC package.

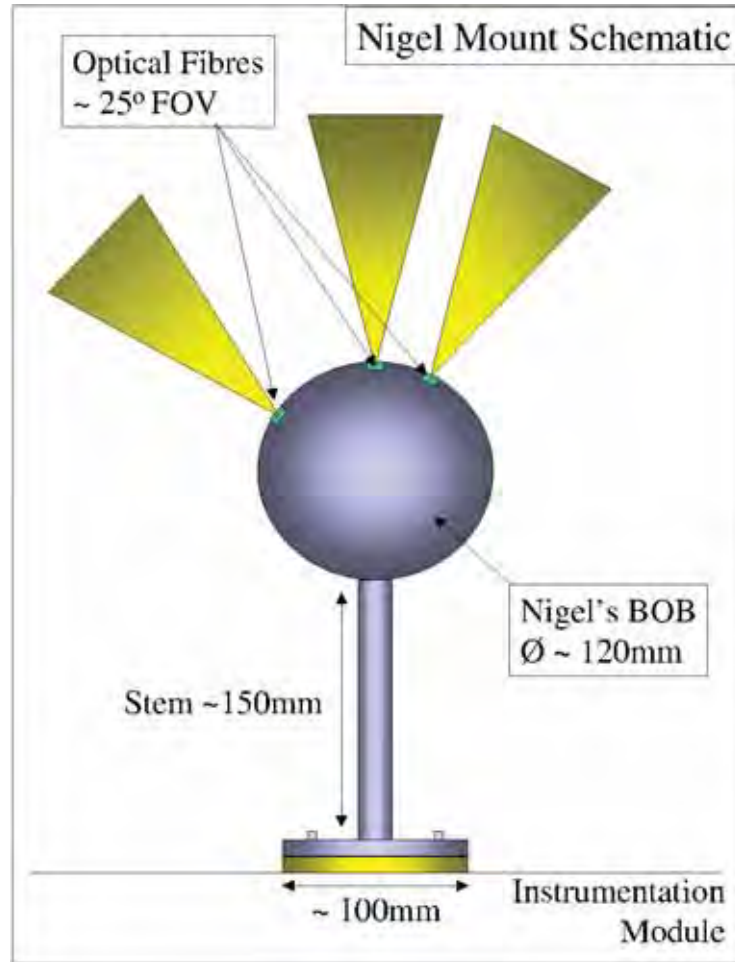


Figure A.3: Nigel's BOB

The figure shows a basic schematic of Nigel's Bob. The Bob houses the optical fibres inside a stainless steel sphere, which stream through the 'stem' to Nigel's instrumentation rack. The whole structure is mounted on a flange that is bolted on the roof of the PLATO instrumentation module.

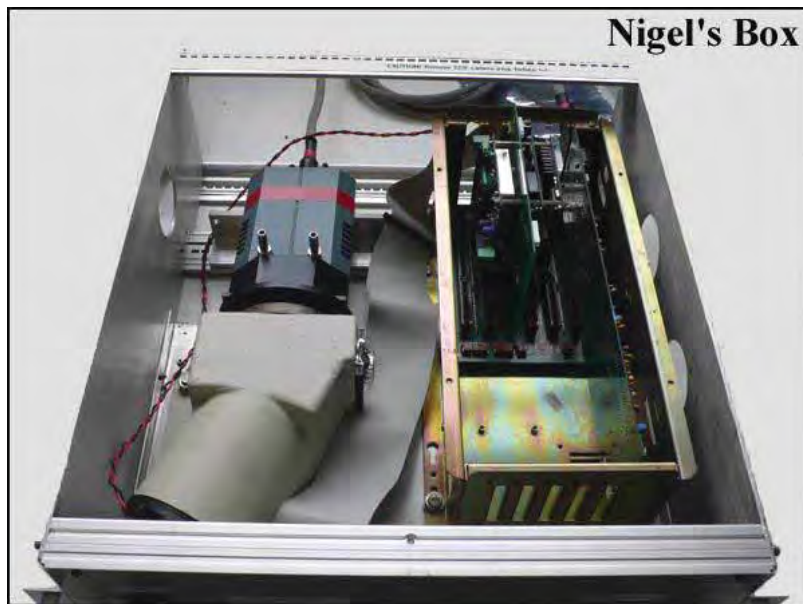


Figure A.4: Nigel Instrumentation Rack

Photograph showing the instrumentation rack for Nigel. Inside, on the left, is the spectrograph that houses the diffraction grating (bottom-end) and CCD camera (top-end). On the right-hand side of the box is the Nigel computer that links the CCD camera to the PLATO Supervisor computer.

ERIC (Extensible Remote Instrument Control) was developed as a ‘remote-controlled’ kernel to communicate with instruments in Antarctica via the Internet (Ashley *et al.* 1996).

A Perl script is executed from the supervisor computer, which directs the CCD camera to take an exposure. The number of exposures to be taken is dependent on two aspects: the position of the Sun and the available space on the hard-drive. No exposure is taken when the Sun is within the fibres’ field-of-view.

The exposure times were set based on the results from the previous exposure in order to avoid saturation on the sky. The CCD images were analysed on the supervisor computers at Dome A because of the limited bandwidth via the Iridium Satellite. The images were dark-subtracted and spectra were modified on the basis of their signal-to-noise. The six 2D spectra on each image were transformed into 1D information, which was then sent via the Iridium satellite modem. The original raw images observed during the 2009 winter months have been stored on solid-state disks, which have now been retrieved by the 2009/2010 Chinese traverse team (Sims *et al.* 2010).

A.5 Nigel Testing

A.5.1 Focusing the CCD

A test for the focusing of the CCD onto the spectrograph was achieved by taking successive spectra and determining the full-width-half-maximum (FWHM) of the same emission line on each spectrum. The light source was a 80W mercury vapour gas lamp (Ferguson, MF80SB).

The best focused position for the CCD camera was determined to be approximately 1.6mm of screw thread away from the housing of the spectrograph, see Figure A.5.

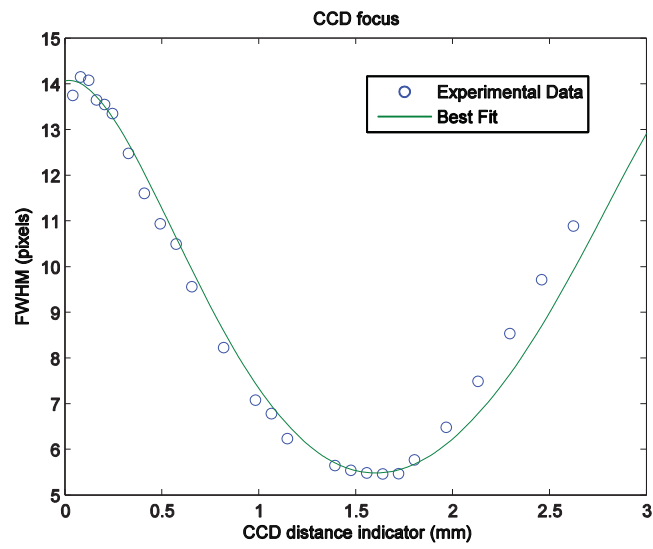


Figure A.5: CCD Focus

The FWHM of the first emission spike of each successive Mercury Gas Spectra were obtained by using the program Matlab. It was determined that having the screw thread length of about 1.6mm yielded the best focused position.

A.5.2 Initial Results from Siding Spring Observatory

Spectra were obtained with the instrument Nigel from October 19th to the 22nd (2008) at the Automated Patrol Telescope (APT) building, Siding Spring Observatory. The operation consisted of a combination of taking individual exposures and executing a script. The first test run was on Monday 20th of October from about 8:20pm until it was cut short due to an unexpected power glitch at about 9:25pm. This resulted in the sudden power down of the Nigel computer. The second test run was on the early morning of October 21st from about 4:20am to 7:20am to gather information from the moonshine, sunrise/twilight and morning daytime. The third test run was from about 6:30pm for 3 hours to gather exposures of twilight and night time. The final test run is another early morning run on October 22nd from 4:30pm to 7:30pm.

An attempt was made to couple the light beam through the inline filter assembly. Unfortunately, this was not successful on site. As a result, any information obtained was not scientifically significant and so, this initial testing was simply an exercise to test the operation of Nigel.

Figures A.6-A.8 each show the raw image exposed corresponding to the six emission spectra that show raw counts as a function of pixel position (arbitrary wavelength) for each fibre.

Daytime

The daytime spectra were taken late afternoon and in the morning. Figures A.6 and A.7 show example daytime spectra before and after the (attempted) alignment of the inline filters respectively. The exposure time in each case was 2 seconds. They clearly show that the filters were attenuating the wavelengths below 515nm for the ‘red’ fibre, which showed that the system achieved its goal in eliminating the 2nd order contamination.

Controlled Testing

Tests carried out under controlled conditions were undertaken with an incandescent light bulb and the mercury vapour gas lamp. The incandescent light bulb was used to shine on the white ceiling; see Figure A.8 for an 100s exposure. The illumination of the white wall was also used for the mercury gas vapour lamp; see Figure A.9 for a 600s exposure.

Initial Results Conclusions

It was clear that there was severe loss in transmission due to mis-aligned filters. An attempt to re-align each fibre that are coupled with an in-line filter holder was undertaken in the UNSW Optics lab. The re-alignment improved the light transmission through each fibre. However, an absolute flux calibration would be needed at the Dome A site for optimal performance (see section A.6). A final polish on the fibre exposed ends was undertaken before deployment.

A.6 Preliminary Results from Dome A

Nigel was successfully deployed on the summer 2008/09 Chinese traverse. Since then it has taken a wealth of data, which still needs to be fully analysed. This task was begun by honours student Matthew Nguyen and now being continued by Masters student Geoff Sims. The following discussion summarises their findings.

Wavelength calibration has been achieved by using known Fraunhofer lines in the daytime spectra and known auroral and airglow lines in the nighttime spectra. Figures A.10 and A.11 show the relative flux as a function of wavelength for twilight and nighttime spectra respectively at Dome A (Sims *et al.* 2010).

For future work, an absolute flux calibration for Nigel will be performed. This needs to consider the various spectral responses from the optical fibres, Schott filters, spectrograph and the CCD camera. A convolution of all these responses has been calculated to yield an expected overall spectral response (see Figure A.12). The convolved uncalibrated flux data from Nigel is intended to be compared with the calibrated flux data observed with the Gattini camera (Sims *et al.* 2010).

Preliminary data suggest that Dome A has exceedingly low water vapour content and a large amount of available dark time, which is advantageous for astronomical observations. See (Sims *et al.* 2010) for an overview.

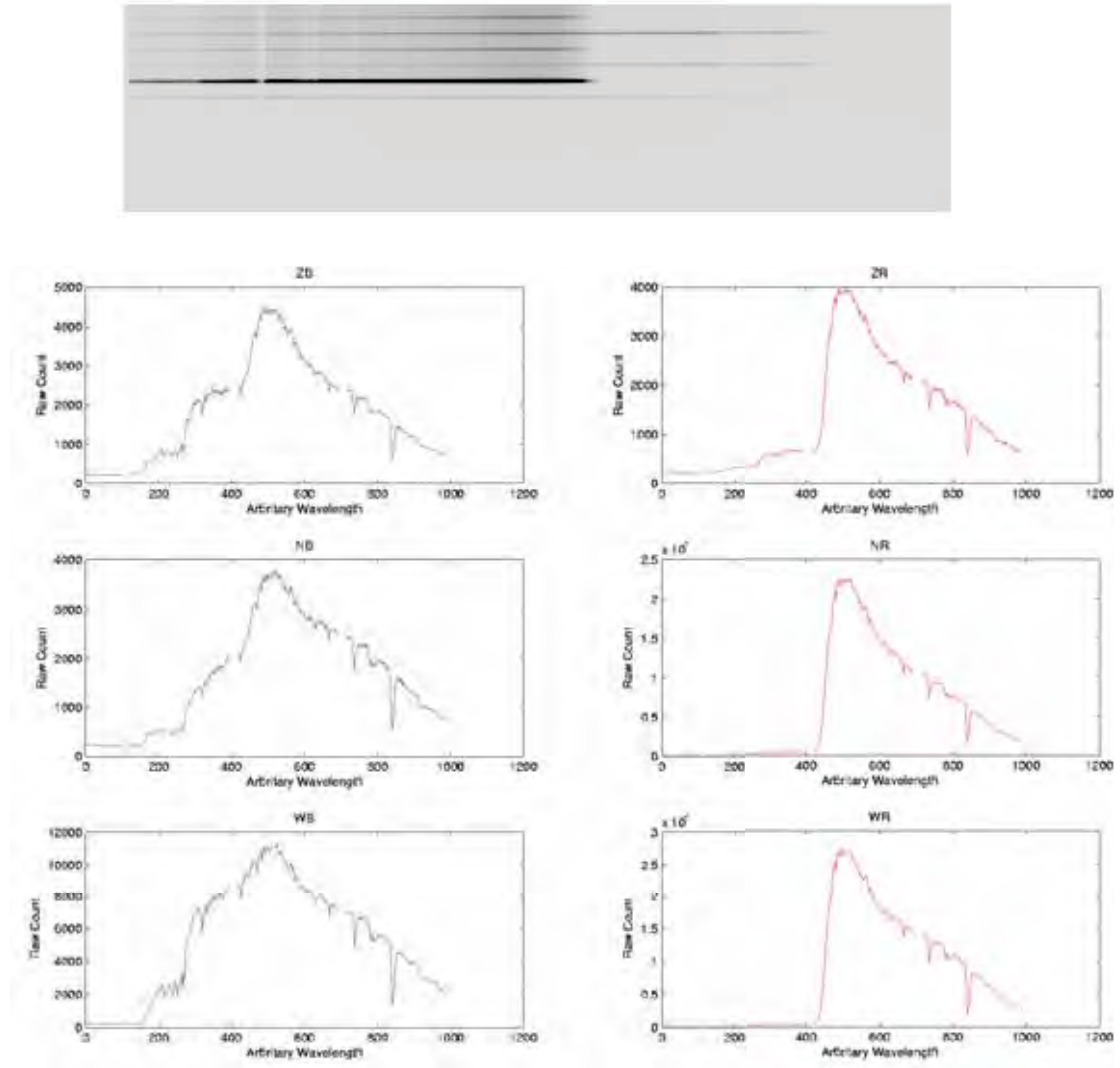


Figure A.6: Daytime Image and Spectra at SSO (unaligned filters)
19th of October exposure 2 seconds

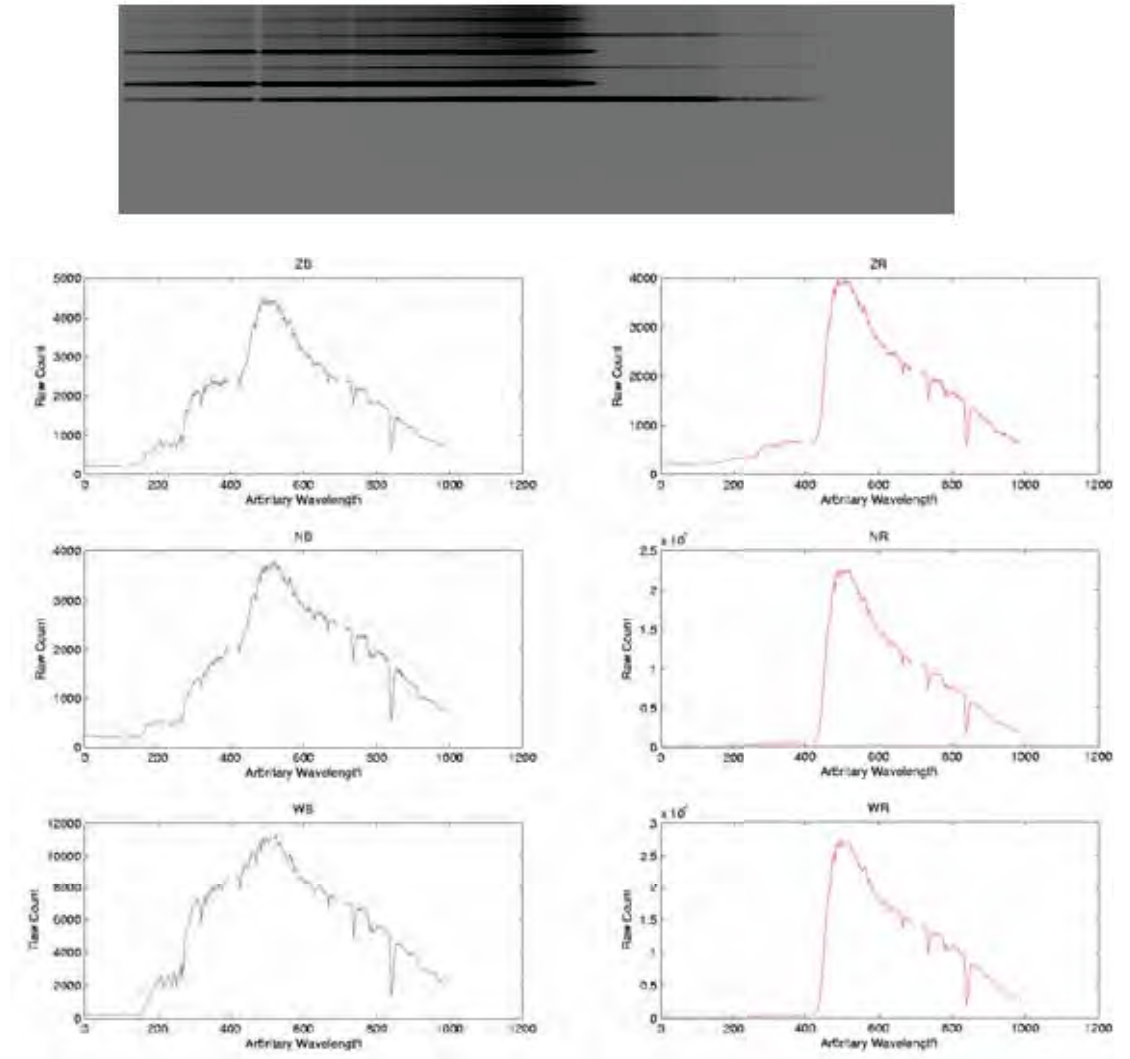


Figure A.7: Daytime Image and Spectra at SSO (aligned filters)
21st of October exposure 2 seconds

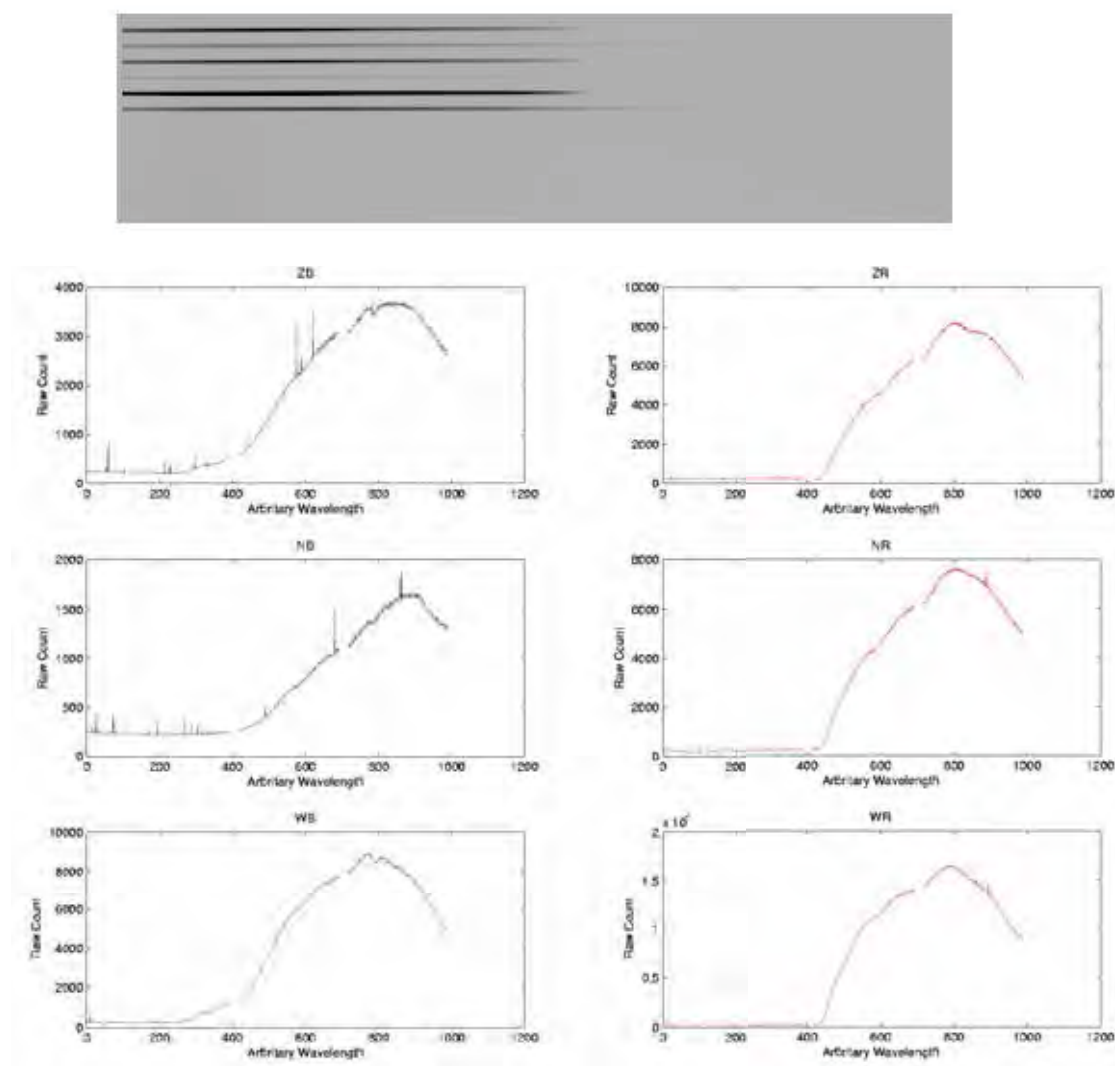


Figure A.8: Light Bulb Spectra Image and Spectra
20th of October exposure 100 seconds

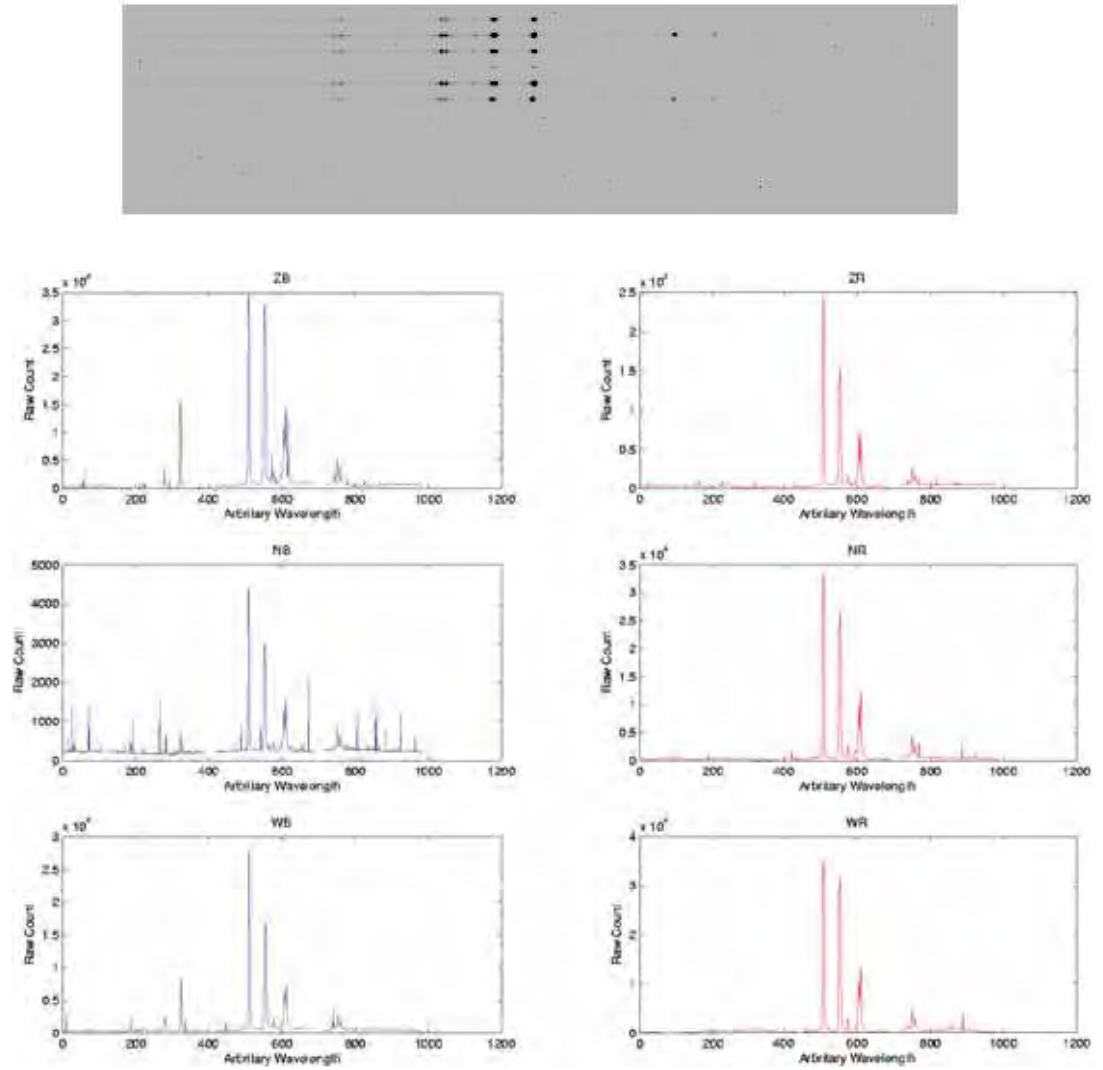


Figure A.9: Mercury Gas Vapour Image and Spectra
21st of October exposure 600 seconds

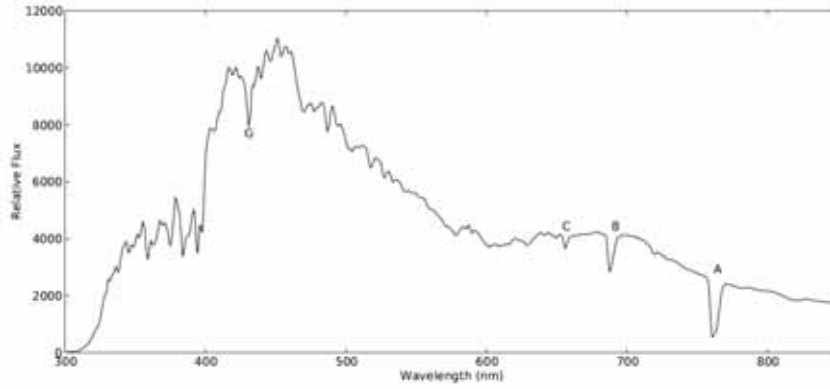


Figure A.10: Dome A Twilight Spectra

This spectrum has been composited from red and blue fibre output that has been spliced at ~ 530 nm. Fraunhofer absorption bands due to molecular oxygen (A-759.4 nm and B-687.7 nm), $H\alpha$ (C-653.3 nm) and from iron (G-430.8 nm) (Sims et al. 2010). (Data Credit: CCAA, PRIC, UNSW)

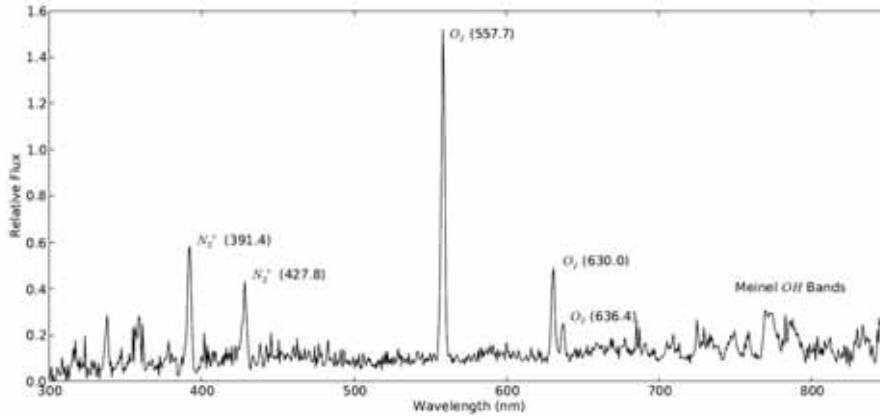


Figure A.11: Dome A Nighttime Spectra

This spectrum has been averaged over 86 spectra. This spectrum has been composited from red and blue fibre output that has been spliced at ~ 530 nm. Strong emission lines due to molecular nitrogen (391.4 nm and 427.8 nm), excited oxygen atoms (557.7 nm, 630.0 nm and 636.4 nm) and Meinel rotation-vibration bands of OH (Sims et al. 2010) (Data Credit: CCAA, PRIC, UNSW)

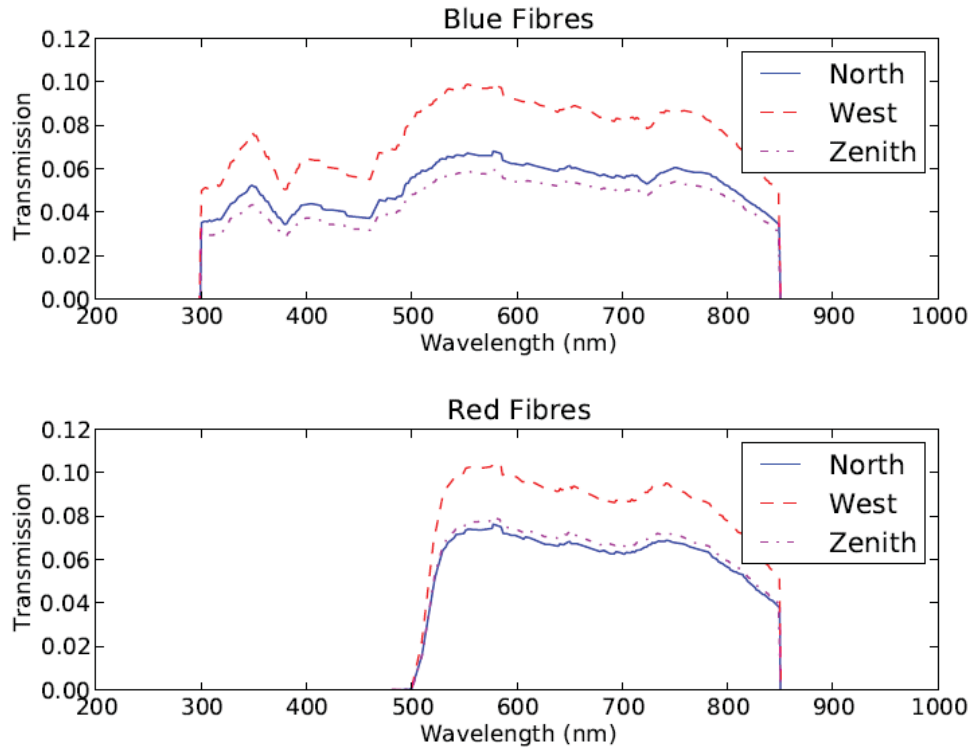


Figure A.12: Convolved spectra response for all fibres.

This is the predicted overall response from each of the six fibres considering the spectral transmission from the optical fibres, Schott filters, spectrograph and the CCD camera (Sims et al. 2010).

Appendix B

Engine Raw Data

Parameter	Definition
RPM	Engine Speed (revolutions per minute)
ST	Engine Start Time (seconds)
ET	Engine Stop Time (seconds)
SL	Initial Fuel Level (millilitres)
EL	Final Fuel Level (millilitres)
FC(g/h)	Fuel Consumption (grams per hour)
Av. Volts	Average Voltage Output (volts)
Av. Curr	Average Current Output (volts)
Adj. Curr	Adjusted Current (Amps)
Power (W)	Total Useable Electrical Output (Watts)
EGT (C)	Exhaust Gas Temperature (Celsius)
DV	Difference in Voltage from no-load scenario (volts)
R(Alt)	Alternator Resistance (Ohms)
P(Alt)	Alternator Power Output (Watts)
Total P	Total Power from Electrical and Alternator Output (Watts)
Efficiency	Fuel-to-electricity efficiency (g/kWh)
Pm[Pa]	Internal Pressure Estimate (Pascals)
Eff(load) [†]	Load Efficiency
Alt Eff [†]	Alternator Efficiency

Table B.1: Legend for Table Values

Table of parameters that define the column titles of Tables B.2-B.13

[†]Additional legend values for one of the test runs for an engine speed of 2200rpm (see Table B.7).

Date: 7/1/2008		Sea Level																	
RPM	ST	ET	SL	EL	FC (g/h)	Av. Volts	Av. Curr	Adj. Curr	Power (W)	EGT (C)	DV	R(Alt)	P(Alt. W)	Total P	Efficiency	Pm(Pa)			
1630	25.02	361.47	93.0	61.5	289.63	75.6231	-0.0507	0.0000	0.0000	91.8	0.000	4.560	0.000	0.000					
1560	38.36	457.15	81.5	41.0	140.86	72.2525	0.6885	0.7392	53.4090	99.0	3.371	4.560	2.492	55.901	2521.821	11617.863			
1580	59.70	438.66	89.5	64.5	189.89	71.1883	2.1050	2.1557	153.4583	108.5	4.437	2.058	9.584	163.021	1185.457	34681.589			
1580	53.55	503.76	90.0	58.5	201.51	60.3492	3.4321	3.4828	241.5294	117.7	6.274	1.801	21.851	263.380	765.077	56032.365			
1570	97.64	521.52	88.0	53.0	237.80	67.3219	6.7076	6.7583	454.9818	138.5	6.301	1.228	56.102	511.084	465.292	109422.189			
1570	21.15	528.48	90.0	40.0	283.84	63.5485	11.3069	11.3606	721.9264	167.5	12.077	1.063	137.197	658.124	330.364	183937.010			
1610	86.31	547.78	88.0	38.5	308.93	64.0048	12.6864	12.7171	813.9507	178.5	11.818	0.914	147.750	981.707	321.227	200784.284			
1565	19.29	472.81	93.5	44.5	311.17	60.9329	13.9106	13.9613	850.7025	185.5	14.890	1.052	205.054	1055.707	294.721	228766.566			
1610	59.88	483.30	81.0	32.0	333.29	61.5423	15.2648	15.3155	942.5511	195.8	14.081	0.919	215.854	1158.206	287.768	241800.194			
1560	26.95	448.06	90.5	40.0	345.37	58.8477	17.0870	17.1377	1006.5142	205.2	16.775	0.979	287.492	1296.006	266.480	273982.550			
1580	29.15	467.72	83.5	20.0	416.99	60.3945	20.6545	20.7052	1250.4802	216.8	15.229	0.735	315.311	1565.781	268.314	333111.671			
1560	34.80	481.05	92.5	42.0	325.26	58.5334	22.6032	22.6539	1292.0087	236.5*	10.060	0.835	436.274	1728.283	188.186	372304.476			

*Altitude was overloading

*Alternator was overheating

Date: 9/1/2008		Altitude																	
RPM	ST	ET	SL	EL	FC (g/h)	Av. Volts	Av. Curr.	Adj. Curr.	Power (W)	EGT (C)	DV	R(Alt)	P(Alt)W	Total P	Efficiency	Pm(Pa)			
1600	145.90	345.84	71.0	52.0	273.68	74.5394	-0.0547	0.0000	0.0000	135.5	0.000	3.484	0.000	0.000		0.0			
1580	53.15	450.80	89.0	56.5	220.90	71.9643	0.6829	0.7392	53.1960	134.1	2.575	3.484	1.904	55.100	4009.066	11722.1			
1560	105.75	551.60	89.0	57.5	203.48	70.1803	2.0738	2.1557	151.2877	138.5	4.359	2.022	9.397	160.685	1266.310	34822.8			
1580	23.05	488.10	91.0	58.5	210.31	68.0367	3.4147	3.4828	240.4410	152.8	5.503	1.580	19.165	259.606	810.128	55937.5			
1585	28.74	426.35	90.0	55.0	253.51	67.7383	6.7383	6.7583	457.7958	188.1	6.801	1.008	45.984	503.780	503.245	106833.4			
1590	29.91	429.85	96.0	55.5	261.79	65.4785	9.7024	11.3606	743.8750	221.6	9.061	0.788	102.937	846.812	344.574	179020.8			
1570	40.10	527.75	88.5	37.0	310.06	63.3045	11.2576	12.7171	805.0751	243.5	11.233	0.883	142.850	947.925	327.092	202949.2			
1575	40.53	554.50	89.0	29.0	336.21	60.7078	13.8497	13.9613	847.5588	279.5	13.832	0.991	193.107	1040.667	323.085	222097.8			
1585	23.02	488.15	94.0	35.0	381.73	58.0048	16.8872	15.3155	888.9725	322.2	16.535	1.080	253.236	1141.608	334.360	242103.4			
1560	32.46	412.05	94.5	41.0	405.91	54.7682	18.8958	17.1377	938.5607	348.5	19.773	1.154	338.867	1277.434	317.756	275249.7			
1560	32.50	240.05	77.5	47.0	423.22	52.6547	20.6178	20.7052	1060.2261	372.9	21.885	1.057	453.127	1543.353	274.223	332547.6			

Table B.2: Engine Data - 1600rpm

Date: 22/4/2008

Sea Level

RPM	ST	ET	SL	EL	FC (g/h)	Av. Volts	Av. Curr.	Adj. Curr.	Power (W)	EGT (C)	DV	R(Alt)	P(Alt)W	Total P	Efficiency	Pm(Pa)
1830	32.91	289.75	92.5	73.5	213.05	83.8872	-0.0550	0.0000	0.0000	103.2	0.000	1.935	1.347	69.995	3082.976	12891.996
1825	22.58	376.25	73.5	47.0	215.79	82.2724	0.7794	0.8344	68.6481	108.8	1.615	1.302	20.308	331.321	750.546	61699.925
1805	27.82	479.50	93.5	54.5	248.67	78.7454	3.8948	3.9496	311.0128	128.9	5.142	1.069	60.950	633.415	448.859	118614.353
1795	29.52	449.90	97.0	55.5	284.31	75.8152	7.4958	7.5508	572.4654	151.6	8.072	1.117	87.326	741.789	380.953	139686.810
1785	30.56	453.51	95.5	54.0	282.59	74.0117	8.7877	8.8427	654.4633	160.7	9.876	1.064	123.833	904.807	340.510	169908.894
1790	20.89	455.56	94.0	47.5	308.10	72.4063	10.7310	10.7860	780.9744	173.9	11.481	1.034	166.128	1063.430	308.872	196695.722
1790	481.94	872.12	94.0	49.5	328.46	70.7824	12.6219	12.6769	897.3014	185.5	13.105	1.054	200.851	1158.172	319.546	217486.850
1790	29.54	438.09	96.0	43.5	370.09	69.3394	13.7513	13.8063	957.3206	191.5	14.548	1.071	255.789	1296.569	275.890	246226.834
1770	27.73	430.29	95.0	45.0	357.71	67.3378	15.4011	15.4561	1040.7798	202.8	16.549	1.013	282.055	1399.574	265.298	262818.468
1790	27.73	419.43	95.0	44.5	371.30	66.9815	16.6290	16.6840	1117.5193	210.7	16.906	0.984	356.509	1567.137	250.276	299082.285
1795	29.53	422.20	96.5	42.0	399.72	65.1621	18.9841	19.0391	1240.6277	224.2	18.725	0.986	555.375	1991.063	223.946	375991.444
1780	100.57	417.06	93.5	44.5	445.89	60.4882	23.6800	23.7350	1435.6874	252.9	23.399					

Altitude

RPM	ST	ET	SL	EL	FC (g/h)	Av. Volts	Av. Curr.	Adj. Curr.	Power (W)	EGT (C)	DV	R(Alt)	P(Alt)W	Total P	Efficiency	Pm(Pa)
1805	19.01	188.39	98.0	86.0	204.04	83.8872	-0.0550	0.0000	0.0000	103.2	0.000	6.809	4.375	67.244	3083.256	12557.2
1800	22.47	341.96	86.0	63.0	207.33	78.4289	0.7466	0.8016	62.8686	149.5	5.458	1.799	26.894	324.316	703.586	60228.7
1810	29.34	395.36	63.0	34.0	228.18	76.9308	3.8111	3.8661	297.4222	183.3	6.956	1.311	71.809	620.732	428.702	116239.2
1795	27.02	394.99	92.0	58.0	266.11	74.1827	7.3446	7.3996	548.9223	219.2	9.705	1.239	94.792	733.820	375.577	137416.3
1795	24.24	389.98	95.0	60.0	275.61	73.0510	8.6927	8.7477	639.0282	235.4	10.836	1.163	132.440	895.102	338.800	167618.1
1795	22.42	378.55	96.0	58.5	303.26	71.4752	10.6153	10.6703	762.8618	258.8	12.412	1.147	178.535	1046.786	315.853	196022.8
1795	32.77	376.84	92.0	52.5	330.63	69.5798	12.4235	12.4785	868.2515	279.3	14.307	1.134	211.001	1144.213	298.594	213671.9
1800	32.66	420.42	93.0	47.0	341.65	68.4178	13.5849	13.6399	933.2120	296.0	15.469	1.194	273.078	1268.594	280.944	239558.9
1780	31.04	447.20	91.0	39.5	356.40	65.8295	15.0675	15.1225	995.5066	314.9	18.058	1.189	310.154	1354.812	273.021	254412.8
1790	28.46	374.94	91.0	46.5	388.89	64.8831	16.0954	16.1504	1044.6579	328.0	19.204	1.215	397.886	1518.342	262.716	286723.0
1780	34.42	377.37	89.5	42.0	398.89	61.9043	18.0448	18.0998	1120.4554	351.7	21.983	1.1837	598.373437	1886.12	234.49	355176.4
1785	28.60	347.68	86.5	36.0	442.27	57.2739	22.4290	22.4840	1287.7464	406.8	26.6133					

Table B.3: Engine Date - 1800rpm

Date: 23/4/2008 Sea Level

RPM	ST	ET	SL	EL	FC (g/h)	Av. Volts	Av. Curr.	Adj. Curr	Power (W)	EGT (C)	DV	R(Alt)	P(Alt)/W	Total P	Efficiency	Pm[Pa]
1990	29.73	272.02	94.5	73.5	249.62	90.6997	-0.0550	0.0000	0.0000	100.0	0.000	1.653	0.000	0.000	2694.023	13853.672
1995	24.90	482.24	73.5	38.5	220.40	89.2090	0.8470	0.9020	80.4665	108.6	1.491	0.906	1.345	81.811	670.020	66186.391
2000	36.14	434.54	93.5	57.0	263.86	86.7673	4.2869	4.3419	376.7349	131.5	3.932	0.906	17.074	393.809	416.620	126146.569
1990	27.03	431.71	93.0	49.5	309.58	82.4165	8.1376	8.1926	675.2054	154.7	8.283	1.011	67.861	743.066	328.600	181664.340
1995	15.26	456.43	95.5	41.5	352.52	79.5450	11.7730	11.8280	940.8583	179.0	11.155	0.943	131.938	1072.796	282.466	233141.573
1990	16.45	454.48	93.0	34.0	387.92	76.1021	15.0864	15.1414	1152.2923	198.5	14.598	0.964	221.028	1373.320	260039.767	276398.728
1990	13.75	410.63	92.5	35.5	413.70	74.0704	16.9186	16.9736	1257.2413	210.5	16.629	0.980	282.259	1539.500	231.056	313314.159
1990	13.43	407.42	91.5	33.5	423.97	72.4213	17.9864	18.0414	1306.5816	215.9	18.278	1.013	329.768	1636.350	219.710	352634.336
1995	13.40	474.65	88.0	17.0	443.31	69.8774	20.3446	20.3996	1425.4710	231.6	20.822	1.021	424.767	1850.238	209.136	408386.543
2000	15.54	383.86	90.5	28.5	484.80	67.5413	23.0782	23.1332	1562.4464	247.5	23.158	1.001	535.728	2098.174		
1990	15.27	373.08	89.5	27.5	499.04	63.8759	24.9877	25.0427	1599.6250	259.0	26.824	1.071	671.740	2271.365		
1990	17.19	389.28	91.0	26.0	503.10	59.9087	26.4677	26.5227	1588.9405	268.3	30.791	1.161	816.660	2405.601		

Altitude

RPM	ST	ET	SL	EL	FC (g/h)	Av. Volts	Av. Curr.	Adj. Curr	Power (W)	EGT (C)	DV	R(Alt)	P(Alt)/W	Total P	Efficiency	Pm[Pa]
1995	20.88	202.62	49.5	33.5	253.55	87.0000	-0.0550	0.0000	0.0000	160.4	0.000	0.911	0.701	76.343	3839.694	12672.3
2025	24.68	383.29	86.0	49.5	293.13	86.2009	0.8225	0.8775	75.6413	171.3	0.799	1.048	18.015	360.650	765.340	61071.4
1985	79.56	403.02	91.0	60.0	276.02	82.6542	4.0904	4.1454	342.6347	191.5	4.346	0.879	55.873	693.486	438.543	116552.2
2000	17.08	395.87	93.0	53.0	304.12	79.9906	7.9161	7.9711	637.6131	228.8	7.009	0.878	115.266	996.555	346.424	167505.0
2000	20.88	383.73	89.5	46.0	345.26	76.9382	11.4008	11.4558	881.3886	265.1	10.062	0.914	196.368	1275.298	304.345	214873.0
1995	22.68	397.40	89.5	39.0	388.13	73.6039	14.6036	14.6586	1078.9301	300.9	13.396	0.960	256.765	1423.163	291.449	240389.1
1990	43.84	373.66	93.0	45.5	414.78	71.3036	16.3032	16.3582	1166.3985	322.0	15.696	0.990	299.553	1513.696	278.969	254402.6
2000	18.98	386.59	94.5	40.6	422.27	69.7831	17.3438	17.3988	1214.1422	338.1	17.217	1.031	393.429	1699.562	266.267	285640.7
2000	18.98	384.91	93.0	35.5	452.54	66.8605	19.4802	19.5352	1306.1332	365.2	20.140	1.213	442.670	1661.961	290.694	278624.6
2005	19.05	376.72	87.0	27.0	483.12	63.8272	19.0480	19.1030	1219.2910	396.3	23.173	1.173	641.194	2033.860	245.545	344408.3
1995	22.79	388.99	92.0	28.5	499.40	59.5724	23.3227	23.3777	1392.6657	415.2	27.428	1.421	795.90178	2058.94	168.37	344319.1
2010	32.29	198.45	82.5	62.5	346.66	53.3694	23.6110	23.6660	1263.0402	423.6	33.6306	1.421	795.90178	2058.94		

Table B.4: Engine Data - 2000rpm

Date: 29/4/2008

Sea Level

RPM	ST	ET	SL	EL	FC (g/h)	Av. Volts	Av. Curr.	Adj. Curr.	Power (W)	EGT (C)	DV	R(Alt)	P(Alt) W	Total P	Efficiency	Pm[Pa]
2065	24.78	148.38	95.5	84.5	256.29	93.1608	-0.0550	0.0000	0.0000	104.8	0.000	1.824	0.000	0.000	2835.435	13898.268
2060	23.12	405.12	95.0	62.5	245.03	91.4684	0.8726	0.9276	84.8461	111.8	1.692	1.824	1.570	86.416	663.459	65833.806
2095	4.35	406.36	93.5	55.5	272.23	88.3812	4.3494	4.4044	399.2662	133.8	4.780	1.085	21.051	410.317	425.221	125704.713
2090	22.80	408.42	94.0	49.5	332.35	84.5183	8.3348	8.3898	709.0916	157.8	8.643	1.030	72.509	781.600	338.324	180965.143
2100	32.61	420.31	95.5	44.0	382.57	81.7113	12.0628	12.1378	991.7954	181.2	11.450	0.943	138.972	1130.767	292.927	211949.461
2095	15.24	405.98	93.0	40.5	386.96	79.3275	14.1248	14.1798	1124.8481	193.9	13.833	0.976	196.153	1321.002	287.101	228998.275
2090	24.71	435.24	95.0	36.5	410.40	77.2654	15.2889	15.3439	1185.5526	200.2	15.895	1.036	243.897	1429.450	266.896	259254.330
2075	32.30	389.58	95.5	42.5	427.14	75.0861	17.1240	17.1790	1289.9041	210.4	18.075	1.052	310.505	1600.409	261.928	268327.618
2095	15.21	393.26	93.0	35.5	438.04	74.0677	17.8966	17.9516	1329.6337	213.8	19.093	1.064	342.752	1672.385	250.405	293138.692
2090	24.74	419.12	95.5	33.0	456.40	71.8094	19.5097	19.5647	1404.9284	222.8	21.351	1.091	417.734	1822.663	240.660	307552.274
2095	30.62	442.67	90.5	24.5	461.31	70.5310	20.5208	20.5758	1451.2317	228.5	22.630	1.100	465.626	1916.858	228.471	347179.484
2105	19.06	401.72	95.5	29.5	496.73	68.2692	23.2828	23.3378	1593.2529	243.7	24.892	1.067	580.915	2174.168		

Altitude

RPM	ST	ET	SL	EL	FC (g/h)	Av. Volts	Av. Curr.	Adj. Curr.	Power (W)	EGT (C)	DV	R(Alt)	P(Alt) W	Total P	Efficiency	Pm[Pa]
2080	32.05	120.94	97.0	88.0	291.57	89.2000	-0.0550	0.0000	0.0000	158.3	0.000	1.301	0.000	0.000	3314.903	12788.5
2100	26.38	379.79	88.0	55.5	264.85	88.0350	0.8407	0.8957	78.8529	167.4	1.165	0.776	1.043	79.896	763.781	60738.0
2110	28.48	399.35	93.0	55.5	291.20	85.8815	4.2193	4.2743	367.0833	202.3	3.319	0.776	14.184	381.268	441.063	117133.4
2110	28.36	436.87	95.5	49.5	324.30	82.9883	8.1890	8.2430	684.0726	240.0	6.212	0.754	51.203	735.276	343.316	168471.3
2100	17.44	436.85	95.0	42.0	361.35	79.3853	11.7446	11.7996	936.7148	276.2	9.815	0.832	115.810	1052.524	312.335	197535.9
2080	26.55	399.96	92.5	43.0	381.78	76.6195	13.6485	13.7035	1049.9553	295.8	12.581	0.918	172.397	1222.352	300.911	214267.4
2080	30.39	402.15	93.5	42.0	398.97	74.8548	14.8092	14.8642	1112.6567	309.8	14.345	0.965	213.230	1325.887	281.702	239812.1
2075	32.50	401.97	94.5	41.0	417.03	72.4833	16.5413	16.5963	1202.9546	331.2	16.717	1.007	277.435	1480.390	279.426	248598.2
2080	51.56	393.27	96.5	45.5	429.85	71.1361	17.1908	17.2458	1226.7990	345.7	18.064	1.047	311.526	1538.325	273.383	272467.6
2070	30.41	378.87	96.5	41.0	458.72	69.0012	18.7558	18.8108	1297.9678	369.0	20.199	1.074	379.956	1677.923	269.204	283331.1
2090	28.67	393.04	98.0	38.0	474.25	67.6999	19.6948	19.7498	1336.4670	384.3	21.530	1.090	425.215	1761.682	261.96	317703.6
2105	23.25	360.33	94.5	33.5	521.19	65.2128	22.2497	22.3047	1454.5519	425.0	23.9872	1.0754	535.0273	1989.58		

Table B.5: Engine Data - 2100rpm

Date: 5/3/2006		Sea Level																
RPM	ST	ET	SL	EL	FC (g/h)	Av. Volts	Av. Curr.	Adj. Curr.	Power (W)	EGT (C)	Eff (load)	DV	R(Air)	P(Air)W	Total P	Efficiency	Pm(Pa)	Alt Eff
2215	23.104	151.839	93	82.5	234.901	98.289	-0.055	0	0.000	104.1	2723.859	2.130	0.000	0.000	0.000	2664.842	14544.386	0.978
2195	26.712	415.586	90	65	253.086	96.1594	0.9113	0.9663	92.919	111.8	1026.105	4.093	2.204	2.058	64.977	983.484	42659.319	0.958
2195	30.764	414.456	84.5	58	273.970	94.2064	2.7792	2.8342	267.000	123	783.940	5.915	1.285	1.571	278.571	736.763	69110.157	0.940
2200	23.174	403.421	85.5	51.5	333.257	92.374	4.547	4.802	425.105	134.8	783.940	9.988	1.140	87.496	860.692	369.800	132150.260	0.898
2160	21.09	431.26	93	44	344.052	88.3007	8.7048	8.7588	773.488	160.4	444.802	9.988	1.140	87.496	860.692	317.214	189509.004	0.863
2195	21.241	428.416	95	39.5	392.559	84.8304	12.5356	12.5906	1066.066	184.5	367.542	13.459	1.069	168.452	1237.517	276.450	243122.627	0.822
2180	25.236	401.838	96	39	435.898	80.8234	15.9872	16.0422	1296.585	204	336.189	17.466	1.069	280.187	1576.772	276.450	243122.627	0.822
2205	38.365	459.371	83	24.5	468.592	78.4268	18.9264	18.9844	1486.886	222.8	314.727	19.682	1.046	377.072	1865.956	251.127	284450.190	0.798
2195	24.946	415.968	93.5	26	497.159	74.2314	21.59	21.645	1608.739	236.1	309.421	24.056	1.111	520.727	2127.465	233.688	325792.447	0.755
2205	21.571	401.307	93.5	23.5	530.695	71.2701	24.3129	24.3679	1736.703	253.1	305.691	27.019	1.109	659.394	2395.097	221.659	365113.134	0.725
2195	25.056	445.53	98.5	15.5	554.802	68.0265	26.5728	26.6278	1811.396	265.3	306.284	30.263	1.137	805.824	2617.220	211.982	400791.980	0.692
2220	21.14	418.993	97.5	17	582.728	65.268	29.7768	29.8316	1947.062	278.6	299.286	33.021	1.107	965.076	2932.136	196.738	443960.601	0.664
Mean																		
Altitude																		
Date: 5/3/2006		Altitude																
RPM	ST	ET	SL	EL	FC (g/h)	Av. Volts	Av. Curr.	Adj. Curr.	Power (W)	EGT (C)	Eff (load)	DV	R(Air)	P(Air)W	Total P	Efficiency	Pm(Pa)	Alt Eff
2200	11.637	239.785	94.5	75	246.178	91.98	-0.0548	0	0.000	169.8	3142.885	0.420	0.435	0.400	86.992	3128.504	13485.119	0.995
2215	23.119	447.854	95.5	54.5	278.005	91.5597	0.9113	0.9661	98.450	181.8	1105.522	0.870	0.917	2.368	252.549	1095.067	38325.320	0.991
2215	23.6008	403.781	91	54.5	276.559	91.1102	2.6008	2.7457	250.161	201.1	1105.522	0.870	0.917	2.368	252.549	1095.067	38325.320	0.991
2205	23.073	430.639	95	52.5	300.316	89.147	4.3926	4.4474	396.472	217	757.479	2.833	0.637	12.599	409.072	734.148	82356.702	0.969
2205	21.05	420.264	93.5	48	342.848	86.2099	8.5084	8.5832	738.233	256.7	484.148	5.770	0.674	49.411	787.643	435.029	120069.839	0.937
2195	60.316	466.07	95.5	39	361.380	82.3151	12.1829	12.2437	1007.641	294.6	378.419	9.065	0.789	118.334	1128.176	338.656	172458.494	0.895
2175	23.354	335.342	92.5	50.5	367.707	76.3875	13.6183	13.6731	1044.591	315.8	371.157	15.583	1.140	213.081	1257.852	306.279	194363.255	0.831
2195	55.12	445.391	93.5	34.5	435.380	79.0657	15.053	15.7078	1242.262	336.7	350.481	12.694	0.821	202.541	1444.803	301.349	221252.035	0.860
2190	19.117	446.031	90.5	21.5	465.480	75.1854	18.1474	18.2022	1368.540	369	340.129	16.795	0.923	306.698	1874.238	278.026	256972.235	0.817
2200	19.268	402.86	93	24	516.077	71.8312	20.9021	20.9589	1505.359	405.4	344.155	20.149	0.961	422.256	1927.616	268.768	294517.290	0.781
Mean																		
0.897																		

Table B.6: Engine Data - 2200rpm (First Test)

Date: 9/4/2008 to 10/4/2008																	Sea Level																
RPM	ST	ET	SL	EL	FC (g/h)	Av. Volts	Av. Curr.	Adj. Curr	Power (W)	EGT (C)	DV	R(Alt)	P(Alt)W	Total P	Efficiency	Pm(Pa)																	
2220	33.05	262.14	93.0	77.0	201.14	97.6500	-0.0505	0.0000	0.0000	124.0	0.000	0.000	0.000	0.000																			
2225	26.99	434.28	95.0	62.5	229.81	96.3820	0.9306	0.9811	94.5604	123.5	1.268	1.292	1.244	95.804	2398.759	14473.332																	
2200	43.40	460.56	90.5	53.5	255.44	94.8088	2.8115	2.8620	271.3428	133.6	2.841	0.993	8.132	279.474	914.007	42700.428																	
2185	32.60	424.16	89.0	49.5	290.53	93.1048	4.6087	4.6592	433.7939	144.5	4.545	0.976	21.177	454.971	638.569	69991.482																	
2165	21.07	430.20	89.5	39.5	351.97	89.5510	8.8940	8.9445	800.9889	171.5	8.099	0.905	72.442	873.430	402.970	135607.417																	
2200	19.34	445.66	81.5	20.0	415.46	87.8139	12.9801	13.0306	1144.2678	200.1	9.836	0.755	128.170	1272.438	326.509	194413.765																	
2190	19.35	450.10	90.5	21.5	461.33	84.0571	16.5654	16.6159	1396.6844	222.1	13.593	0.818	225.858	1622.543	284.328	249037.663																	
2175	38.93	407.54	93.0	22.0	554.73	85.5097	20.6530	20.7035	1770.3501	241.6	12.140	0.586	251.347	2021.697	274.360	312442.272																	
2175	109.45	417.25	90.0	21.0	645.61	79.6839	27.1646	27.2151	2168.6053	286.0	17.966	0.660	488.949	2657.555	242.935	410710.637																	
2210	15.45	315.80	93.0	14.0	757.52	71.1127	35.1173	35.1678	2500.8772	337.4	26.537	0.755	933.258	3434.136	220.584	522321.863																	

Date: 10/4/2008																	Altitude																
RPM	ST	ET	SL	EL	FC (g/h)	Av. Volts	Av. Curr.	Adj. Curr	Power (W)	EGT (C)	DV	R(Alt)	P(Alt)W	Total P	Efficiency	Pm(Pa)																	
2117	72.63	247.0	90.5	64.0	437.64	102.1864	-0.0548	0.0000	0.0000	193.0	0.000	0.000	0.000	0.000																			
2240	34.34	399.06	64.0	20.5	343.50	101.9636	0.9855	1.0403	106.0727	192.2	0.223	0.214	0.232	106.305	3231.249	15952.058																	
2225	52.66	460.90	96.0	44.0	366.93	99.0967	2.9372	2.9920	296.4973	209.0	3.090	1.033	9.244	305.742	1200.140	46188.909																	
2210	26.75	402.25	92.0	48.0	337.47	96.4054	4.7689	4.8237	465.0307	224.5	5.781	1.198	27.886	492.917	684.639	74971.145																	
2190	28.95	422.80	93.0	41.5	376.59	91.4349	9.0750	9.1298	834.7824	266.2	10.752	1.178	98.159	932.941	403.659	143193.491																	
2170	27.04	427.27	92.0	32.5	428.15	86.9289	12.8449	12.8997	1121.3567	311.0	15.258	1.183	196.817	1318.174	324.808	204186.021																	
2190	67.37	448.92	98.5	33.0	494.40	83.3780	16.4329	16.4877	1374.7115	360.9	18.808	1.141	310.107	1694.819	293.447	258596.172																	
2160	28.76	352.36	95.0	35.0	533.99	78.7126	19.0273	19.0821	1502.0017	395.0	23.474	1.230	447.929	1949.931	273.852	303443.994																	
2290	36.41	198.29	92.0	52.5	702.74	79.0776	22.9639	23.0187	1820.2636	480.8	23.109	1.004	531.935	2352.198	298.760	345264.113																	

High rpm

*High rpm

Table B.7: Engine Data - 2200rpm (Second Test)

Date: 23/4/2008

Sea Level

RPM	ST	ET	SL	EL	FC (g/h)	Av. Volts	Av. Curr.	Adj. Curr	Power (W)	EGT (C)	DV	R(Alt)	P(Alt)W	Total P	Efficiency	Pm[Pa]
2420	22.78	122.40	94.0	85.0	260.20	104.1570	-0.0550	0.0000	0.0000	117.9	0.000	0.000	0.000	0.000		15013.779
2400	23.00	386.20	85.0	52.0	261.88	102.0349	0.9742	1.0292	105.9143	125.4	2.122	2.062	2.184	107.198	2441.079	43920.188
2390	17.32	381.86	93.5	56.5	292.31	99.8544	2.9432	2.9982	299.3835	138.1	4.303	1.435	12.900	312.284	938.042	71690.017
2390	17.17	380.88	95.5	55.0	320.87	98.0981	4.8389	4.8939	480.0872	150.0	6.058	1.238	29.647	508.734	829.483	98469.037
2385	28.68	390.32	92.0	48.0	348.47	96.1961	6.6528	6.7079	645.2738	161.9	7.961	1.187	53.401	698.675	498.784	135825.654
2395	25.12	392.98	94.5	45.5	383.61	94.0037	9.2365	9.2915	873.4354	180.0	10.153	1.093	94.339	967.775	396.389	161617.654
2390	24.94	391.52	95.0	43.0	408.53	92.6001	10.9778	11.0328	1021.6384	190.6	11.557	1.048	127.505	1149.143	355.504	195210.602
2390	19.33	404.54	90.0	31.0	441.11	89.8024	13.2710	13.3260	1196.7068	205.0	14.355	1.077	191.289	1387.996	317.800	217095.987
2390	22.92	382.74	91.5	33.0	466.24	88.0550	14.7850	14.8200	1304.9751	214.5	16.102	1.087	238.632	1543.607	303.340	248608.530
2395	13.46	374.89	92.5	31.0	490.05	85.6372	16.9517	17.0067	1456.4062	228.3	18.520	1.089	314.961	1771.367	276.653	292348.604
2390	17.20	379.68	94.0	27.5	528.34	82.3813	19.9021	19.9571	1644.0918	247.0	21.776	1.091	434.580	2078.672	254.174	335693.082
2415	23.12	360.12	92.5	23.5	589.85	76.5349	23.1214	23.1764	1843.3327	268.8	24.622	1.062	570.652	2413.984	244.276	

Altitude

RPM	ST	ET	SL	EL	FC (g/h)	Av. Volts	Av. Curr.	Adj. Curr	Power (W)	EGT (C)	DV	R(Alt)	P(Alt)W	Total P	Efficiency	Pm[Pa]
2400	24.97	157.22	89.0	78.0	239.55	101.7366	-0.0550	0.0000	0.0000	192.7	0	0.00	0.00	0.00		14586.521
2400	26.46	383.03	78.0	36.5	335.19	100.9794	0.9697	1.0237	103.3726	206.9	0.7572	0.7397	0.78	104.15	3216.4	42585.458
2400	18.91	382.51	92.5	47.5	358.43	99.4026	2.9337	2.9887	297.0846	229.7	2.334	0.781	6.976	304.060	1172.2	69495.767
2400	17.03	412.65	95.0	45.0	363.99	97.7750	4.8223	4.8773	476.8780	249.6	3.962	0.812	19.322	496.200	733.5	95571.885
2410	18.99	373.27	93.5	46.5	382.07	96.5516	6.6803	6.7353	650.3040	272.3	5.185	0.770	34.923	885.227	557.6	131606.409
2400	13.44	410.29	93.0	38.0	399.14	93.0998	9.1813	9.2363	859.8977	293.9	8.637	0.935	79.772	939.670	424.8	154254.914
2400	17.11	383.40	89.5	37.5	409.88	90.9230	10.7709	10.8258	984.3142	310.5	10.814	0.899	117.066	1101.380	371.2	187343.283
2390	17.11	387.53	95.0	37.5	447.07	88.1795	13.0382	13.0832	1154.5125	335.1	13.560	1.036	177.545	1332.058	335.6	207966.249
2380	19.15	385.48	91.5	33.5	455.97	85.9475	14.4187	14.4737	1243.9783	349.6	15.769	1.091	228.527	1472.505	309.7	237389.007
2370	19.25	378.44	93.0	32.5	465.08	82.7731	16.3970	16.4520	1361.7830	370.8	18.964	1.153	311.988	1673.771	289.8	279390.218
2395	19.02	386.10	92.0	22.5	545.28	80.7894	19.5121	19.5671	1580.8143	412.0	20.947	1.071	409.876	1990.690	273.9	307567.848
2415	21.07	361.14	96.0	28.5	571.65	74.4703	21.6654	21.7204	1617.5247	437.4	27.266	1.255	592.235	2208.760	258.7	

Table B.8: Engine Data - 2400rpm

Date: 28/4/2008

Sea Level

RPM	ST	ET	SL	EL	FC(g/h)	Av. Volts	Av. Curr.	Adj. Curr.	Power (W)	EGT (C)	DV	R(Alt)	P(Alt)W	Total P	Efficiency	Pm[Pa]
2620	22.74	188.48	92.5	75.0	304.13	115.4817	-0.0551	0.0000	0.0000	122.5	0.000	2.229	0.000	0.000		
2610	24.73	395.97	96.0	55.5	314.19	112.9185	1.0858	1.1409	128.8287	129.6	2.543	2.229	2.902	131.730	2385.084	16965.164
2580	20.93	391.91	95.5	51.5	341.56	109.8095	3.2428	3.2880	362.4815	143.0	5.552	1.684	18.311	380.793	887.021	49416.900
2585	22.91	391.07	92.5	45.5	367.67	107.5282	5.2960	5.3511	575.3942	157.6	7.934	1.483	42.453	617.847	595.078	80340.309
2590	30.43	408.33	97.0	44.0	403.82	105.4538	7.2818	7.3368	773.7040	171.3	10.008	1.364	73.427	847.131	476.814	109842.046
2595	17.23	378.39	92.0	36.5	442.56	102.1625	10.0505	10.1056	1032.4134	189.8	13.299	1.316	134.396	1166.810	379.293	151138.713
2600	36.69	401.28	95.5	35.5	473.99	100.6294	11.8937	11.9488	1202.4006	201.6	14.832	1.241	177.228	1379.629	343.564	178361.831
2600	26.58	385.71	95.5	34.0	493.20	97.6310	13.5300	13.5851	1329.0439	213.5	17.831	1.298	239.515	1568.559	314.427	202787.168
2605	35.39	393.09	93.0	30.5	503.22	96.7132	14.3524	14.4075	1393.3654	218.8	18.749	1.301	270.119	1663.514	302.506	214650.487
2595	18.36	386.92	88.0	30.0	453.22	95.1060	16.0013	16.0564	1527.0600	228.8	20.358	1.288	326.839	1853.899	244.470	240138.500
2590	24.78	396.14	96.5	26.0	546.74	92.6556	17.4437	17.4988	1621.3618	238.3	22.808	1.303	399.079	2020.441	270.606	262216.177
2610	30.70	414.94	97.0	15.0	614.63	89.9118	21.5313	21.5864	1927.9202	265.3	26.150	1.211	564.482	2492.402	248.600	320889.400

Altitude

RPM	ST	ET	SL	EL	FC(g/h)	Av. Volts	Av. Curr.	Adj. Curr.	Power (W)	EGT (C)	DV	R(Alt)	P(Alt)W	Total P	Efficiency	Pm[Pa]
2600	24.62	117.95	97.0	63.5	416.57	108.3114	-0.0550	0.0000	0.0000	226.9	0	0.3663	0.3629	0.00		
2600	18.04	373.39	95.5	48.5	386.25	107.9151	1.0371	1.0921	117.8541	240.0	0.3663	0.3629	0.43	118.29	3366.8	15292.421
2595	22.74	380.35	95.5	44.5	410.73	106.5363	3.1444	3.1984	340.8522	262.7	1.775	0.555	5.679	346.531	1185.3	44886.772
2600	26.49	377.36	96.0	44.0	426.79	105.1260	5.1823	5.2373	550.5869	286.7	3.183	0.608	16.672	567.259	752.4	73336.890
2605	24.88	408.60	93.5	35.5	435.32	103.3882	7.1417	7.1967	744.0539	308.2	4.923	0.684	35.431	779.485	558.5	100580.287
2600	20.81	401.33	92.0	31.0	461.81	100.2115	9.8653	9.9203	994.1261	337.4	8.100	0.816	80.353	1074.482	429.6	138911.646
2600	24.67	392.62	95.0	33.5	481.37	97.7090	11.5560	11.6110	1134.4992	358.3	10.602	0.913	123.104	1257.604	382.8	162586.124
2590	24.68	384.22	92.0	30.0	496.80	94.8708	13.1185	13.1715	1249.8711	372.0	13.435	1.020	178.953	1426.624	348.1	185149.555
2570	24.62	390.71	92.5	30.0	491.67	92.9740	13.7432	13.7982	1282.8738	375.2	15.337	1.112	211.629	1494.502	329.0	195468.379
2570	24.61	369.48	94.5	33.5	509.40	90.7225	15.2046	15.2596	1384.3991	387.7	17.589	1.153	268.400	1652.789	308.2	216170.897
2565	20.89	362.50	95.0	33.5	518.49	88.9269	16.9536	16.986	1466.9862	402.0	19.985	1.203	331.915	1796.901	288.2	235739.770
2590	19.20	372.06	93.5	23.5	571.34	81.4632	19.6553	19.7103	1605.6641	431.1	26.848	1.362	529.188	2134.850	267.8	277064.364

Table B.9: Engine Data - 2600rpm

Date: 10/4/2008

Sea Level

RPM	ST	ET	SL	EL	FC (g/h)	Av. Volts	Av. Curr.	Adj. Curr.	Power (W)	EGT (C)	DV	R(AH)	P(AH) W	Total P	Efficiency	Pm(Pa)
2820	28.75	214.85	94.0	74.0	309.51	123.8265	-0.0549	0.0000	0.0000	138.5	0.000	0.000	0.000	0.000		
2805	19.63	412.35	74.0	30.0	322.67	123.2297	1.1973	1.2522	154.3082	146.4	0.597	0.477	0.747	155.056	2081.013	18580.931
2790	17.75	431.50	94.0	41.0	368.92	120.1263	3.5687	3.6136	434.0884	161.6	3.700	1.024	13.371	447.459	824.473	53909.152
2780	19.82	419.06	96.5	38.5	418.41	119.0365	5.8726	5.9275	705.6889	179.0	4.790	0.808	28.393	733.982	570.049	88428.852
2755	30.80	432.82	92.5	22.0	505.05	112.4330	11.1224	11.1773	1256.6974	216.9	11.394	1.019	127.349	1384.046	364.908	168865.889
2795	19.34	409.86	93.5	11.0	608.42	108.9861	16.0489	16.1038	1755.0904	253.4	14.840	0.922	238.987	1954.077	305.113	239813.255
2760	30.45	461.27	95.0	10.0	642.84	104.5011	18.4797	18.5346	1936.8891	267.4	19.325	1.043	358.189	2295.075	260.096	279512.197
2760	23.86	389.45	96.0	11.0	669.60	102.0086	20.6310	20.6859	2110.1397	278.6	21.818	1.055	451.323	2561.463	261.414	311955.011
2760	29.02	362.04	96.5	15.0	704.82	98.2686	22.2718	22.3267	2193.7903	283.7	25.568	1.145	570.847	2764.637	254.942	336699.198
2780	31.75	350.17	96.0	14.0	741.66	96.5884	23.8190	23.8759	2305.9418	305.9	27.238	1.141	650.280	2956.221	250.882	357441.688
2840	21.21	236.12	91.5	24.0	896.22	91.7417	31.2459	31.3008	2871.5886	361.3	32.085	1.025	1004.280	3875.869	231.232	458736.952
2800	26.98	251.22	95.0	24.5	905.46	84.1855	32.7737	32.8286	2763.6921	375.9	39.641	1.208	1301.359	4065.051	222.742	488001.277

Date: 11/4/2008

Altitude

RPM	ST	ET	SL	EL	FC (g/h)	Av. Volts	Av. Curr.	Adj. Curr.	Power (W)	EGT (C)	DV	R(AH)	P(AH) W	Total P	Efficiency	Pm(Pa)
2775	38.62	183.45	64.0	35.0	576.68	126.7393	-0.0549	0.0000	0.0000	275.5	0	0	0.00	0.00		
2775	34.92	460.10	90.5	20.0	477.54	125.4397	1.2186	1.2735	159.7475	266.0	1.3996	1.0205	1.66	161.40	2958.7	19550.809
2780	21.36	443.96	93.0	18.5	507.71	121.9471	3.6119	3.6668	447.1556	295.1	4.792	1.307	17.572	464.728	1092.5	56191.000
2770	53.88	428.68	92.5	29.5	454.10	118.6614	5.8661	5.9210	702.5941	328.2	8.078	1.364	47.829	760.423	845.1	91052.512
2760	34.36	427.25	96.0	19.0	554.43	112.1319	11.0894	11.1443	1249.6315	400.4	14.607	1.311	162.789	1412.421	399.6	172015.684
2760	28.60	385.25	90.0	23.0	541.03	104.0695	12.1918	12.2467	1274.5079	443.5	22.670	1.851	277.630	1552.138	348.5	189031.666
2720	41.93	401.60	94.5	14.5	640.69	104.4997	15.4048	15.4597	1615.6340	469.4	22.240	1.439	343.818	1959.352	326.9	242134.399
2760	34.40	453.25	100.0	1.0	680.72	101.6256	17.9684	18.0233	1831.6287	522.9	25.114	1.393	452.632	2284.260	298.0	275193.752
2730	40.74	392.23	91.5	19.0	584.04	98.6415	15.4915	15.5464	1533.5202	472.3	28.098	1.807	436.820	1970.340	301.5	242600.407
2835	30.63	86.26	95.0	79.0	828.33	101.6767	17.2998	17.3547	1764.5666	528.0	25.063	1.444	434.954	2199.523	376.6	250788.467
2790	486.32	747.70	92.0	8.5	920.04	110.0777	7.6951	7.6500	842.0944	399.0	16.862	2.178	127.461	969.556	643.9	116810.415
2760	28.60	385.25	90.0	23.0	541.03	104.0695	12.1918	12.2467	1274.5079	443.5	22.67	1.851	277.63	1652.14	343.6	189031.666

Table B.10: Engine Data - 2800rpm

Sea Level																
RPM	ST	ET	SL	EL	FC (g/h)	Av. Volts	Av. Curr.	Adj. Curr.	Power (W)	EGT (C)	DV	R(Alt)	P(Alt)W	Total P	Efficiency	Pm(Pa)
3015	24.69	108.44	83.0	71.5	395.46	133.3593	-0.0591	0.0000	0.0000	139.2	0.000	2.570	4.428	0.000	2192.845	19678.752
2990	43.61	403.75	94.5	46.5	383.85	129.9857	1.2535	1.3126	170.6192	148.3	3.374	2.570	4.428	175.047	2192.845	19678.752
3000	24.53	369.90	93.5	45.5	400.26	128.4048	2.4886	2.5477	327.1369	159.0	4.955	1.945	12.623	339.759	1178.064	38068.290
3005	22.78	373.52	95.0	42.0	435.20	125.4752	4.9054	4.9645	622.9216	177.3	7.884	1.588	39.141	662.062	657.342	74057.215
3000	22.90	421.49	95.0	32.5	451.60	123.1693	6.2473	6.1004	751.3820	186.0	10.190	1.670	62.163	813.545	555.101	91153.516
3000	24.83	398.73	96.0	33.5	494.64	120.2674	8.0789	8.3380	1002.7896	201.6	13.092	1.570	109.160	1111.950	444.837	124598.218
3005	22.84	383.92	91.5	28.5	531.96	117.5213	10.4414	10.5005	1237.1826	218.0	15.538	1.480	163.157	1400.339	379.877	156639.699
3000	17.17	360.78	94.0	28.5	549.00	116.3896	11.4196	11.4787	1336.0013	224.0	16.970	1.478	194.790	1530.791	358.637	171517.243
2985	19.17	423.46	92.5	9.0	594.82	114.5611	12.3947	12.4538	1426.7210	230.0	18.798	1.509	234.109	1660.830	358.146	187022.513
2990	17.22	368.75	91.0	21.5	569.40	112.9707	13.3282	13.3873	1512.3727	235.0	20.389	1.523	272.948	1785.321	318.936	200704.978
2990	29.67	357.80	93.5	21.0	636.35	112.0618	14.3673	14.4264	1616.6484	243.0	21.298	1.476	307.246	1923.895	330.761	216283.365
2980	15.32	290.12	92.0	32.5	623.59	108.7543	16.0821	16.1412	1755.4249	254.1	24.605	1.524	397.154	2152.579	289.695	242804.031
Altitude																
RPM	ST	ET	SL	EL	FC (g/h)	Av. Volts	Av. Curr.	Adj. Curr.	Power (W)	EGT (C)	DV	R(Alt)	P(Alt)W	Total P	Efficiency	Pm(Pa)
3015	15.52	121.68	88.5	72.5	434.09	129.0000	-0.0555	0.0000	0.0000	320.2	0	2.9929	2.3633	0.00	3247.4	18334.827
2995	28.35	370.36	98.5	35.5	530.51	126.0071	1.2109	1.2664	159.5754	331.9	2.9929	2.3633	3.79	163.37	3247.4	18334.827
3000	22.42	400.92	93.0	24.5	521.22	124.7975	2.4193	2.4748	308.8489	343.0	4.203	1.698	10.400	319.249	1632.6	35770.218
3010	15.25	392.78	93.0	22.5	537.82	122.0466	4.7738	4.8293	589.3996	369.0	6.953	1.440	33.580	622.980	863.3	69569.748
2985	32.28	360.40	91.5	19.0	636.35	121.2007	5.9314	5.9869	725.6165	373.6	7.799	1.303	46.694	772.310	824.0	86968.185
2990	20.93	365.08	93.0	28.0	543.96	118.6840	8.1560	8.2115	974.5737	397.2	10.316	1.256	84.710	1059.284	513.5	119084.174
3005	25.94	318.70	93.5	35.5	569.79	115.6974	10.2505	10.3060	1192.3774	427.0	13.303	1.291	137.097	1329.474	428.6	148712.818
2995	17.19	322.65	92.0	31.5	570.40	113.4699	11.1458	11.2013	1271.0104	440.6	15.530	1.386	173.957	1444.968	394.8	162171.429
2985	15.16	302.59	92.5	34.5	581.16	111.0886	12.0129	12.0684	1340.6617	455.2	17.911	1.484	216.162	1556.824	373.3	175310.570
2975	15.24	321.27	95.0	32.0	592.88	108.6857	12.8301	12.8856	1400.4805	465.8	20.314	1.577	261.762	1662.242	356.7	188126.916
2970	25.20	230.34	96.5	52.0	624.73	107.9235	13.3985	13.3041	1391.9618	464.0	25.077	1.872	335.877	1727.259	361.6	195292.247

Table B.11: Engine Data - 3000rpm

Date: 5/4/2008 Sea Level													
RPM	ST	ET	SL	EL	FC (g/h)	Av Volts	Av Curr	Adj Curr	Power (W/EGT/C)	DV	R	P (Alt)	Total Pow Efficiency Pm(Pa)
3220	22.62	143.52	96.00	80.00	381.16	140.8171	-0.0563	0.0000	0.00	146.4	0.000	0.000	
3200	23.84	367.13	97.50	50.00	398.50	138.4697	1.3380	1.3943	193.07	157.3	2.347	1.664	3.273 195.341 2029.649 20624.1
3195	22.99	437.63	94.50	24.00	489.68	132.4895	6.4780	6.5343	895.70	196.8	8.332	1.275	54.441 920.141 532.182 96904.7
3195	24.76	323.44	95.50	37.50	559.26	127.3821	10.0548	10.1111	1287.97	224.0	13.435	1.329	136.843 1423.816 392.790 149794.5
3175	15.80	214.27	96.00	54.00	609.48	124.2358	12.1779	12.2342	1519.93	238.3	16.581	1.355	202.859 1722.785 353.775 182389.7
Date: 5/4/2008 Altitude													
RPM	ST	ET	SL	EL	FC (g/h)	Av Volts	Av Curr	Adj Curr	Power (W/EGT/C)	DV	R	P (Alt)	Total Pow Efficiency Pm(Pa)
3195	22.64	150.73	94.50	63.50	697.04	138.6500	-0.0547	0.0000	0.00	422.0	0.000		
3190	24.05	310.14	97.00	34.50	629.18	134.6008	1.3027	1.3574	182.71	439.3	6.216	4.580	8.438 191.145 3291.648 20141.2
3185	25.99	328.06	99.00	30.00	657.85	129.2463	6.3255	6.3802	624.62	490.7	11.571	1.814	73.824 898.441 732.212 94816.5
3200	26.16	330.44	95.50	23.00	686.21	124.7794	9.8347	9.8894	1233.99	541.5	16.039	1.622	168.603 1392.597 492.759 146281.2
3185	26.24	309.98	92.00	21.50	715.69	120.8922	11.8585	11.9132	1440.21	563.3	18.925	1.673	237.369 1677.582 426.560 177046.5
3200	26.01	113.91	91.50	63.50	817.33	108.3167	15.9987	16.0544	1738.96	617.6	32.500	2.024	521.774 2260.734 405.768 237472.1

Table B.12: Engine Data - 3200rpm (First Test)

Date: 10/4/2008

Sea Level

RPM	ST	ET	SL	EL	FC(gph)	Av. Volts	Av. Curr.	Adj. Curr.	Power(W)	EGT (C)	DV	R	P (Alt)	Total Pow	Efficiency	Pmp(Pa)
3215	28.22	164.12	95.00	70.00	529.50	139.1700	0.0546	0.0000	0.00	170.6	0.000					
3220	34.68	345.36	97.00	54.00	398.58	137.9900	1.3299	1.3847	191.07	174.2	1.180	0.852	1.634	192.709	2068.323	20115.8
3220	44.18	397.28	93.50	40.50	432.29	137.3526	2.6701	2.7249	374.27	184.5	1.617	0.667	4.952	378.224	1139.920	39687.1
3220	38.86	390.75	95.00	38.00	466.51	136.3516	4.0349	4.0907	557.64	193.0	2.916	0.689	11.526	669.164	819.640	59414.7
3210	40.70	392.53	95.50	35.00	485.24	135.3266	6.2977	5.3625	794.34	202.6	3.843	0.718	20.572	744.907	664.833	78000.8
3200	29.00	420.89	94.00	13.50	591.59	133.8518	6.5922	6.6470	889.71	212.6	5.316	0.800	35.350	925.063	639.518	97170.5
3150	31.97	384.65	95.00	30.00	535.61	132.1073	7.8116	7.8666	1039.24	221.1	7.063	0.896	55.659	1094.795	492.153	115359.9
3170	19.33	438.35	94.00	12.00	563.60	130.6417	9.9978	9.0528	1182.65	230.4	8.828	0.942	77.203	1259.850	447.356	133589.6
3160	26.99	375.88	95.00	25.50	582.29	128.1065	10.1326	10.1874	1305.09	238.5	11.062	1.086	112.688	1417.780	410.708	150811.7
3160	13.45	365.13	89.00	11.00	638.94	126.4679	11.2001	11.2649	1433.38	247.5	12.702	1.129	142.961	1566.344	407.921	166614.7
3140	23.07	245.21	94.50	46.00	628.79	124.5542	12.9022	12.3570	1639.12	263.1	14.616	1.183	361.216	1900.331	330.886	203426.9
3270	13.43	203.68	81.50	62.50	439.21	150.8938	-0.0612	0.0000	-0.00	162.4	0.000					
3245	45.74	389.36	62.50	10.00	448.20	146.3276	1.4152	1.4764	216.04	171.5	4.556	0.323	1.410	217.448	2047.406	22524.4
3240	26.46	374.00	97.50	2.00	785.97	127.2110	18.5922	18.6534	2372.92	306.2	23.883	0.788	548.114	2921.032	272.487	303043.0
3230	20.13	222.71	96.00	31.50	916.97	117.4504	33.0619	23.1231	2715.62	335.6	33.443	0.691	739.353	3459.180	265.390	399566.2

Date: 22/4/2008

Altitude

RPM	ST	ET	SL	EL	FC(gph)	Av. Volts	Av. Curr.	Adj. Curr.	Power(W)	EGT (C)	DV	R	P (Alt)	Total Pow	Efficiency	Pmp(Pa)
3340	34.68	138.33	94.50	21.50	2028.36	148.8383	-0.0583	0.0000	0.00	641.0	0.000					
3485	26.60	244.67	97.50	18.50	1043.33	195.0000	1.5046	1.5609	241.94	616.4	6.161	3.947	9.616	251.556	4187.529	24263.0
3290	26.38	265.26	96.00	38.50	637.17	146.4470	-0.0953	0.0000			0.000					
3250	28.35	336.20	94.00	21.00	682.83	142.1912	1.3746	1.4298	203.32	469.4	4.256	2.976	8.085	308.405	3261.295	21657.9
3220	37.91	318.90	96.00	21.50	755.52	134.2042	6.5022	6.5576	860.04	855.2	12.243	1.687	80.352	764.445	784.445	100246.1
3180	32.06	337.70	94.50	17.00	730.27	128.9200	8.8736	8.9288	1148.97	591.6	17.655	1.977	157.640	1307.1	568.477	139217.9

Table B.13: Engine Data - 3200rpm (Second Test)

Appendix C

Published Papers

The following papers on which Hengst is first author are included in their published form:

- **A small, high-efficiency diesel generator for high-altitude use in Antarctica**, 2009, S. Hengst, D. Luong-Van, J.R. Everett, J.S. Lawrence, M.C.B. Ashley, D. Castel and J.W.V. Storey, International Journal of Energy Research, **34**, 827-838
- **PLATO Power—a robust, low environmental impact power generation system for the Antarctic plateau**, 2008, S. Hengst, G.R. Allen, M.C.B. Ashley, J.R. Everett, J.S. Lawrence, D. Luong-Van and J.W.V. Storey, Proc. SPIE, **7013**, 70124E–70124E-10

Refereed papers on which Hengst is a co-author are:

- **The PLATO Dome A site testing observatory: power generation and control systems**, 2009, J.S. Lawrence, M.C.B. Ashley, S. Hengst, D.M. Luong-Van, J.W.V. Storey, H. Yang, X. Zhou, and Z. Zhu, Review of Scientific Instruments, **80**, 064501-1064501-10
- **The PLATO Dome A Site-Testing Observatory: Instrumentation and First Results**, 2009, H. Yang, G. Allen, M.C.B. Ashley, C.S. Bonner, S. Bradley, X. Cui, J.R. Everett, L. Feng, X. Gong, S. Hengst,

J. Hu, Z. Jiang, C.A. Kulesa, J.S. Lawrence, Y. Li, D. Luong-Van, M.J. McCaughrean, A. Moore, C. Pennypacker, W. Qin, R. Riddle, Z. Shang, J.W.S. Storey, B. Sun, N. Suntzeff, N.F.H Tothill, T. Travouillon, C.K. Walker, L. Wang, J. Yan, J. Yang, D. York, X. Yuan, X. Zhang, Z. Zhang, X. Zhou and Z. Zhu, Z., Publications of the Astronomical Society of the Pacific, **121**(876), 174-184

Conference papers on which Hengst is a co-author are:

- **Performance of the autonomous PLATO Antarctic Observatory over two full years**, 2010, D.M. Luong-Van, M.C.B. Ashley, X.Cui, J.R. Everett, L. Feng, X. Gong, S. Hengst, J.S. Lawrence, J.W.V. Storey, L. Wang, H. Yang, J. Yang, X. Zhou and Z. Zhu, Ground-based and Airborne Telescopes III, Proceedings of SPIE, **7733**, 77331T-77331T-8
- **Optical sky brightness at Dome A, Antarctica, from the Nigel experiment**, 2010, G. Sims, M.C.B. Ashley, X. Cui, J.R. Everett, L. Feng, X. Gong, S. Hengst, Z. Hu, J.S. Lawrence, D.M. Luong-van, Z. Shang, J.W.V. Storey, L. Wang, H. Yang, J. Yang, X. Zhou and Zhenxi Zhu, Ground-based and Airborne Telescopes III, Proceedings of the SPIE, **7733**, 77334M-77334M-9
- **Dome A site testing and future plans**, 2010, X. Gong, L. Wang, X. Cui, L. Feng, X. Yuan, M.C.B. Ashley, G. Allen, C.S. Bonner, S.G. Bradley, J.R. Everett, S. Hengst, J. Hu, Z. Jiang, C.A. Kulesa, J.S. Lawrence, Y. Li, D.M. Luong-van, M.J. McCaughrean, A.M. Moore, C. Pennypacker, W. Qin, R. Riddle, Z. Shang, J.W.V. Storey, B. Sun, N. Suntzeff, N.F.H. Tothill, T. Travouillon, C.K. Walker, J. Yan, H. Yang, J. Yang, D.G. York, X. Zhang, Z. Zhang, X. Zhou, Z. Zhu, EAS Publications Series, **40**, 65-72

- **PLATO—a robotic observatory for the Antarctic plateau**, 2010, M.C.B. Ashley, G. Allen, C.S. Bonner, S.G. Bradley, X. Cui, J.R. Everett, L. Feng, X. Gong, X., S. Hengst, J. Hu, Z. Jiang, C.A. Kulesa, J.S. Lawrence, Y. Li, D.M. Luong-van, M.J. McCaughrean, A.M. Moore, C. Pennypacker, W. Qin, R. Riddle, Z. Shang, J.W.V. Storey, B. Sun, N. Suntzeff, N.F.H. Tothill, T. Travouillon, C.K. Walker, L. Wang, J. Yan, H. Yang, J. Yang, D.G. York, X. Yuan, X. Zhang, Z. Zhang, X. Zhou, Z. and Zhu, EAS Publications Series, **40**, 7984
- **The PLATO Antarctic site testing observatory**, 2008, J.S. Lawrence, G.R. Allen. M.C.B. Ashley, C. Bonner, S. Bradley, X. Cui, J. Everett, X. Feng, S. Hengst, J. Hu, Z. Jian, C.A. Kulesa, Y. Li, D. Luong-Van, A.M. Moore, C. Pennypacker, W. Qin, R. Riddle, Z. Shang, J.W.V. Storey, B. Sun, N. Suntzeff, N.F.H. Tothill, T. Travouillon, C.K. Walker, L. Wang, J. Yan, J. Yang, H. Yang, D. York, X. Yuan, X. Zhang, Z. Zhang, X. Zhou and Z. Zhu, , Proceedings of SPIE, **7012**, 701227701227-12
- **Astrophysics from Dome A**, 2007, N.F.H. Tothill, C.A. Kulesa, C.K. Walker, M.C.B. Ashley, C. Bonner, X. Cui, J. Everett, Feng, L., S. Hengst, Hu, J., Jiang, Z., J.S. Lawrence, Li, Y., D. Luong-Van, A. M. Moore, Pennypacker, C., Qin, W., R. Riddle, J.W.V. Storey, Shang, Z., Sun, B., T. Travouillon, L. Wang, Z. Xu, H. Yang, J. Yan, D. York, X. Yuan, and Z. Zhu, EAS Publications Series, **33**, 301306

SHORT COMMUNICATION

A small, high-efficiency diesel generator for high-altitude use in Antarctica

Shane Hengst^{1,*†}, D. M. Luong-Van¹, J. R. Everett¹, J. S. Lawrence^{1,‡}, M. C. B. Ashley¹,
D. Castel^{1,2} and J. W. V. Storey¹

¹*School of Physics, University of New South Wales, Sydney, NSW 2052, Australia*

²*Institut Supérieur de l'Électronique et du Numérique, 20 rue Cuirassé Bretagne, CS 42807-29228 Brest Cedex 2, France*

SUMMARY

We have characterised a small, high-efficiency diesel generator selected to power remote experiments on the Antarctic plateau at altitudes of up to 5000 m. We describe the design of an environmental chamber to simulate these high altitudes and present an experimental investigation of the engine operation at high altitude on Jet A-1, comparing this to the engine's performance at sea level. Although attention must be paid to the provision of adequate cooling, no modification to the engine itself is required. Our final system provides very high reliability and produces 1500 W of electrical power with a fuel consumption of 280 g kWh⁻¹. A bank of ultracapacitors is used to start the engine in the cold environment of Antarctica. We describe the low-temperature operation and survival tests that we performed on the ultracapacitors and the engine. Copyright © 2009 John Wiley & Sons, Ltd.

KEY WORDS: diesel engine; high altitude; antarctica; remote generation

1. INTRODUCTION

The Antarctic plateau is a vast, largely unexplored region in East Antarctica. Most of it is at an elevation of over 3000 m, with Dome A being the highest point at 4093 m. Scientific interest in the Antarctic plateau is growing, both for the historical climate information that can be gained

from deep ice cores [[1], references therein], and the potential it offers for new astronomical observatories with 'space-like' observing conditions [[2], references therein]. Permanent stations now exist at the South Pole (on the edge of the plateau), Vostok and Dome C, with new stations under construction at Dome A and Dome F.

*Correspondence to: Shane Hengst, School of Physics, University of New South Wales, Sydney, NSW 2052, Australia.

†E-mail: shane@phys.unsw.edu.au

‡Present address: Macquarie University/Anglo-Australian Observatory, Sydney, NSW, Australia.

Contract/grant sponsor: Australian Research Council

To facilitate the exploration of these, and other high Antarctic sites, we have developed a system of small, high-efficiency diesel generators. Six of these generators are installed in PLATO, the PLATeau Observatory [3–5], a robotic observatory that was deployed to Dome A, in January 2008 by the Polar Research Institute of China. PLATO is measuring the atmospheric conditions at Dome A in order to gather information for future large astronomical telescopes. PLATO also provides a scientific platform for small telescopes and other experiments [6,7]. The PLATO facility itself is composed of two modules, each built into a 10-foot shipping container: an instrument module with a flexible computer-controlled system for the instrument suite [8]; and an engine module that provides the primary power during the winter months [9].

There are five astronomical instruments on PLATO, each of which is designed to run on less than 100 W (average) power. Electrical power is also required for heaters to keep the instruments warm and to provide additional heat to the instrument module itself. Yang *et al.* [3] present a detailed description of PLATO and first season (2008) results for the above-mentioned instruments. Lawrence *et al.* [5] present a detailed description of PLATO's power generation and control systems, together with an overview of the system performance for 2008.

PLATO must operate unmanned throughout the year because of the remoteness of Dome A. Except for a period of a few weeks in January each year when the annual servicing missions take place, communications with the observatory are only possible via the Iridium satellite network. Thus, the power generation system needs to be maintenance-free for a period of 11 months.

During the summer months, when the sun is above the horizon, PLATO can be powered largely by an array of solar panels. However, moving into winter there is progressively less sun available and for approximately 3.5 months of the year the sun is continuously below the horizon. Unlike the Antarctic coast, where wind turbines can provide large amounts of power, the plateau is remarkably free of wind. Dome A has possibly the lowest average wind speed of any place on earth [10], making wind power impractical.

Several other possible power sources are discussed in Lawrence *et al.* [11]. Perhaps the most promising in the longer term are fuel cells. These have been tested in an Antarctic environment [12] but the technology is still relatively immature. In addition, the energy density of the most suitable fuel, methanol, is less than half that of jet fuel.

These arguments lead to the selection of diesel engines to augment the solar power. Six 4-volt 320 AHr lead-acid batteries are used to provide temporary energy storage. To provide redundancy and increase the flexibility of PLATO's power system, six independent engines are used in PLATO [5]. The factors leading to the choice of Jet A-1 fuel are described in Section 2.3. However, in principle almost any hydrocarbon fuel could be used, including bio-diesel or other renewable fuel.

Dome A, the highest point on the Antarctic plateau has a physical elevation of 4093 m above sea level. However, the low temperatures in Antarctica lead to a reduced atmospheric scale height; i.e. the atmospheric pressure falls off more rapidly with altitude than at a temperate site. Thus, the average pressure at Dome A is about 575 hPa [10] (roughly half that at sea level), corresponding to a pressure altitude of 4530 m. The average summertime temperature at Dome A is about -35°C , dropping to as low as -90°C in winter. This is well below the freezing point of any commonly available fuel. The design philosophy of PLATO is therefore for the engines to keep themselves and their fuel warm throughout the year using waste engine heat. The engine must be able to start reliably from cold in the summer time, but thereafter the engines are in a warm, highly insulated, temperature-regulated environment. However, should all the engines fail during the winter, they may need to survive temperatures as low as -90°C before the service crew arrives the following January.

The development of the PLATO engine system therefore consisted of the following steps:

- Selection of an appropriate engine and alternator.
- Selection of an appropriate fuel.
- Measurement of the engine performance at high (simulated) altitude.

- Design and testing of a low-temperature starting system.
- Verification of the survival of the engine system at extreme low temperatures.

These steps are detailed in the following sections.

2. DESIGN OF THE GENERATOR SYSTEM

2.1. Design criteria

2.1.2. Engine selection. For our purposes, only a small amount of power is needed (~ 1.5 kW) making turbocharging unnecessary. The simplest and lowest cost choice is thus that of naturally aspirated single-cylinder diesel engine.

The engine we selected is a commercially available Hatz 1B30 single-cylinder, naturally aspirated diesel four-stroke with a displacement of 347 ml. It is a direct-injection, air-cooled engine with a bore of 80 mm and stroke of 69 mm, and a compression ratio of 21.5. The design speed of operation is 1500–3600 rpm. At 3600 rpm the engine can produce 5000 W at sea level. However, the minimum brake specific fuel consumption (BSFC) is at 2200 rpm, and the engine wear rate is much reduced at this lower speed. Allowing for the lower atmospheric pressure at Dome A, we expect a maximum power output of ~ 2 kW at 2200 rpm. In practice, we would plan to run the engine at still lower power levels, partly to ensure complete combustion and reduce pollution to an absolute minimum.

The choice of an air-cooled engine was also motivated by the desire to keep everything as simple as possible. The standard engine-cooling fan was retained, and the warm air passing over the cylinder head allowed to circulate within the engine module. The overall internal temperature of the engine module is regulated by a separate thermal management system [8].

2.1.2. Engine lubrication. The crankcase oil selected was Mobil 1 Delvac 5w-40, chosen for its low pour point of -45°C and for its recommended use in

high performance applications of heavy-duty diesel engines [13].

For operation in PLATO, each engine's running time is much longer than the manufacturer's recommended service interval of 200 h. In order to achieve this, the engine lubrication system has been extensively modified. Each of the two banks of three engines has a 60 l external oil tank. Oil from the tank is continuously pumped into each engine with a Thomas Magnete LHP27 metering pump at a rate of approximately 11 cc min^{-1} at 3 Hz. At each crankcase, a simple overflow pipe is used to return the excess oil to the storage tank. Large-area filters are used to clean the oil.

2.2. Electrical output

Although small generator sets are already commercially available, including some with diesel engines, they are normally directly coupled to 50/60 Hz alternators producing a nominal 220/110 V AC. There are two main reasons why we chose not to take this path.

1. Such engines must run at 3000 or 3600 rpm, at which speed BSFC is considerably higher and the life of the engine is greatly reduced.
2. The alternators used are normally relatively inefficient, especially where voltage regulation via a slip-ring field excitation is used.

Given that PLATO would be operating alone for 11 months, we decided to deploy two different types of generator in order to maximise the chance of success. The generators chosen were

- A three-phase brushless bearing-less alternator made by eCycle. These units are lightweight and compact, with the NdFeB permanent magnet rotor mounted directly onto the crankshaft. The output of the alternator is rectified with an IR 70MTKB diode bridge. The manufacturer quotes an efficiency of about 90% under our operating conditions, not including the losses in the diode bridge.
- A DC servo motor MSS-22 made by Mavilor. This disc motor has very high efficiency (both as a motor and as a generator) as it does not suffer from iron loss.

During engine testing, only an eCycle alternator was used, as its compact design made it easier to install in the test chamber. For these tests we used a unit with a voltage constant of 40 V krpm^{-1} .

2.3. Fuel selection

The high cost (typically $\$4$ – $\$10 \text{ kg}^{-1}$) of transporting fuel to and across Antarctica implies that the optimum strategy is to use a fuel of the highest possible energy density. Similarly, the environmental issues associated with transport logistics tend to outweigh the environmental effects of burning the fuel itself, leading to the selection of diesel or jet fuel—the highest energy-density fuels that are readily available. Jet fuel is cleaner burning and has a significantly lower freezing point (or, more accurately, pour point) than even SAB (Special Antarctic Blend) diesel, and was therefore chosen for our application.

There are many types of jet fuels available [14]. The most common is Jet A-1, a kerosene grade that contains a complex mixture of higher-order hydrocarbons. Jet A-1 (and its US counterpart Jet A) is widely used for commercial aircraft with turbine engines, while JP-8 is used for military aircraft. JP-8 is essentially Jet A-1 but with three additives to reduce ice build-up, corrosion and electric charge [15]. We chose Jet A-1 because of its ready availability in Antarctica.

The use of jet fuel in diesel engines is not unusual. NATO's Single Fuel Concept (SFC), for example, specifies JP-8 (or NATO code: F-34) as the single fuel to be used for all of their land and air military transports. Also, Jet A-1 has previously been used for a bank of six diesel engines for the

winter operation of the Italian Antarctic coastal station at Terra Nova Bay [16].

As Jet A-1 is primarily used for turbine engines, it is usually combined with additives before use in compression-ignition engines. Diesel oil has a typical cetane index of about 55, corresponding to a shorter ignition delay than Jet A-1 (or JP-8, which has a cetane index closer to 47). Jet A-1 will thus perform better as a diesel fuel if it is mixed with a cetane enhancer and an oil to improve its lubrication properties. However, as the Hatz 1B30 is already specified for use with Jet A-1, we elected not to add a cetane enhancer. We mixed the fuel with $\sim 2\%$ fully synthetic 'Racing 2T' two-stroke oil to provide lubrication for the fuel pump and the injection system [17]. In order to keep the fuel warm during the winter months, the fuel in PLATO is kept inside the well-insulated engine module in a 4000l aluminium tank. The tank is reinforced by aluminium webs that also act to conduct heat to the fuel at the bottom of the tank. Fuel is pumped from the bottom of the tank with a Thomas Magnete LHP27 metering pump and passes through a large-area filter on its way to the engine.

In Table I we present typical values of the basic properties of Jet A-1, automotive diesel and SAB. There is no specified value for the cetane index of Jet A-1, but it is assumed to be similar to that of JP-8. Jet fuel properties also vary from source to source [26].

2.4. Engine starting

The Hatz engine is electromechanically started in the usual way, with a solenoid engaging the starter

Table I. Fuel properties of Jet A-1, Automotive Diesel and Special Antarctic Blend (SAB) [18–24].

Fuel	Density at 15°C (kg l^{-1})	Energy density (MJ kg^{-1})	Cetane index (–)	Max. viscosity (mm^2s)@ 40°C	Freezing point ($^\circ\text{C}$)	Flash point ($^\circ\text{C}$)	Auto-ignition point ($^\circ\text{C}$)
Jet A-1	~ 0.81	42.8 (min)	$\sim 47^*$	~ 2	< -47	> 38.0	~ 240
Diesel	0.85 (max)	45.6	~ 55	~ 6	< -35	> 60.0	~ 240
SAB Diesel	~ 0.82	46.4	~ 51	~ 7	< -35	> 61.5	$\sim 240^\dagger$

*Cetane Index (CI) quoted for Jet A-1 is actually the CI for JP-8 [25].

† Since Diesel and SAB Diesel are chemically similar then the auto-ignition temperatures are also similar.

motor pinion with the ring gear on the crankshaft. The peak current required is 300 A at 12 V, and the motor will normally start within 1–2 s.

In order to improve the reliability of starting at low temperatures, we use ultracapacitors in place of the usual lead-acid battery. This is because the internal resistance of lead-acid batteries rises rapidly with decreasing temperature, whereas ultracapacitors can deliver thousands of amperes even at -40°C . The ultracapacitors are type BCAP3000 manufactured by Maxwell under the trade name Boostcap; each capacitor is about the size of a soft-drink can and is rated at 3000 F, 2.7 V.

For PLATO, two banks of ultracapacitor are used: one of 500 F (6×3000 F capacitors in series) and the other of 1000 F (12×3000 F capacitors in series-parallel). The capacitor banks are charged with a 12 V DC/DC converter that is current-limited to 9 A. Each of the capacitors is shunted with a simple clamp circuit that limits the voltage across it to a conservative value of 2 V. The clamp circuit must be able to pass the full charging current (9 A) from the time it turns on for as long as it takes for the sum of the voltages across the capacitors to rise to the value set by the DC/DC converter—in this case 12.0 V. In addition, the circuit creates a shunt current path of 45 mA. This is ten times the leakage current of the capacitors, and thus helps to equalise the voltage across each one. This shunt current will also discharge the capacitors with a time constant of 19 h after the system has been powered down.

3. COLD TEMPERATURE TESTS

Several important cold-temperature tests were carried out to ensure that the system would operate satisfactorily in Antarctica and would survive both the low temperatures that would be experienced during transport and the even lower temperatures that would occur during winter in the event of a power failure. The tests were carried out in a Forma Scientific Model 8558 laboratory freezer.

3.1. Fuel separation

Because of the possibility that the fuel for PLATO will freeze at least once before being used by the engines, it was important to determine if this

would cause any separation of the Jet A-1 and oil. A sample of the fuel mix was placed in the laboratory freezer and cooled to -90°C . The freezing point of the fuel mix was determined to be about -57°C , somewhat lower than the nominal Jet A-1 freezing point. Upon thawing, the fuel mix showed no visible stratification between the jet fuel and the two-stroke oil.

3.2. Engine survival

The engine manufacturer, Hatz, Germany, specifies that the Hatz 1B30 engine has a minimum storage temperature of -46°C . However, with the possibility of the engine experiencing much lower temperatures than this in Antarctica, it was important to determine what, if anything, would happen if it were exposed to extreme cold. Problems that might be anticipated include permanent distortion of metal components and cracking of elastomeric seals. A 1B30 engine was frozen to -90°C overnight in the laboratory freezer and then allowed to stand at room temperature to thaw. Once thawed, the engine was found to restart successfully and to perform well. No oil leaks or other issues were discovered.

3.3. Ultracapacitor current delivery

A BCAP3000 ultracapacitor was charged to 2.0 V and discharged at various currents (5, 62.5 and 121 A) while monitoring the charge and discharge time. This test was carried out as a function of temperature, with little change in behaviour being evident between room temperature and -40°C . At -46°C the ultracapacitor made an abrupt transition from capacitor to insulator, presumably because the electrolyte froze.

The internal resistance of the ultracapacitor was measured at -40°C by measuring the change in voltage across its terminals when the current drawn from it was switched from 0 to 107 A. The resulting value of 0.19 milliohm is consistent with the data sheet value of 0.29 milliohm $\pm 35\%$.

3.4. Ultracapacitor and clamp circuit survival

A BCAP3000 ultracapacitor was tested at room temperature then frozen to -90°C . Upon thawing

the capacitor was found to have the same capacitance and discharge current capability as before. The clamp circuit was similarly (mis) treated, and was also found to perform flawlessly on thawing to -40°C . This gave us confidence that the ultracapacitor bank would survive a winter without heat, and be capable of starting the engines the following spring.

4. ENGINE TEST RIG

4.1. Mechanical

In order to simulate the low atmospheric pressure of Dome A in the laboratory, an environmental chamber was designed and built with the capability of maintaining a constant pressure down to half an atmosphere with the engine running at full power. The chamber consists of a base plate and a bell-jar made from mild steel. The base plate is a circular disk, 30 mm thick, with an outer diameter of 1100 mm. The bell-jar has a wall thickness of 5 mm, with a welded dome-shaped top and a welded bottom flange. Two lifting hooks were welded on either side of the bell-jar to accommodate a crane. The bell-jar is sealed over the base plate via an O-ring. See Figure 1.

An $8\text{ m}^3\text{ min}^{-1}$ Longtech LTV-100 Roots blower, driven by a Teco CNS-C4088 15 kW three-phase



Figure 1. Engine test rig. The air flows through the air-filter box to the environmental chamber. The rate of airflow is controlled by the butterfly valve. The Roots blower runs at constant speed, pumping air from the environmental chamber.

electric motor, extracts air from the chamber and vents it outside the building. The flow rate was chosen to be an order of magnitude greater than the rate at which the engine consumed air, so that the engine exhaust was well diluted before reaching the Roots blower. Air was continuously introduced into the chamber via an air-filter box and butterfly valve. The butterfly valve was manually adjusted to set the desired pressure within the chamber.

The engine was attached via rubber isolation dampeners to the base plate of the chamber. See Figure 2. The eCycle alternator was directly attached to the engine crankshaft, and the three-phase electrical output coupled via a diode bridge to a pair of resistor load banks. The engine breathed the reduced pressure air from inside the chamber, while the exhaust exited via a diffuser that allowed the exhaust gases to be well mixed with the main airflow before reaching the Roots blower.

A motor-driven lead screw was attached to the engine governor lever in order to control the speed of the engine. The actuator was mounted on the engine plate and was electrically controlled via a switch that was external to the chamber.

Fuel consumption was measured using an externally mounted graduated cylinder, which delivers fuel via a fuel line that passes through a seal in the base plate to the engine. By having the fuel-feed system mounted externally to the pressure chamber,



Figure 2. Engine mounted on base-plate of the environmental chamber with peripherals.

less vibration was coupled to the graduated cylinder, thus allowing a more accurate reading of the fuel level. The graduated cylinder could be read by eye to ± 0.5 ml. Typical consumption during a run was 60 ml, leading to a formal error in the amount of fuel consumed of $\pm 2\%$.

4.2. Data acquisition

Several sensors were placed on and around the engine to monitor various engine parameters. The processed signals from the sensors were fed into a desktop PC running Windows XP.

K-type thermocouples were used to measure the temperatures of the ambient air, oil sump, cylinder head, exhaust gas, alternator and the intake air. Two Motorola MPX4115AP pressure sensors with a specified accuracy of $\pm 1.5\%$ were placed inside the chamber. Output from the thermocouples, pressure sensors, and the resistor load bank sensors were all processed by ADAM modules connected via a serial device server (Moxa NPort 5410) to the Desktop PC. The formal accuracy of the temperature measurement is about 0.1°C and that of the voltage and current 0.1% . The engine speed was also monitored by a tachometer directly connected to the serial device server. All information received from sensors was then processed and logged in real time by the National Instrument's software package, LabVIEW. Virtual Instrument (VI) software created in LabVIEW allowed all parameters and data to be displayed on the computer monitor in real time and also stored to an output file. The output '*.csv' file was packed by the VI with the first column being allocated to time and subsequent columns being the calibrated sensor values.

The file was loaded into Matlab to produce plots of the engine sensor values as a function of time (see Section 4.3). Matlab was used to calculate the means of the pressure, voltage, current and engine speed over the duration of the run. These average values were imported into Microsoft Excel to calculate the overall BSFC.

4.3. Test procedure

The engine was started and stopped at a variety of simulated altitudes. It was found to start reliably,

from ambient (typically $\sim 25^\circ\text{C}$), at altitudes of more than 5000 m. Tests of starting at low temperatures were not performed, as the concept of PLATO is that one engine is always running, and thus keeps the other engines warm.

The majority of tests were conducted at a fuel injection timing of 18° crank angle before top dead centre (CA BTDC). Tests were made under otherwise identical conditions at both sea-level atmospheric pressure (1000 hPa) and at a pressure of about 540 hPa (hereinafter described as 'at altitude'). The corresponding pressure altitude is 5000 m, which is well above that of Dome A. Each test was allowed to go for no more than 10 min in order to avoid possible overheating of the engine within the chamber.

The engine speed was set at discrete intervals from 1600 to 3200 rpm and the load varied from 50 W up to 3 kW. At each setting, the following parameters were recorded:

- Fuel consumed
- Load-bank voltage and current
- Exhaust gas temperature

A typical data set for an engine test is presented in Figures 3–5. This particular engine test was conducted at a simulated altitude of 4500 m and at a crankshaft speed of 2200 rpm. The engine run-time was 390 s (5.5 min).

The ambient temperature inside the chamber was observed to increase by about 10°C during the

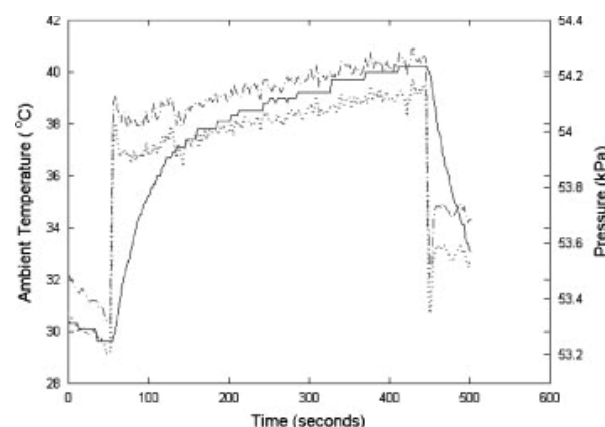


Figure 3. Ambient temperature (solid line) and air pressure (dotted and dot-dashed lines) inside the chamber during a typical test run.

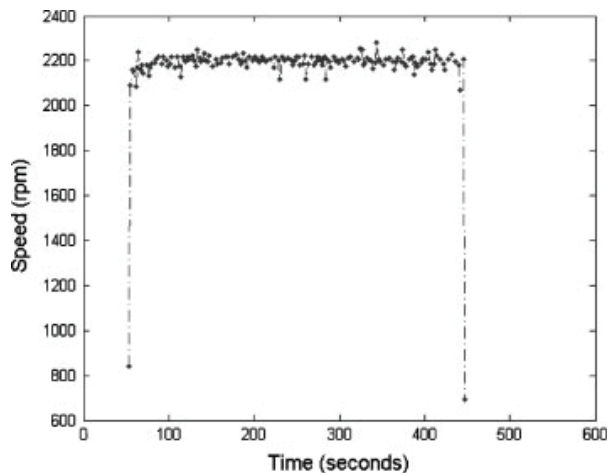


Figure 4. Engine speed during a typical test run showing the stability of the engine governor.

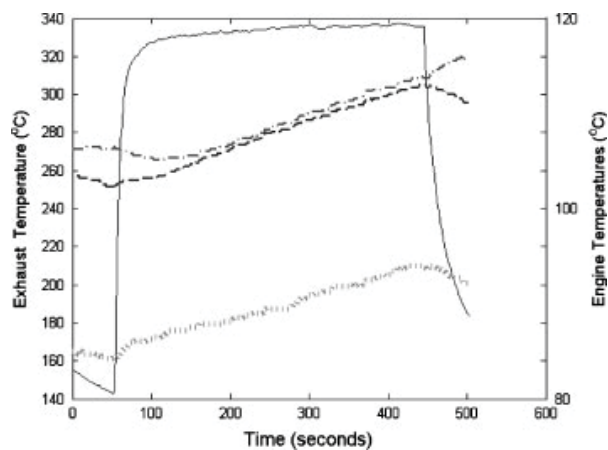


Figure 5. The exhaust gas temperature (left scale, solid line), and other engine temperatures (right scale) during a typical test run. The engine temperatures are: the cylinder head (dot-dashed line); the generator (dashed line) and the oil sump (dotted line).

operation of the engine. This increase in intake air temperature resulted in a small decrease in power output from the engine as the run progressed and a slight increase in the chamber air pressure (see Figure 3). However, the engine governor was able to keep the engine speed very constant, as shown in Figure 4.

The cylinder head, generator, oil sump and exhaust gas temperatures (Figure 5) were also monitored so that the observer could initiate an

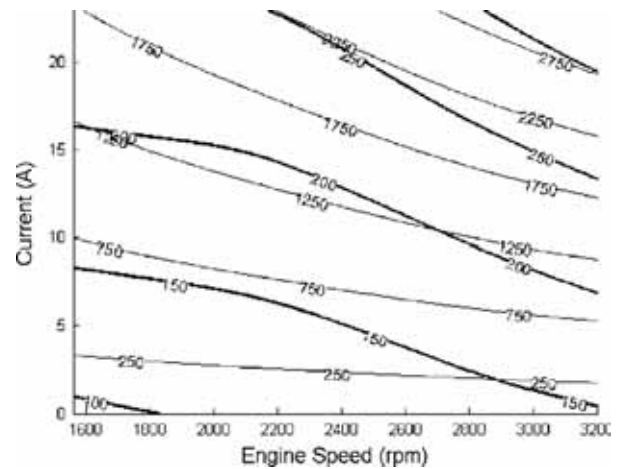


Figure 6. Sea level engine map, showing the exhaust gas temperature ($^{\circ}\text{C}$, thick line) and power output (W, thin line) as a function of current (y-axis) and engine speed (x-axis).

immediate shutdown of the engine and the Roots blower in the event of a serious system failure.

The Hatz engine is supplied for the EPA market with an injection timing of 18° CA BTDC, and for the non-EPA market with 13° CA BTDC. Although we expected the advanced injection timing would give better performance at altitude, we nevertheless conducted a further set of tests at an injection timing of 13° CA BTDC. These tests were conducted at a fixed engine speed of 2200 rpm.

5. RESULTS AND DISCUSSION

5.1. Engine map data and engine efficiency

Figures 6 and 7 are smoothed engine contour maps at sea level and at altitude, respectively. Each contour map shows exhaust gas temperature and the total power as a function of current (y-axis) and engine speed (x-axis). The current is directly proportional to the torque developed by the engine.

The engine maps of Figure 6 and 7 show a greatly increased exhaust temperature at altitude. This is to be expected: for a given power output and rpm, a specific amount of thermodynamic work has to be performed each cycle. At altitude, only 54% of the mass of air is present in the

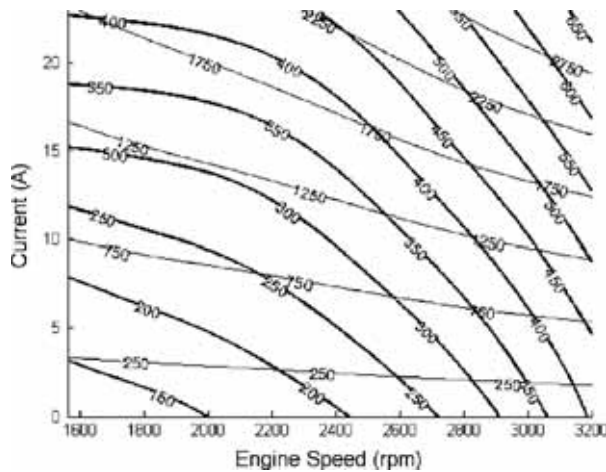


Figure 7. At altitude engine map, showing the exhaust gas temperature ($^{\circ}\text{C}$, thick line) and power output (W, thin line) as a function of current (y-axis) and engine speed (x-axis).

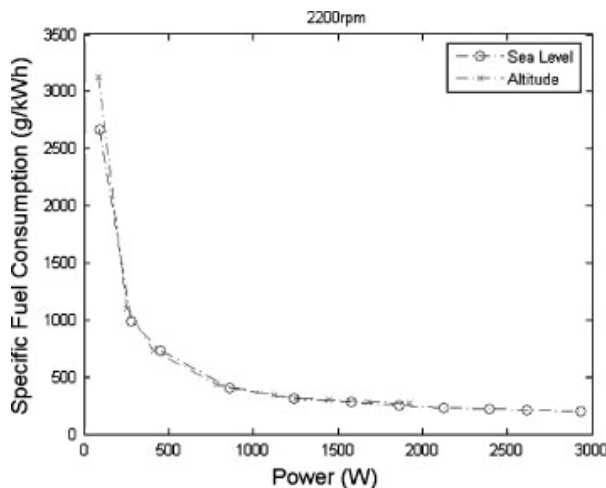


Figure 8. Brake specific fuel consumption (g kWh^{-1}) as a function of power at a fixed engine speed of 2200 rpm.

cylinder compared to sea level, and so this air must undergo a greater temperature excursion to perform the same work. In addition, the amount of air available for cooling is also reduced by nearly 50%.

In Figure 8, the power that was recorded was the electrical output power from the alternator, and thus included the alternator and rectifier losses. BSFC figures (in g kWh^{-1}) are therefore an overall fuel-to-electricity efficiency. At an

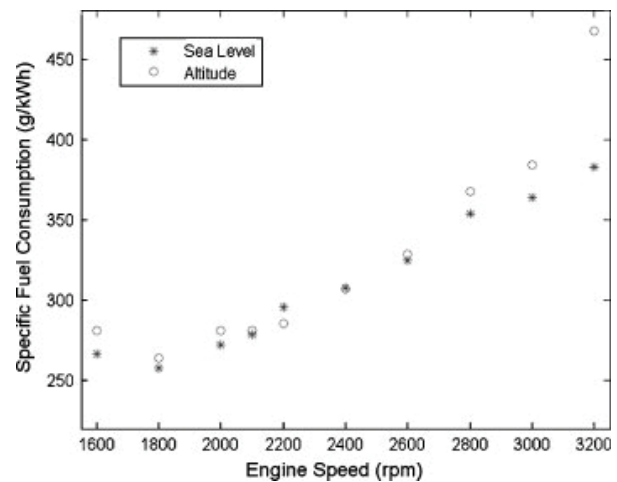


Figure 9. Brake specific fuel consumption (g kWh^{-1}) for a fixed power output of 1500 W as function of engine speed.

engine speed of 2200 rpm, the engine efficiency changed remarkably little between sea level and at altitude. However, as the engine speed was increased above 2600 rpm the engine became progressively less efficient at altitude than it was at sea level (see Figure 9). At our preferred engine speed of 2200 rpm and a power output of 1500 W, the engine's BSFC at altitude is 280 g kWh^{-1} .

5.2. Injection timing

In Figures 10 and 11 we present the results of tests at an injection timing of 18° CA BTDC ('Test A'), 13° CA BTDC, then again at 18° CA BTDC ('Test B'). The engine speed was fixed at 2200 rpm.

From Figure 10 it was clear that at 2200 rpm the injection timing has little effect on the fuel consumption. However, as seen in Figure 11, the engine ran hotter at 13° CA BTDC than at 18° CA BTDC both at sea level and at altitude. At altitude, the exhaust gas temperature could be as much as 65°C hotter with the less advanced timing.

This increase in exhaust temperature is likely to be because of a slower combustion due to the reduced air density. Heat that is liberated towards end of the expansion stroke does no useful work

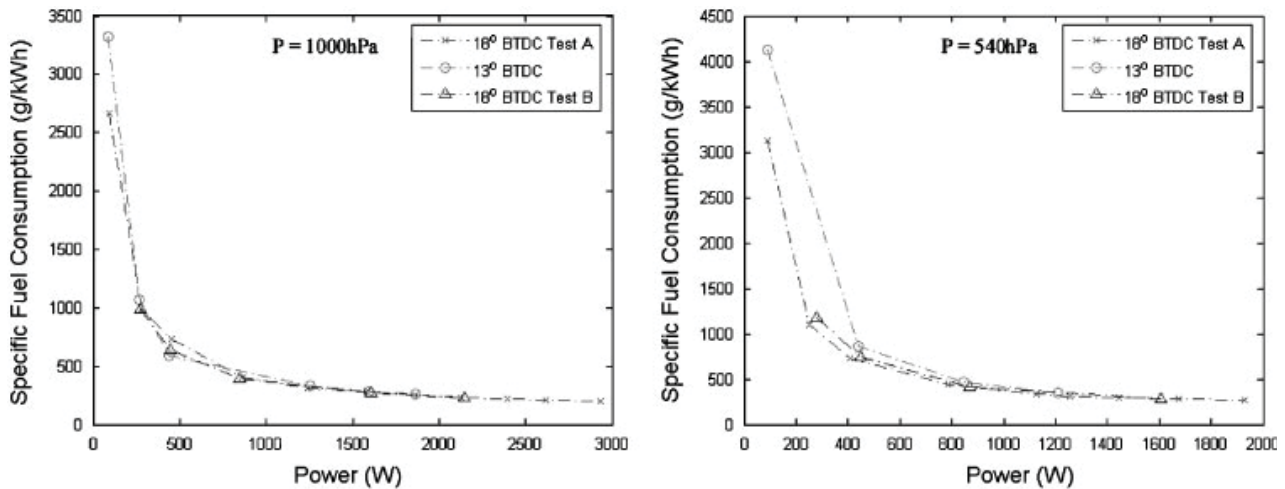


Figure 10. Brake specific fuel consumption at sea level (left) and at altitude (right) at fuel injection timings of 13° and 18° CA BTDC.

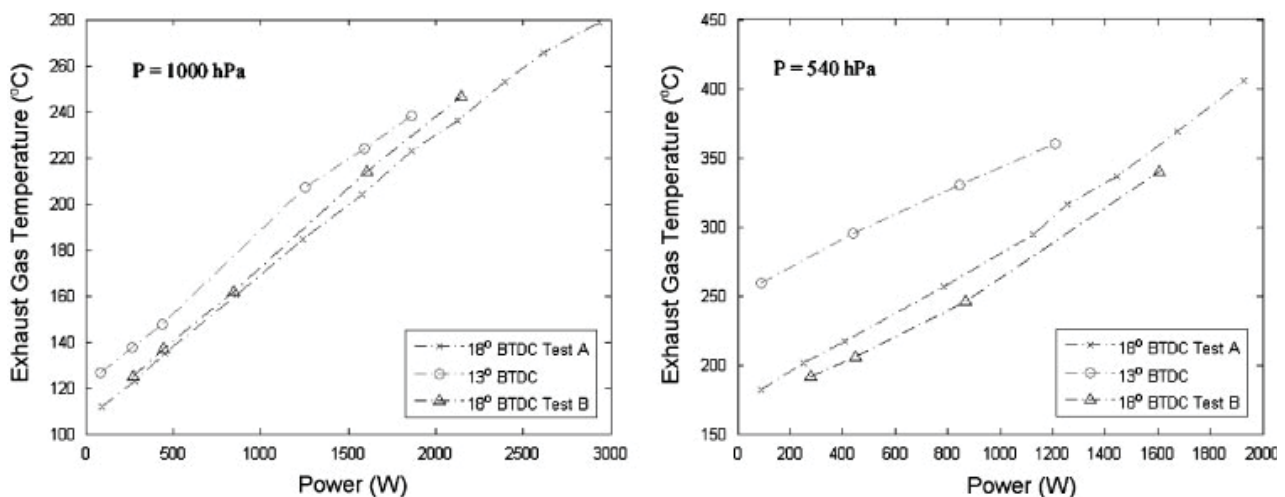


Figure 11. Exhaust gas temperature at sea level (left) and at altitude (right) at fuel injection timings of 13° and 18° CA BTDC.

and only serves to heat up the exhaust valve and pipe [27]. Nevertheless, it is surprising that the injection timing has such a profound effect on the exhaust temperature, while having little or no effect on the fuel consumption.

6. CONCLUSION

Little modification to the Hatz 1B30 engine was required for it to start and run satisfactorily at an

altitude of up to 5000 m. Because the maximum power output at a given speed was reduced in direct proportion to the air pressure, so the maximum fuel delivery must also be correspondingly reduced. However, because the air is less dense, there is less working fluid available to do the thermodynamic work and less cooling is available, and so the temperature rise (cylinder head, exhaust gas, etc.) is greatly increased for a given power output. By advancing the start of the fuel delivery timing there is more time for

combustion early in the power stroke, liberating useful work and minimising this increase in exhaust gas temperature.

Allowing for an alternator efficiency of approximately 90%, we find that BSFC of the engine at sea level is consistent with published data. Furthermore, little loss of efficiency, if any, is encountered when the engine is running at high altitude.

An ultracapacitor starting bank has been shown to provide ample cranking current at temperatures as low as -40°C . Both the engine and the starting bank survive temperature cycling to -90°C with no discernable ill effect.

The PLATO power generation system is an innovative and scalable system that can be implemented for remote sites anywhere on the Antarctic plateau and at other high-altitude locations up to 5000 m.

ACKNOWLEDGEMENTS

This research is supported by the Australian Research Council. We thank the UNSW School of Mechanical and Manufacturing Engineering for access to the Internal Combustion Laboratory, Hatz Australia, and in particular Sami Almogoawish, Ian O'Callaghan and Tissa Pathiratna, provided us with the invaluable assistance and generously shared their deep understanding of diesel engines with us. We also thank Jason and Graham Allen for their help in modifying the oil and fuel systems. One of the resistor load banks was generously lent to us by Graeme Arnold and Bob Bell from Swithgear Commissioning & Maintenance Pty Ltd and the other by Ian Davis from Eaton Electric Systems Pty Ltd.

REFERENCES

1. Lüthi D, Le Floch M, Bereiter B, Blunier T, Barnola J, Siegenthaler U, Raynaud D, Jouzel J, Fischer H, Kawamura K, Stocker TF. High-resolution carbon dioxide concentration record 650,000–800,000 years before. *Nature* 2008; **453**:379–382.
2. Storey JWV. Astronomy from Antarctica. *Antarctic Science* 2005; **17**(4):555–560.
3. Yang H, Allen G, Ashley MCB, Bonner CS, Bradley S, Cui X, Everett JR, Feng L, Gong X, Hengst S, Hu S, Jiang Z, Kulesa CA, Lawrence JS, Li Y, Luong-Van D, McCaughrean MJ, Moore AM, Pennypacker C, Qin W, Riddle R, Shang Z, Storey JWV, Sun Z, Suntzeff N, Tothill NFH, Travouillon T, Walker CK, Wang L, Yan J, Yang J, York D, Yuan X, Zhang X, Zhang Z, Zhou X, Zhu Z. The PLATO Dome A site-testing observatory: instrumentation and first results. *PASP* 2009; **121**:174–184.
4. Lawrence JS, Allen GR, Ashley MCB, Bonner C, Bradley S, Cui X, Everett JR, Feng X, Hengst S, Hu J, Jian Z, Kulesa CA, Li Y, Luong-Van D, Moore AM, Pennypacker C, Qin W, Riddle R, Shang Z, Storey JWV, Sun B, Suntzeff N, Tothill NFH, Travouillon T, Walker CK, Wang L, Yan J, Yang J, Yang H, York D, Yuan X, Zhang X, Zhang Z, Zhou X, Zhu Z. The PLATO Antarctic site testing observatory. *Proceedings of SPIE* 2008; **7012**:701227.
5. Lawrence JS, Ashley MCB, Hengst S, Luong-Van DM, Storey JWV, Yang H, Zhou X, Zhu Z. The PLATO Dome A site testing observatory: power generation and control systems. *Review of Scientific Instruments* 2009; **80**:064501.
6. Lawrence JS, Ashley MCB, Burton MG, Cui X, Everett JR, Kenyon SL, Luong-Van D, Moore AM, Storey JWV, Tokovinin A, Travouillon T, Pennypacker C, Wang L, York D. Site testing Dome A, Antarctica. *Proceedings of SPIE* 2006; **6237**:62671L1–62671L9.
7. Tothill NFH, Kulesa CK, Ashley MCB, Bonner C, Everett J, Feng L, Hengst S, Hu J, Jian Z, Lawrence JS, Li Y, Luong-Van D, Moore AM, Pennypacker C, Qin W, Riddle R, Storey JWV, Shang Z, Sun B, Travouillon T, Wang L, Xu Z, Yang H, Yan J, York D, Yuan X, Zhu Z. Astrophysics from Dome A. *EAS Publication Series*. In *Proceedings of the 2nd ARENA Conference*, Potsdam, Germany, Zinnecker H, Rauer H, Epchtein N (eds). EAS Publications Series, vol. 33, 2008; 301–306.
8. Luong-Van DM, Ashley MCB, Everett JR, Lawrence JS, Storey JWV. PLATO control and robotics. *Proceedings of SPIE* 2008; **7019**:70192U.
9. Hengst S, Allen GR, Ashley MCB, Everett JR, Lawrence JS, Luong-Van D, Storey JWV. PLATO Power—a robust, low environmental impact power generation system for the Antarctic plateau. *Proceedings of SPIE* 2008; **7012**:70124E.
10. Available from: <http://www.aad.gov.au/weather/aws/dome-a/index.html> (January 2009).
11. Lawrence JS, Ashley MCB, Storey JWV. A remote, autonomous laboratory for Antarctica with hybrid power generation. *Australian Journal of Electrical & Electronic Engineering* 2005; **2**:1–12.
12. Datta BK, Velayutham G, Goud AP. Fuel cell power source for a cold region. *Journal of Power Sources* 2002; **106**:370–376.
13. Available from: http://www.mobil.com/USA-English/Lubes/PDS/NAXXENCVLMOMobil_Delvac_1_5W-40.asp (January 2009).
14. Maurice LQ, Lander H, Edwards T, Harrison III WE. Advanced aviation fuels: a look ahead via a historical perspective. *Fuel* 2001; **80**:747–756.
15. Batchelor G, Moses C, Fletcher R. Impact study on the use of Jet A fuel in military aircraft during operations in Europe; *AGARD Report 801*, 1997.
16. Meloni A, De Santis A, Morelli A, Palangio P, Romeo G, Bozzo E, Caneva G. The geophysical observatory at Terra Nova Bay. *Recent Progress in Antarctic Earth Science TERRAPUB* 1992; 585–588.
17. Available from: http://www.mobil.com/Australia-English/Lubes/PDS/glxenpvlmomobil1_racing_2t.pdf (January 2009).

18. Product Specification: Jet A-1. *Fuels Technical Services*, BP Australia Pty. Ltd., 2008.
19. Product Specification: BP Automotive Diesel Fuel. *Fuels Technical Services*, BP Australia Pty. Ltd., 2006.
20. Product Specification: BP Antarctic Diesel. *Fuels Technical Services*, BP Australia Pty. Ltd., 2008.
21. Safety Data Sheet: Jet A-1. Shell Company of Australia Ltd., 2005.
22. Material Safety Data Sheet: Jet A-1. *BP Australia Pty. Ltd.*, 2008.
23. Material Safety Data Sheet: Automotive Diesel, *BP Australia Pty. Ltd.*, 2008.
24. Material Safety Data Sheet: BP Antarctic Diesel Fuel (SAB). *BP Australia Pty. Ltd.*, 2008.
25. Assanis D, Fernandes G, Fuschetto J, Filipi Z, McKee H. Impact of military JP-8 fuel on heavy duty diesel engine performance and emissions. *Proceedings of the Institution of Mechanical Engineers: Part D* 2007; **221**.
26. Colket M, Edwards T, Williams S, Cernasky NP, Miller DL, Egolfopoulos F, Lindstedt P, Seshadri K, Dryer FL, Law CK, Friend D, Lenhert DB, Pitsch H, Sarofim A, Smooke M, Tsang W. Development of an experimental database and kinetic models for surrogate jet fuels. *AIAA* 2007; 2007–2770.
27. Ricardo HR, Hempson JGG. *The High Speed Internal Combustion Engine*. Blackie: London, U.K., 1968.

PLATO Power—a robust, low environmental impact power generation system for the Antarctic plateau

Shane Hengst^{*a}, Graham R. Allen^b, Michael C.B. Ashley^a, Jon R. Everett^a, Jon S. Lawrence^a,
Daniel M. Luong-Van^a, John W.V. Storey^a

^aSchool of Physics, University of New South Wales, Sydney, NSW, Australia 2052;

^bSolar Mobility Pty Ltd, PO Box 951, Epping, NSW, Australia 2121

ABSTRACT

PLATO (PLATeau Observatory) is the third-generation astronomical site-testing laboratory designed by the University of New South Wales. This facility is operating autonomously to collect both scientific and site-testing data from Dome A, the highest point on the Antarctic plateau, at an elevation of 4093m. We describe the power generation and management system of PLATO. Two redundant arrays of solar panels and a multiply-redundant set of small diesel engines are intended to provide 1–2kW of electrical power for a full year without refueling or other intervention. An environmental chamber has been constructed to study the high-altitude performance of the diesel engines, and suitable cold-starting procedures and engine lubrication techniques have been developed. PLATO's power system is an innovative solution with wide applicability to small astronomical facilities on the Antarctic plateau, offering minimum environmental impact and requiring minimal human intervention.

Keywords: Diesel engine, remote power generation, Antarctica, Dome A

1. INTRODUCTION

PLATO (PLATeau Observatory)¹ is a remote facility that has been successfully deployed to Dome A, Antarctica (see Fig. 1) in January 2008 by an expedition of the Polar Research Institute of China. PLATO was designed and built at the University of New South Wales to provide heat, power and communications for a suite of site-testing instrumentation. The UNSW Antarctic Group has previously developed remote facilities for the South Pole (AASTO, or Automated Astrophysical Site-Testing Observatory), and for Dome C (AASTINO, or Automated Astrophysical Site-Testing InterNational Observatory). Fig. 1 shows the locations of these sites.

The AASTO² was built by Lockheed and was based closely on the US Automated Geophysical Observatory. It used a propane-fuelled thermoelectric generator, producing some 50W of electrical power and 2.5kW of heat.

AASTINO³ was powered by a pair of WhisperGen PPS16 24VDC⁴ Stirling engines burning Jet A-1 fuel. The two engines were cooled with a glycol loop that fed directly into large heat exchangers, keeping the AASTINO warm via the waste engine heat. At sea level the WhisperGen engines produced 750W of electrical power but, as with any naturally-aspirated combustion engine, they produce less power as the altitude increases. At Dome C each engine was able to produce about 500W. AASTINO also used two solar panels to provide additional power during summer.

In developing PLATO, several new factors had to be taken into account, building upon the experience from the earlier AASTO and AASTINO facilities. New challenges to be faced at Dome A include:

- **No preferred wind direction.** Unlike at Dome C and the South Pole, the wind at Dome A has almost no preferred direction⁵. This means that it is impossible to protect the astronomical instruments from the exhaust stream by simply placing them upwind of the engines, as was done with the AASTINO. Instead, a separate engine and instrument module are required, spaced at a sufficient distance that the exhaust stream is less likely to intrude into the atmosphere through which the instruments are observing. The disadvantage of this approach is that it is then no longer possible to use waste engine heat to keep the instrument module warm, unless the engine coolant is plumbed between the two units. This option was, however, considered to be impractical, leading us to a solution in which the instrument module is heated purely by electrical power.

* shane@phys.unsw.edu.au; phone 61 2 9385 6695; fax 61 2 9385 6060

- **Higher altitude.** The physical altitude of Dome A is 4093m. However, the cold air above Antarctica results in a smaller scale height for the atmosphere, resulting in a pressure altitude at Dome A of typically 4500m. The engines must be able to start reliably at this altitude, and their power output must be sufficient even with the thinner air they will be breathing. In practice, this means choosing an engine of a significantly larger displacement than would be required at sea level.
- **Colder.** Dome A is almost certainly the coldest place on earth, although this is not yet firmly established as meteorological records are only recognized if made by a human observer! Nevertheless, temperatures as low as -90°C appear possible. This is well below “dry ice” temperature, emphasizing the need for extremely well-insulated structures and very efficient use of energy.
- **More remote.** The greater difficulty of bringing materials to Dome A makes it even more important that the power solution be optimized in terms of fuel type, fuel efficiency, and power management.

In addition, increasingly sophisticated astronomical instruments require ever greater amounts of electrical power. The PLATO power solution is therefore designed to be both adaptable and scalable—that is, it can provide additional power for short periods when required, and future versions can be built to provide higher base loads if necessary.

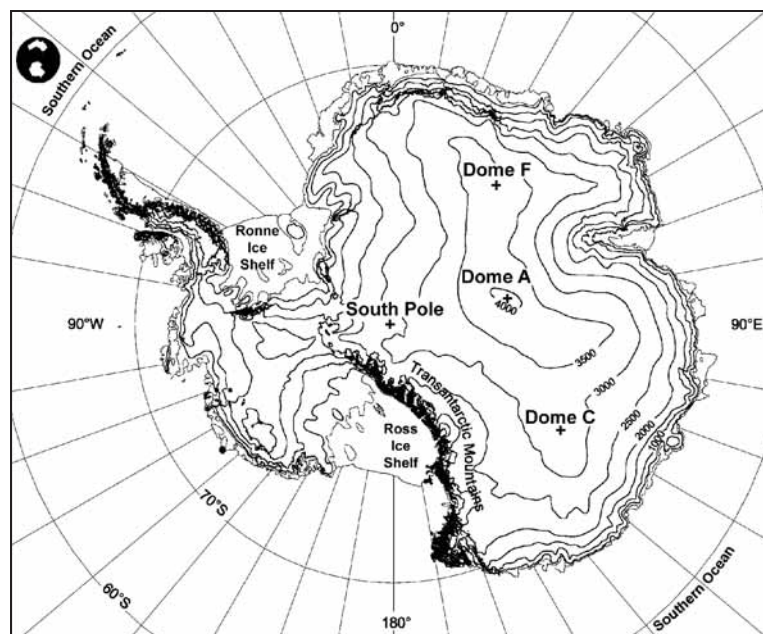


Fig. 1: Contour map of Antarctica (courtesy of AAD)

2. POWER GENERATION AND THERMAL MANAGEMENT

Fig. 2 shows that, during the course of a year, the Sun is continuously above the horizon at Dome A for approximately four and a half months, rises and sets each day for three months and is continuously below the horizon for four and a half months. The ideal power system will therefore be one that uses solar power during the summer, short-term electrical storage in the form of batteries, and uses a high energy-density fuel in an efficient manner during the dark winter months. PLATO therefore uses a hybrid solar/diesel power solution, burns Jet A-1, and has lead-acid batteries for energy storage.

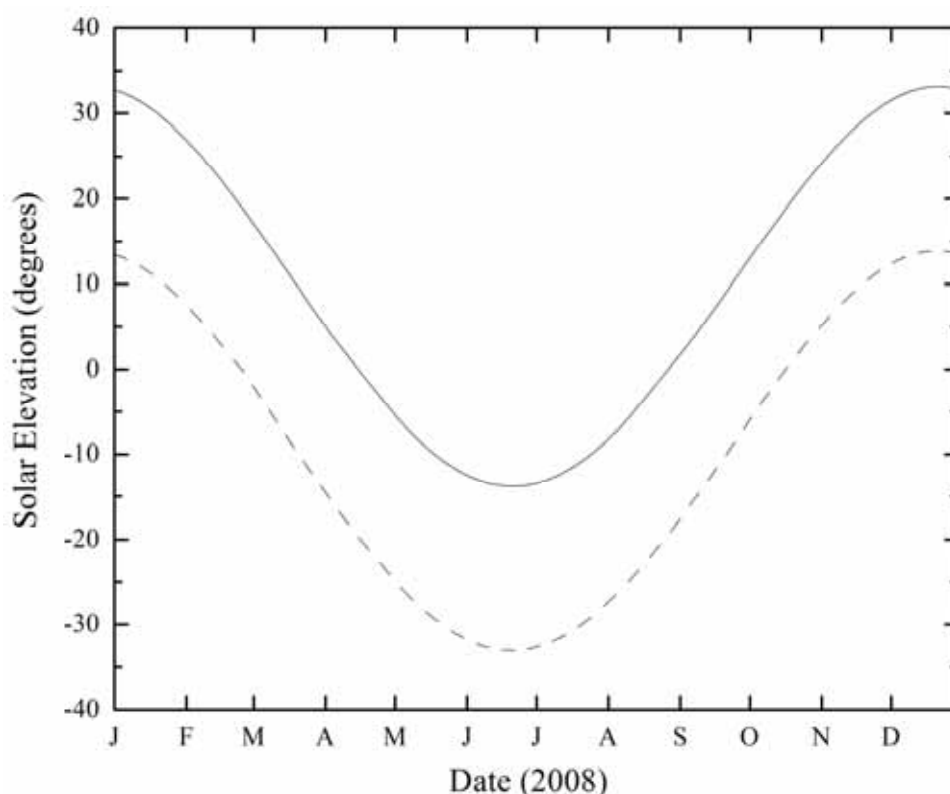


Fig. 2 Maximum and minimum daily solar elevation at Dome A for 2008.

PLATO consists of a power module and a separate instrumentation module¹. The two modules are separated by about 50m, and are joined only by the two pairs of high-voltage power cables, a Controller Area Network (CAN) bus cable, and a 28V power bus. Both modules are extremely well insulated: the engine module with 150mm thick polyurethane foam on all six internal surfaces and the instrument module similarly insulated with 200mm of foam.

The engine module is kept warm by the waste heat of the engines. A Eurotherm 3200 PID (Proportional-Integral-Derivative) controller activates two brushless axial-flow fans that exhaust warm air from the module, causing cold air to be drawn in. This maintains the temperature at a steady 20°C. All the fuel required for a year's operation (4000 litres) is also contained within the engine module, where it is kept warm.

The instrument module is kept warm mainly by the waste heat from the electronics. When this is insufficient, up to 1200W of resistive heaters can be switched on. Two anti-stratification fans keep the air within the module well mixed. Should the module become too warm (as can occur during the summer), a Eurotherm 3200 PID controller turns on two exhaust fans, in a manner similar to the thermal management system of the engine module.

The battery bank is a set of six, 4 Volt Sungel 4SG320 sealed lead-acid batteries, giving a nominal power bus of 28V. The batteries have their own 180W heater. Despite their modest energy density (34Wh/kg), sealed lead-acid batteries remain a good choice for short-term energy storage in Antarctica. They have good charge/discharge efficiency, work down to very low temperatures ($\sim -30^{\circ}\text{C}$), can be frozen and re-thawed without serious ill-effect, require only basic charge management, and are remarkably tolerant of accidental abuse.

3. SOLAR POWER

The solar panels are arranged in two arrays of three paralleled panels. Each panel is a polycrystalline silicon Conergy C167P, with a nominal power output of 167W at 25°C; 1.5 air-masses. Fig. 3 shows one array of solar panels that was erected at UNSW for testing.

Each panel is mounted vertically, roughly 1 metre above the snow to allow air to freely flow beneath it, thus minimizing snow accumulation. The two arrays are oriented north-east and north-west respectively, to maximize the amount of energy captured in the late autumn and early spring.



Fig. 3. One of the two solar arrays erected at UNSW for testing.

Each array of three panels is fed to an Apollo Solar T80 maximum-power-point tracker (MPPT)⁶. The two T80 MPPTs are arranged in a master/slave configuration, so that both units will switch from boost charging to float charging and back again at the same time. The master T80 MPPT has its own battery temperature sensor, allowing the output voltage to automatically track the battery's charging requirements.

Solar arrays are remarkably effective in Antarctica, as we have previously noted with the AASTINO³. Silicon solar cells are significantly more efficient at low temperatures, producing 5% more power for every 10°C drop in temperature. This, combined with the enhanced solar input from the snow reflection, results in a power output of up to 220W from each 167W panel. The bright reflection from the snow has another advantage: even when the sun is directly behind the panel, it can produce several watts of power.

When the Sun is above the horizon, it also provides a significant amount of useful radiant heat to the modules.

4. DIESEL POWER

Within the engine module are six Hatz 1B30 diesel engines⁷ arranged in two banks of three. See Fig. 4. The engines are air-cooled single-cylinder units with a capacity of 350cc and a nominal power output of 5.4kW at 3600rpm at sea level. Generally, only one engine is running at any time, although the possibility exists to run any number of engines simultaneously. This gives a very high degree of redundancy, plus the ability to boost the power output whenever it is required while maintaining a highly efficient "base load" generating capacity.

These engines have a nominal service interval of 200 hours. However, in PLATO they will see no human being for over eleven months. In order to achieve this extended running time, the engine lubrication system has been extensively modified. Each bank of three engines shares a 60 litre external oil tank. Oil is continuously pumped into each engine from the storage tank with a Thomas Magnete LHP27 metering pump at a rate of approximately 11cc/minute at 3Hz. A simple overflow pipe in each crankcase returns the excess oil to the storage tank. Large-area filters are used to clean the oil. The lubricating oil is fully synthetic Delvac 5W-40⁸. Operating the engines at only 2200rpm further enhances engine longevity.



Fig. 4. Left photo: Inside the engine module showing all six engines with electronics mounted on the top of the 4,000 litre fuel tank. Right photo: Inside the engine module showing one bank of the engines. The Mavilor generator is attached to the left-most engine, while the centre and right engines have the eCycle alternators mounted.

The engines sit on top of a 4000 litre aluminum fuel tank. Several thick aluminum webs within the tank provide stiffening and also contribute to the conduction of heat from the engines down to the bottom of the tank. Fuel circulation is further assisted by returning the hot, unused fuel from the injector nozzles back to the vicinity of the pick-up pipe. Fuel is pumped from the bottom of the tank with a Thomas Magnete LHP27 metering pump and passes through a large-area filter on its way to the engine. To help keep the fuel in a liquid state, the fuel pumps on all of the non-running engines are also run continuously, circulating fuel from the bottom of the tank through the warm environment of the engine module before returning it to the vicinity of the pickup lines. If the fuel at the bottom of the tank were to drop much below -40°C , it would freeze and the engines would stop in an unrecoverable state. The fuel tank, when full of fuel, has a thermal time constant of several days, which gives some time to recover from momentary power outages.

The fuel used for the engines is Jet A-1, mixed with $\sim 2\%$ fully synthetic “Racing 2T” 2-stroke oil to provide lubrication for the fuel pumps and injectors.

Two different approaches are used to generate electrical power from the engines: eCycle alternators and Mavilor generators. This was done as a risk-mitigation measure, as neither unit had been tested at this altitude before.

Four of the engines are equipped with brushless alternators made by eCycle⁹. In these units the rotor is mounted directly onto the crankshaft, resulting in an extremely lightweight and compact unit. NdFeB magnets are used to achieve maximum efficiency. The three-phase output of the alternator is rectified with an IR 70MTKB diode bridge to produce 120–150VDC.

The two remaining engines (one on each bank) use MSS 22 axial-flux disc servo motors made by Mavilor¹⁰. These motors are very efficient (both as motors and as generators) because they have no iron in their armature and hence no hysteresis loss. However, at 16kg they are significantly heavier than the eCycle alternators and, because they have their own bearings, must be coupled to the engine via a flexible shaft coupling. The Mavilor motors produce a DC output of 120–150V. A single IRK166 diode is placed in series with each motor to prevent reverse current flow.

The DC output from each of the three engines in a bank is paralleled after the diode bridges (or blocking diode in the case of the Mavilor) and sent to the instrument module.

4.1 Engine Starting

Each engine has a conventional starter motor that engages with a ring gear on the crankshaft when activated by the starter solenoid. The starter motors draw up to 300A at 12V. At the low temperatures that could be experienced in the engine module, lead-acid batteries lose their ability to deliver high currents. In the interests of reliability, and to ensure

that the full starting current would be available at all temperatures, it was decided to instead use a stack of ultracapacitors.

Each bank of engines has its own stack of Maxwell BCAP3000P ultracapacitors¹¹. One bank has six paralleled pairs of 3000F capacitors in series, giving 1000F at 12V. This was found to give more than enough capacity for multiple engine start attempts, and so the second bank was constructed with just six 3000F capacitors in series, giving 500F at 12V.

Each ultracapacitor has a voltage clamp across it, to ensure that no capacitor is charged beyond its absolute maximum voltage rating of 2.7V. Additional shunt resistors are used to help distribute the charge equally across the capacitors.

Each capacitor stack is charged from a DC/DC converter that takes its input from the 28V PLATO power bus. The DC/DC converters must be able to deliver their rated current into a short circuit, as this is the load presented to them by a discharged ultracapacitor stack. At a current of 9A it takes 11 minutes to fully charge the 500F stack to 12V, and twice as long as this to charge the 1000F stack.

The 120–150VDC from each engine bank is brought to the instrument module via separate cables. In the instrument module, each bank feeds into a parallel pair of Kepco RKW 28–55K¹² switched-mode power supplies. Although nominally rated at 1500W each, these units (like everything else) must be de-rated to account for the reduced air-cooling from the altitude, and so two are used for each engine bank.

The output voltage from each Kepco pair is set by a feedback loop incorporating a Unitrode UC2906 lead-acid battery charger IC. This automatically tracks the temperature of the batteries with an appropriate compensation. The voltage set-point can also be trimmed by either of two “Supervisor” computers within PLATO over a range of $\pm 5\%$. Thus, when the sun is up, the set point of the engines can be adjusted below the set point of the solar panels, giving priority to the panels. The UC2906 chip also includes current limiting. This is set to 45A (approx 1400W) so that the engines can never be overloaded.

5. LABORATORY TESTING OF DIESEL ENGINE

Testing of the diesel engine was undertaken in the Internal Combustion Laboratory of the School of Mechanical and Manufacturing Engineering at the University of New South Wales. See Fig. 5.

To simulate the pressure altitude of Dome A at UNSW, an environmental chamber was constructed that can maintain a constant pressure of down to half an atmosphere with the engine running at full power. The chamber consists of a base plate and a bell-jar made from mild steel. The base plate is a circular disk, 30mm thick, with an outer diameter of 1100mm. This is sealed via an O-ring to a 1000mm diameter steel bell jar. The bell-jar has a wall thickness of 5mm, and has a welded dome-shaped head and a welded bottom flange. Two lifting hooks are welded on either side of the bell-jar to accommodate a crane. See Fig. 5.

An 8 cubic metre/minute Roots blower, driven by a 15kW 3-phase electric motor, extracts air from the chamber and discharges it outside the building. The flow rate is chosen to be an order of magnitude greater than the rate at which the engine is consuming air, so that the engine exhaust is well diluted before reaching the Roots blower. Air is continuously introduced into the chamber via an air-filter box and butterfly valve. Manual control of the butterfly valve allows any required pressure to be achieved within the bell-jar.

The engine is attached via rubber isolators to the base plate of the bell-jar. See Fig. 8. A brushless, bearing-less eCycle alternator, similar to those used in the PLATO module, is directly attached to the engine crankshaft. The three-phase electrical output is coupled via a diode bridge to a pair of resistive load banks. The engine breathes the reduced pressure air from inside the bell-jar, and exhausts it via an exhaust diffuser that ensures that the exhaust gases are well mixed with the main airflow before they reach the Roots blower.

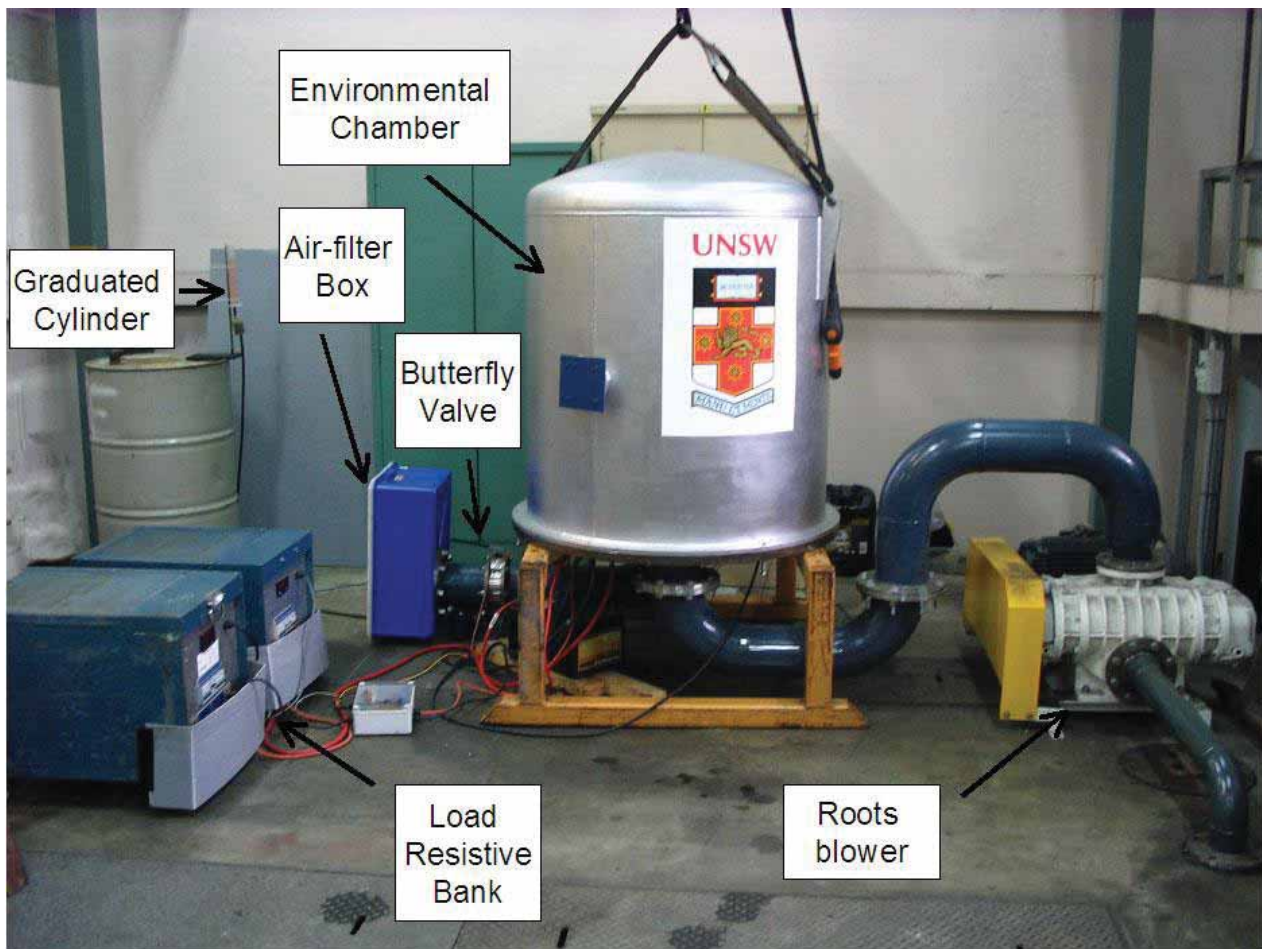


Fig. 5 Engine test rig. Air flows through the air-filter box to the environmental chamber. The rate of airflow is controlled by the butterfly valve. The Roots blower runs at constant speed, pumping air from the environmental chamber.

Fuel consumption is measured using an externally-mounted graduated cylinder, which delivers fuel via a fuel line that leads through the base plate to the engine. By having the fuel-feed system mounted externally to the pressure chamber, there is less vibration coupled to the graduated cylinder, thus allowing a more accurate reading of the fuel level.

To control the speed of the engine, a motor-drive lead screw is attached to the engine governor lever. The actuator is mounted on the engine plate and is electronically controlled via a switch that is external to the chamber.

K-type thermocouple sensors measure the temperatures of the ambient air, oil sump, cylinder head, exhaust gas, alternator/generator and the intake air. The exhaust gas temperature (EGT) is a particularly important indicator of engine performance. The other temperatures are monitored largely to ensure that none of the engine components is overheating.

Readings from the thermocouple sensors, pressure sensors and load bank are all monitored via ADAM modules. ADAM modules are input/output devices that both execute commands and receive voltage signals. The received voltage signals can be calibrated to the desired output of a sensor. A LabVIEW application monitors all systems and records all measurements.

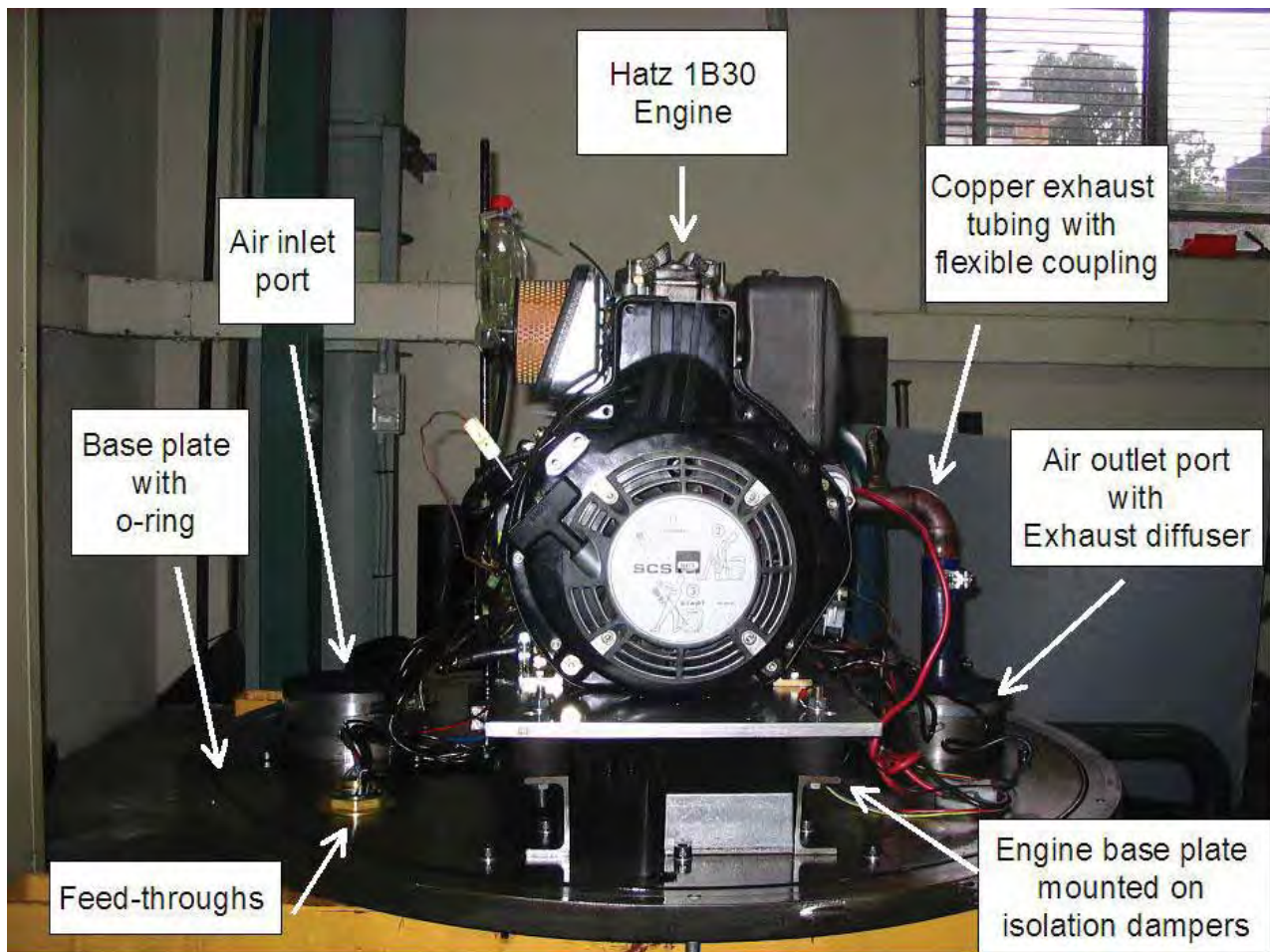


Fig. 6 Hatz test engine mounted on the base plate with peripherals.

5.1 Laboratory test results

The engine was started and stopped at a variety of simulated altitudes. It was found to start reliably, from cold (typically $\sim 25^{\circ}\text{C}$), at altitudes of more than 5000m. The engine was then run for approximately ten minutes at each speed and load, at both sea-level atmospheric pressure (1000hPa) and at a pressure of about 540hPa, which is well below the typical pressure at Dome A of 575hPa. At each setting, the following parameters were recorded:

- Fuel consumed
- Engine run time
- Load-bank voltage and current
- Exhaust gas temperature

From these data points, a set of engine maps can be constructed for each altitude. We present two examples of this data in Fig. 7, for an engine speed of 2200rpm. In these plots, the power recorded is the electrical output power from the alternator, and thus includes the alternator and rectifier losses. The brake specific fuel consumption figure is therefore an overall fuel-to-electricity efficiency.

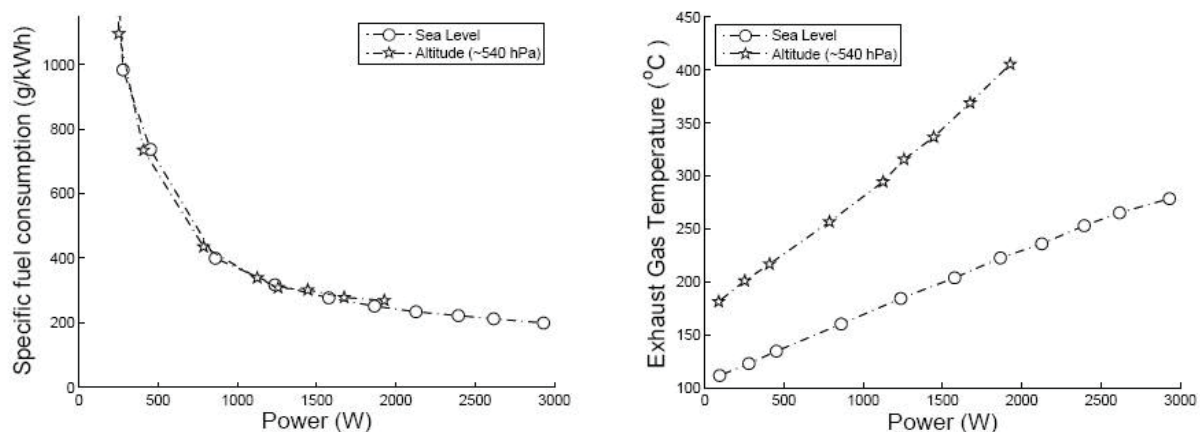


Fig. 7 Left: Brake specific fuel consumption versus power output at 2200rpm. Right: Exhaust gas temperature versus power output at 2200rpm.

The increased exhaust temperature at high altitude observed in the right-hand plot of Fig. 9 agrees with theoretical expectations. As similar amounts of heat must be generated to produce a given power, but only 0.54 times the mass of air is present in the cylinder, the combustion will raise the temperature of the gas by almost twice as much.

The high altitude plots end at 1900W, as this is the maximum power that the engine can produce at 540hPa, no more air being available for combustion.

6. CONCLUSION

Little modification to the engines is required for them to run satisfactorily at an altitude of up to 5,000 m. This is as expected: assuming adiabatic compression, the air in the cylinder will reach the same temperature regardless of altitude (ignoring cylinder wall losses), and will be sufficient to ignite the fuel at each injection stroke. However, the maximum power output at a given speed is reduced in direct proportion to the air pressure, and so the maximum fuel delivery must also be correspondingly reduced. Most importantly, because the air is less dense, there is less working fluid available to do the thermodynamic work and less cooling is available, so the temperature rise (cylinder head, exhaust gas etc.) is greatly increased for a given power output.

At high altitude, the mixture is expected to burn slower than at sea level. To partially compensate for this, the engines are run with an injection timing appropriate for a speed of 3600rpm, even though the actual running speed is 2200rpm.

Allowing for an alternator efficiency of around 85%, we find that the brake specific fuel consumption of the engine at sea level is consistent with published data. Furthermore, little loss of efficiency, if any, is encountered when the engine is run at high altitude.

At the time of writing (May 2008), PLATO has run unattended for 4 months. All engines are still functional, although one is becoming difficult to start and some will not run for more than a few hours without having to be restarted. Power has been continuously available to the instrument module since PLATO was switched on.

7. ACKNOWLEDGEMENTS

This research is supported by the Australian Research Council. We thank the UNSW School of Mechanical and Manufacturing Engineering for access to the Internal Combustion Laboratory. Hatz Australia, and in particular Sami Almogawish, Ian O'Callaghan and Tissa Pathiratna, provided us with invaluable assistance and generously shared their deep understanding of diesel engines with us. Apollo Solar kindly provided us with information on the T80 Maximum Power Point Trackers that was vital to the development of our remote monitoring scheme. Jason Allen was responsible for many of the refinements to the oil circulation system that proved essential to the longevity of the engines. One of the electrical load banks was generously lent to us by Graeme Arnold and Bob Bell from Switchgear Commissioning & Maintenance Pty Ltd and the other by Ian Davis from Eaton Electric Systems Pty Ltd. The Astronomical Society of Australia provided partial funding for SH to attend the SPIE meeting.

REFERENCES

- [1] Lawrence, J. S., Allen, G.R., Ashley, M. C. B., Bonner, C., Bradley, S., Cui, X., Everett, J. R., Feng, X., Hengst, S., Hu, J., Jian, Z., Kulesa, C. A., Li, Y., Luong-Van, D., Moore, A. M., Pennypacker, C., Qin, W., Riddle, R., Shang, Z., Sun, B., Suntzeff, N., Tothill, N. F. H., Travouillon, T., Walker, C. K., Wang, L., Yan, J., Yang, J., Yang, H., York, D., Yuan, X., Zhang, X., Zhang, Z., Zhou, X., Zhu, Z., "The PLATO Antarctic site testing observatory", Proc. SPIE Astronomical and Telescopes conference paper, *this volume*
- [2] Storey, J.W.V., Ashley, M.C.B. Burton, M.G., "An automated astrophysical observatory for Antarctica", PASA, 13, 35 – 38 (1996)
- [3] Lawrence, J.S., Ashley, M.C.B. and Storey, J.W.V., "A remote, autonomous laboratory for Antarctica with hybrid power generation. " Aust. Journal Elec. Electronics Engineering, 2(1), 1-12 (2004)
- [4] WhisperTech Limited. Whispergen Personnel Power Station Users Manual: PPS16 marine and land version. Christchurch, New Zealand (2003)
- [5] Tothill, N. F.H., Kulesa, C. A., Walker, C. K., Ashley M. C., Bonner, C., Cui, X., Everett, J., Feng, L., Hengst, S., Hu, J., Jiang, Z., Lawrence, J. S., Li, Y., Luong-Van, D., Moore, A. M., Pennypacker, C., Qin, W., Riddle, R., Storey J. W. V., Shang, Z., Sun, B., Travouillon, T., Wang, L., Xu, Z., Yang, H., Yan, J., York, D., Yuan, X., and Zhu, Z., "Astrophysics from Dome A", EDP Sciences, EAS Publications, *in press*
- [6] <http://www.apollow-solar.net/T80-turbocharger.htm>, (May, 2008)
- [7] <http://www.hatz.com.au/products/b-series/index.html>, (May, 2008)
- [8] http://www.mobil.com/USA-English/Lubes/PDS/GLXXENCVLMOMobil_Delvac_1_5W-40.asp, (May, 2008)
- [9] <http://www.ecycle.com/APU.html>, (May, 2008)
- [10] http://www.mavilor.es/pdf_products/mss_series_sc.pdf, (May, 2008)
- [11] <http://www.maxwell.com/ultracapacitors/products/large-cell/bcap3000.asp>, (May, 2008)
- [12] <http://www.kepcopower.com/specs/rkw-progspecs.pdf>, (May, 2008)

Bibliography

- Ai, X.P., Xiao, L.F., Cao, Y.L., & Yang, H.X. 2004. Optimization of EC-based multi-solvent electrolytes for low temperature applications of lithium-ion batteries. *Electrochimica Acta*, **49**(27), 4857–4863.
- Aristidi, E., Agabi, K., Azouit, M., Fossat, E., Vernin, J., Travouillon, T., Lawrence, J.S., Meyer, C., Storey, J.W.V., Halter, B., Roth, W.L., & Walden, V. 2005. An analysis of temperatures and wind speeds above Dome C, Antarctica. *Astronomy & Astrophysics*, **430**, 739–746.
- Arnaud, J., Faurobert, M., & Fossat, E. 2006. Dome C: An exceptional site for solar observations. *Memorie della Societa Astronomica Italiana*, **78**, 105.
- Ashley, M.C.B., P.W., Brooks, & Lloyd, P. L. 1996. Remote Control of Astronomical Instruments via the Internet. *Publ. Astron. Soc. Aust*, **13**, 17–21.
- Ashley, M.C.B., Burton, M.G., Calisse, P.G., Phillips, A., & Storey, J.W.V. 2005. Site testing at Dome C - cloud statistics from the ICECAM experiment. *Special Session 2, 25th IAU General Assembly, Sydney, Highlights of Astronomy, ASP Conf. Series*, **13**, 932.
- Ashley, M.C.B., Bonner, C.S., Everett, J.R., Lawrence, J.S., Luong-van, D., McDaid, S., McLaren, C., & Storey, J.W.V. 2010. Future development of the PLATO observatory for Antarctic science. *Ground-based and Airborne Instrumentation for Astronomy III, Proc. SPIE*, **7735**, 773540–773540–6.

- Assanis, D., Fernandes, G., Fuschetto, J., Filipi, Z., & McKee, H. 2007. Impact of military JP-8 fuel on heavy duty diesel engine performance and emissions. *Proceedings of the Institution of Mechanical Engineers: Part D* 2007, **221**, 957–970.
- Bareli, A. 2004. Increasing Reliability and Availability of Telecom Sites by Using CCVT Power Solutions. *Telecommunications Energy Conference, INTELEC*, 372–378.
- Batchelor, G., Moses, C., & Fletcher, R. 1997 (January). *Impact Study on the Use of Jet A Fuel in Military Aircraft during Operations in Europe*. Tech. rept. AGARD-R-801. Advisory Group for Aerospace Research and Development, North Atlantic Treaty Organization.
- Belousenko, I.V. 1997. Energy converters prove most reliable for Gazprom. *Pipeline & Gas Journal*, **224**(3), 44–46.
- Boccas, M., Ashley, M.C.B., Phillips, A., Schinckel, A., & Storey, J.W.V. 1998. Antarctic Fiber Optic Spectrometer. *The Astronomical Society of the Pacific*, **11**, 306–316.
- Bonner, C., Ashley, M.C.B., Cui, X., Feng, L., Gong, X., Lawrence, J.S., Luong-Van, D., Shang, Z., Storey, J.W.V., Wang, L., Yang, H., Yang, J., Zhou, X., & Zhu, Z. 2010. Thickness of the Atmospheric Boundary Layer Above Dome A, Antarctica, during 2009. *Publications of the Astronomical Society of the Pacific*, **122**(895), 1122–1131.
- Bonner, C.S., Ashley, M.C.B., Lawrence, J.S., Storey, J.W.V., Luong-Van, D.M., & Bradley, S.G. 2008. SNODAR: a new instrument to measure the height of the atmospheric boundary layer on the Antarctica plateau. *Proc. of SPIE*, **7014**(70146I-7).
- Bosch GmbH, R. 2005. *Diesel-Engine Management: Systems and Components*. 4th edn. John Wiley & Sons Ltd.

- BP Australia. 2006. *Product Specification: BP Automotive Diesel Fuel*. Tech. rept. Fuel Technical Services BP Pty. Ltd.
- BP Australia. 2008. *Product Specification: Jet A-1*. Tech. rept. Fuel Technical Services BP Pty. Ltd.
- BP Australia MSDS. 2008. *Material Safety Data Sheet: Jet A-1*. Tech. rept. BP Pty. Ltd.
- Burton, M. G. 2010. Astronomy in Antarctica. *The Astronomy and Astrophysics Review*, 417–469.
- Burton, M.G., Lawrence, J.S., Ashley, M.C.B., Bailey, J.A., Blake, C., Bedding, T.R., Bland-Hawthorn, J., Bond, I.A., Glazebrook, K., Hidas, M., Lewis, G., Longmore, S.N., Maddison, S.T., Mattila, S., Minier, V., Ryder, S., Sharp, R., Smith, C.H., Storey, J.W.V., Tinney, C.G., Tuthill, P., Walsh, A.J., Walsh, W., Whiting, M., Wong, T., Woods, D., & Yock, P.C.M. 2005. Science Programs for a 2-m Class Telescope at Dome C, Antarctica: PILOT, the Pathfinder for an International Large Optical Telescope. *Publications of the Astronomical Society of Australia*, **22**, 199–235.
- Calisse, P.G., Ashley, M.C.B., Burton, M.G., Lawrence, J.R., Phillips, M.A., Storey, J.W.V., Peterson, J.B., & Radford., S.H. 2004. New submm site testing results from Dome C, antarctica. *Astronomy in Antarctica, 25th meeting of the IAU, Special Session 2, 18 July, 2003 in Sydney, Australia*, **2**.
- Chamberlain, M.A., Ashley, M.C.B., Burton, M.G., Phillips, A., Storey, J.W.V., & Harper, D.A. 2000. Mid-Infrared observing conditions at the south pole. *The Astrophysical Journal*, **535**, 501–511.
- Chen, D. 2008. Proposed Construction and operation of the new Chinese

- Dome A Station Dome A, Antarctic: Final Comprehensive Environmental Evaluation. *Chinese Artic and Antarctica Administration*.
- Chen, J. 1996. Thermodynamic analysis of a solar-driven thermoelectric generator. *Journal of Applied Physics*, **79**(5), 2717–2721.
- Clucas, D.M., & Raine, J.K. 1994a. A New Wobble Drive with Particular Application in a Stirling Engine. *Proceedings of the Institution of Mechanical Engineers, Part C: Journal of Mechanical Engineering Science*, **208**(C5), 337–346.
- Clucas, D.M., & Raine, J.K. 1994b. Development of Hermetically Sealed Stirling Engine Battery Charger. *Proceedings of the Institution of Mechanical Engineers, Part C: Journal of Mechanical Engineering Science*, **208**(C6), 357–366.
- Colket, M., Edwards, T., Williams, S., Cernasky, N.P., Miller, D.L., Egolfopoulos, F., Lindstedt, P., Seshadri, K., Dryer, F.L., Law, C.K., Friend, D., Lenhert, D.B., Pitsch, H., Sarofim, A., Smooke, M., & Tsang, W. 2007. Development of an Experimental Database and Kinetic Models for Surrogate Jet Fuels. *American Institute of Aeronautics and Astronautics: 45th AIAA Aerospace Sciences Meeting and Exhibit*, **2007-770**.
- Cowlshaw, M.F. 1974. The characteristics and use of lead-acid cap lamps. *Trans. British Cave Research Association*, **1**(4), 199–214.
- Dalcanton, J. 2009. 18 years of science with the Hubble Space Telescope. *Nature*, **457**(7225), 41–50.
- Dempsey, J.T., Storey, J.W.V., Ashley, M.C.B, Calisse, M.G. Burton P.G., & Jarnyk, M.A. 2004. AFOS: Probing the UV-visible potential of the Antarctic Plateau. *Proc. of SPIE*, **5492**, 811–821.

- Dempsey, J.T., Storey, J.W.V., & Phillips, A. 2005. Auroral contribution to sky brightness for optical astronomy on the Antarctica plateau. *Publications of the Astronomical Society of Australia*, **22**, 91–104.
- Desonie, D. 2008. *Polar Regions: Human Impacts*. New York, NY USA: Chelsea Home Publishers.
- Doolittle, J.H. 1986. Lockheed Technical Report LMSC F171145. *Lockheed Missiles & Space Co.*, 67.
- Doolittle, J.H. 1992. Automatic geophysical observatories prepared for the polar cap network. *Antarctic Journal of the United States 1992 Review*, 323–324.
- Doolittle, J.H., S.B., S.B. Mende, E.W., E.W. Paschel, M.L., M.L. Trimpi, & Anderson, M.R. 1993. First automated geophysical observatory installed on the Polar Plateau. *Antarctic Journal of the United States*, **28**(5), 301–301.
- Dopita, M.A., Wood, P.R., & Hovey, G.R. 1996. An automated dimm telescope for Antarctica. *Publications of the Astronomical Society of Australia*, **13**, 39–43.
- Dudneny, J.R., Kressmann, R.I., & Rodger, A.S. 1998. Automated observatories for geospace research in polar regions. *Antarctic Science*, **10**(2), 192–203.
- Ealey, M. 1992. Active and Adaptive Optical Components: the technology and future trends. *Proc. of SPIE*, **1543**, 2–34.
- Fossat, E. 2005. The Concordia Station and the Antarctic Plateau: The Best Site on Earth for the 21st Century Astronomers. *Astrophysics & Astronomy*, **26**, 349–357.

- Francey, R. 1992. The impact of climate change on the Antarctic atmosphere. *Impact of Climate Change: Antarctica Workshop*, 33–38.
- Gell, R. 1989. *Antarctica: Future of a Frozen Wilderness*. Houghton Mifflin Australia.
- Gillingham, P.R. 1991. Prospects for an Antarctic Observatory. *Proceedings of Astronomical Society of Australia*, **9**(1), 55–56.
- Goswami, D.Y., & Kreith, F. 2008. *Energy Conversion*. Boca Raton, FL USA: CRC Press: Taylor & Francis Group.
- Gropper, J. 2000. 25 years of experience with closed cycle vapor turbogenerators as primary power source in remote telecommunications projects in Russia and CIS countries. *Telecommunications Energy Special Conference, TELESCon*, 203–207.
- Hengst, S., Allen, G.R., Ashley, M.C.B., Everett, J.R., Lawrence, J.S., Luong-Van, D., & Storey, J.W.V. 2008. PLATO Power – a robust, low environmental impact power generation system for the Antarctic plateau. *Proc. of SPIE*, **7012**(70124E-10).
- Hengst, S., Luong-Van, D.M., Everett, J.R., Lawrence, J.S., Ashley, M.C.B., Castel, D., & Storey, J.W.V. 2009. A Small, High-Efficiency Diesel Generator for High-Altitude use in Antarctica. *International Journal of Energy Research*, **34**.
- Herdman, R.C. 1994. Power Sources for Remote Arctic Applications. *U.S. Congress, Office of Technology Assessment*, June. Washington DC.
- Hickok, F. 1975. *Handbook of Solar and Wind Energy: A Cahners Special Report*. Boston, MA USA: Cahners Publishing Company, Inc.
- Holmes, R.E., Stearns, C.R., & Weidner, G.A. 1997. Antarctic automatic weather stations: 1995-1996. *Antarctic Journal - Review*, 171–174.

- Hongxia, X., Lingai, L., & Fraisse, G. 2007. Development and applications of solar-based thermoelectric technologies. *Renewable and Sustainable Energy Reviews*, **11**(4), 923–936.
- Indermuhle, B.T., Burton, M.G., & Maddison, S.T. 2005. The History of Astrophysics in Antarctica. *Publications of the Astronomical Society of Australia*, **22**, 73–90.
- Jacobson, M. Z. 2009. Review of Solutions to Global Warming, Air Pollution, and Energy Security. *Energy & Environmental Science*, **148**(2).
- Kenyon, S. L., & Storey, J. W. V. 2006. A Review of Optical Sky Brightness and Extinction at Dome C, Antarctica. *Publications of the Astronomical Society of the Pacific*, **118**, 489–502.
- Kenyon, S. L., Ashley, M.C.B., Everett, J. R., Lawrence, & J. S., Storey, J. W. V. 2006. Nigel and the optical sky brightness at Dome C, Antarctica. *Proceedings of SPIE*, **6267**.
- Kniffen, D.A. 2003. Lessons learned from the Compton Gamma-ray Observatory. *Proc. of SPIE*, **4851**, 1092–1103.
- Kolb, G. 2008. *Fuel Processing: for Fuel Cells*. Wiley-Vch Verlag GmbH & Co. KGaA, Weinheim.
- Kouremenos, D.A., Rakopoulos, C.D., & Hountalas, D.T. 1997. Experimental investigations of the performance and exhaust emissions of a swirl chamber diesel engine using JP-8 aviation fuel. *International Journal of Energy Research*, **21**, 1173–1185.
- Kulesa, C.A., CK, C.K. Walker, Schein, M., Golish, D., Tothill, N., Siegel, P., Wienreb, S., Jones, G., Bardin, J., Jacobs, K., Martin, C.L., Storey, J., Ashley, M., Lawrence, J., D, D. Luong-Van, Everett, J., Wang, L., Feng, L., Zhu, Z., Yan, J., Yang, J., Zhang, X.G., Yuan, X. Cui X., Hu, J.,

- Xu, Z., Jiang, Z., Yang, H., Li, Y., Sun, B., & Shang, Z. 2008. Pre-Heat: Submillimeter Site Testing and Astronomical Spectra from Dome A. *Proc. of SPIE*, **7012**(701249-11).
- Lawrence, J.S. 2004. Adaptive-optics performance of Antarctic telescopes. *Applied Optics*, **43**, 1435–1449.
- Lawrence, J.S., Ashley, M.C.B., Burton, M.G., & Storey, J.W.V. 2001. Observations of the Antarctic Infrared Sky Spectral Brightness. *SPIE Conferences Series*, **4836**, 176–176.
- Lawrence, J.S., Ashley, M.C.B., Tokovinin, A., & Travouillon, T. 2004. Exceptional astronomical seeing conditions above Dome C in Antarctica. *Nature*, **431**, 278.
- Lawrence, J.S., Ashley, M.C.B., & Storey, J.W.V. 2005. A remote, autonomous laboratory for Antarctica with hybrid power generation. *Australian Journal of Electr. Electron. Engineering*, **2**, 1–12.
- Lawrence, J.S., Ashley, M.C.B., Burton, M.G., & Storey, J.W.V. 2007. Dome C atmospheric condition: Implications for astronomy. *Acta Astronomica Sinica*, **48**(1), 48–53.
- Lawrence, J.S., Allen, G.R., Ashley, M.C.B., Bonner, C., Bradley, S., Cui, X., Everett, J., Feng, X., Hengst, S., Hu, J., Jian, Z., Kulesa, C.A., Li, Y., Luong-Van, D., Moore, A.M., Pennypacker, C., Qin, W., Riddle, R., Shang, Z., Storey, J.W.V., Sun, B., Suntzeff, N., Tothill, N.F.H., Travouillon, T., Walker, C.K., Wang, L., Yan, J., Yang, J., Yang, H., York, D., Yuan, X., Zhang, X., Zhang, Z., Zhou, X., & Zhu, Z. 2008. The PLATO Antarctic site testing observatory. *Ground-based and Airborne Instrumentation for Astronomy II, Proc. SPIE*, **7012**, 701227–701227–12.
- Lawrence, J.S., Ashley, M.C.B., Hengst, S., Luong-Van, D.M., Storey, J.W.V., Yang, H., Zhou, X., & Zhu, Z. 2009. The PLATO Dome A

- site testing observatory: power generation and control systems. *Review of Scientific Instruments*, **80**(064501).
- Lessard, M.R., Weatherwax, A.T., Spasojevic, M., Inan, U.S., Gerrard, A., Lanzerotti, L., Ridley, A., Engebretson, M.J., Petit, N.J., Clauer, R., LaBelle, J., Mende, S.B., Frey, H.U., Pilipenko, V.A., Rosenberg, T.J., & Detrick, D. 2009. PENQUIn multi-instrument observations of dayside high-altitude injections during the 23 March 2007 substorm. *Journal of Geophysical Research: Space Physics*, **114**(A00C11), 10PP.
- Luong-Van, D.M., Ashley, M.C.B., Everett, J.R., Lawrence, J.S., & Storey, J.W.V. 2008. PLATO control and robotics. *Proc. of SPIE*, **7019**(70192U).
- Luong-Van, D.M., Ashley, M.C.B., Cui, X., Everett, J.R., Feng, L., X. Gong, S. Hengst, Lawrence, J.S., Storey, J.W.V., Wang, L., Yang, H., Yang, J., Zhou, X., & Zhu, Z. 2010. Performance of the autonomous PLATO Antarctic Observatory over two full years. *Ground-based and Airborne Telescopes III Proceedings of the SPIE*, **7733**, 77331T–77331T–8.
- Lüthi, D., Floch, M. Le, Bereiter, B., Blunier, T., Barnola, J., Siegenthaler, U., Raynaud, D., Jouzel, J., Fischer, H., Kawamura, K., & Stocker, T.F. 2008. High-resolution carbon dioxide concentration record 650,000–800,000 years before. *Nature*, **453**, 379–382.
- Mago, P.J., Harrod, J., Srinivasan, K., & Chamra, L.M. 2009. First and Second Law Analysis of a Stirling Engine with Imperfect Regeneration and Dead Volume. *Proceedings of the Institution of Mechanical Engineers, Part C: Journal of Mechanical Engineering Science*, **223**, 2595–2607.
- Mahon, L.L.J. 1992. *Diesel Generator Handbook*. Oxford, UK: Butterworth-Heinemann Ltd.
- Marks, R.D., Vernin, J., Azouit, M., Manigault, J.F., & Clevelin, C. 1999.

- Measurements of optical seeing on the high Antarctic plateau. *Astronomy and Astrophysics Supplement*, **134**, 11–172.
- Maurice, L.Q., Lander, H., Edwards, T., & III, W.E. Harrison. 2001. Advanced aviation fuels: a look ahead via a historical perspective. *Fuel*, **80**, 747–756.
- McEwen, D.J., Chakrabarty, P., & Evans, W.F.J. 1983. Solar UV and Ozone Balloon Measurements. *Adv. Space Res.*, **2**(5), 209–212.
- Meloni, A., Santis, A. De, Morelli, A., Palangio, P., Romeo, G., Bozzo, E., & Caneva, G. 1992. The Geophysical Observatory at Terra Nova Bay. *Recent Progress in Antarctic Earth Science Terra Scientific Publishing Company*, 585–588.
- Miller, R. E. 1983. *The Demonstration At Noorvik Of An Unattended, Pilot Operated Airport Lighting System*. Tech. rept. State Of Alaska, Department Of Transportation And Public Facilities Division Of Planning And Programming, Research Section.
- Moore, A., Allen, G., Aristidi, E., Ashley, M., Bedding, T., Beichman, C., Briguglio, R., Busso, M., Candidi, M., Ciardi, D., Cui, X., Cutispoto, G., Espy, E. Distefano P., Everett, J., Feng, L., Hu, J., Jiang, Z., Kenyon, S., Lawrence, C. Kulesa J., Roux, B. Le, Leslie, T., Li, Y., Luong-Van, D., Phillips, A., Qin, W., Ragazzoni, R., Riddle, R., Sabbatini, L., Salinari, P., Saunders, W., Shang, Z., Stello, D., Storey, J., Sun, B., Suntzeff, N., Taylor, M., Tosti, G., Tothill, N., Travouillon, T., Belle, G. Van, Braun, K. Von, Wang, L., Yan, J., Yang, H., Yuan, X., Zhu, Z., & Zhou, X. 2008. Gattini: a multisite campaign for the measurement of sky brightness in Antarctica. *Proc. of SPIE*, **7012**(701226-10).
- Papagiannakis, R.G., Kotsiopoulos, P.N., Hountalas, D.T., & Yfantis, E. 2006. Single Fuel Research Program Comparative Results of the Use of

- JP-8 Aviation Fuel versus Diesel Fuel on a Direct Injection and Indirect Injection Diesel Engine. *SAE 2006 World Congress & Exhibition*, **2006-01-1673**.
- Papitashvili, P.A. 1999. Comment on "Automated observatories for geospace in polar regions" by J.R. Dudeney, R. I. Kressmann and A.S. Rodger. *Antarctic Science*, **1**(119).
- Parish, T.R., & Cassano, J.J. 2003. The Role of Katabatic Winds on the Antarctic Surface Wind Regime. *Monthly Weather Review*, **131**(2), 317–333.
- Patel, K.C., & Spath, S.R. 2004. Spitzer Space Telescope: observatory, description, and performance. *Proc. of SPIE*, **5487**, 112–123.
- Pavlov, D. 2006. *Essentials of Lead-acid Batteries*. Karaikudi, India: Society for Advancement of Electrochemical Science and Technology.
- Paxton, L.J., & Meng, C.I. 1999. Auroral Imaging and Space-based optical remote sensing. *J. Hopkins APL Tech.*, **20**, 556–569.
- Pietras, C. R. 1993 (September). *Hybrid power system for remote communications stations*. Master of Science in Electrical Engineering, United States Navy - Naval Postgraduate School, Monterey, CA USA.
- Pulkrabek, W.W. 2004. *Engineering Fundamentals of the Internal Combustion Engine*. 2nd edn. Pearson Prentice-Hall: New Jersey.
- Quilty, P.G. 1992. Introduction of Impact of Climate Change: Antarctica, Australia. *Commonwealth of Australia*.
- Rathborne, J.M., & Burton, M.G. 2003. Results from the South Pole Infrared EXplorer Telescope. *Highlights of Astronomy, ASP Conference Series*, **13**, 937–944.

- Ricardo, H.R., & Hempson, J.G.G. 1968. *The High Speed Internal Combustion Engine*. Blackie: London, U.K.
- Sadibekova, T., Fossat, E., Vernin, J., Agabi, A., Aristidi, E., Azouit, M., Chadid, M., Tringuet, H., Genthon, C., Krinner, G., & Sarazin, M. 2007. Choosing Dome C, Antarctic Plateau as Future Astronomical Observatory. *EAS Publication Series*, **25**, 60–72.
- Saunders, W., Gillingham, P., McGrath, A., Haynes, R., Brzeski, J., Storey, J., & Lawrence, J. 2008. PILOT: a wide-field telescope for the Antarctic plateau. *Proc. of SPIE*, **7012**(70124F).
- Saunders, W., Lawrence, J.S., Storey, J.W.V., Ashley, M.C.B., Kato, S., Minnis, P., Winker, D.M., Liu, G., & Kulesa, C. 2009. Where is the best site on Earth? Domes A, B, C and F, and Ridges A and B. *Publications of the Astronomical Society of the Pacific*, **121**, 976–992.
- Scrosati, B., & Garche, J. 2010. Lithium Batteries: Status, Propects and Future. *Journal of Power Sources*, **195**(9), 2419–2430.
- Shell. 2005. *Safety Data Sheet: Jet A-1*. Tech. rept. Shell Company of Australia Ltd.
- Sims, G., Ashley, M. C. B., Everett, J. R., Cui, X., Feng, L., Gong, X., Hengst, S., Lawrence, J.S., Luong-van, D. M., Z.Shang, Storey, J. W. V., Wang, L., Yang, H., Yangc, J., Zhoui, X., & Zhu, Z. 2010. Optical sky brightness at Dome A, Antarctica from the Nigel experiment. *Proc. of SPIE*, **77334M**.
- Smith, R.C. 1995. *Observational Astrophysics*. Cambridge University Press.
- Stearns, C.R., Holmes, R.E., & Weidner, G.A. 1997. Antarctic automatic weather stations: 1996-1997. *Antarctic Journal - Review*, 174–178.

- Steel, J., & Guichard, A. 1993. Alternative Energy Options for Antarctic Stations. **1**(December), 295–300.
- Steel, J. D. 1993 (November). *Alternative Energy Options for Antarctic Stations*. Ph.D. thesis, University of Tasmania. Thesis Submitted in Partial Fulfilment of the Requirements of the Graduate Diploma of Antarctic and Southern Ocean Studies with Honours.
- Storey, J., Angel, R., Lawrence, J., Hinz, P., M., M. Ashley, & Burton. 2006. LAPCAT: the Large Antarctic Plateau Clear-Aperture Telescope. *Proc. of SPIE*, **6267**(62671E).
- Storey, J.W.V. 1998. The AASTO Program. *ASP Conference Series*, **141**.
- Storey, J.W.V. 2005. Astronomy from Antarctica. *Antarctic Science*, **17**(4), 555–560.
- Storey, J.W.V., Ashley, M.C.B., Boccas, M., Phillips, M.A., & A.E.T. Schinckel, A.E.T. 1999. Infrared Sky Brightness Monitors for Antarctica. *The Publications of the Astronomical Society of the Pacific*, **111**(760), 765–771.
- Swain, M.R., & Hubert, G. 2006. Antarctic Boundary Layer Seeing. *The Publications of the Astronomical Society of the Pacific*, **118**(846), 1190–1197.
- Swenson, G.R., Rairden, R.L., Solomon, S.C., & Anath, S. 1998. Imaging Spectroscopy for Two-Dimensional Characterization of Auroral Emissions. *Applied Optics*, **37**(24), 5760–5770.
- Takumra, T. 2002. Trends in advanced batteries and key materials in the new century. *Solid State Ionics*, **152-153**, 19–34.

- Travouillon, T., Ashley, M.C.B., Burton, M.G., Storey, J.W.V., & Loewenstein, R.F. 2003a. Atmospheric turbulence at the south pole and its implications for astronomy. *Astronomy & Astrophysics*, **400**(March), 1163–1172.
- Travouillon, T., Ashley, M.C.B., Burton, M.G., Storey, J.W.V., Conroy, P., Hovey, G., Jarnyk, M., Sutherland, M., & Loewenstein, R.F. 2003b. Automated Shack-Hartmann seeing measurements at the South Pole. *Astronomy & Astrophysics*, **409**, 119–1172.
- Travouillon, T., Aristidi, E., Fossat, E., Lawrence, J.S., Mekarnia, D., Moore, A.M., Skidmore, A.W., & Storey, J.W.V. 2008. Sampling the Ground Layer of the Atmosphere at Dome C using fast Sonic-anemometers. *Proc. of SPIE*, **7012**(70124B).
- Urieli, I., & Berchowitz, D.M. 1984. *Stirling Cycle Engine Analysis*. Adam Hilger Ltd, Bristol.
- Viswanathan, B., & Schibioh, M. Aulice. 2007. *Fuel Cells: Principles and Applications*. University Press.
- Walker, G., & Senft, J.R. 1985. *Free Piston Stirling Engines*. Springer-Verlag.
- Weisskopf, M.C. 2006. Technical report: Synchrotron Radiation from Outer Space and the Chandra X-Ray Observatory. *Synchrotron Radiation News*, **19**(5), 29–35.
- White, S., Nylen, T., & Johns, B. 2006. GNSS Support to the National Science Foundation Office of Polar Programs: Antarctic Program 2005-2006 Season Report. *UNAVCO Community and Facility Activities*.
- Whittingham, M. S. 2004. Lithium Batteries and Cathode Materials. *American Chemical Society: Chemical Review*, **104**, 4271–4301.

- Xiao, C., Li, Y., Allison, I., Bian, L., & Ren, J. 2008. Preliminary evidence indicating Dome A (Antarctica) satisfying preconditions for drilling the oldest ice core. *Chinese Science Bulletin*, **53**(1), 102–106.
- Yang, H., Allen, G., Ashley, M.C.B., Bonner, C.S., Bradley, S., Cui, X., Everett, J.R., Feng, L., Gong, X., Hengst, S., Hu, J., Jiang, Z., Kulesa, C.A., Lawrence, J.S., L, Y., Luong-Van, D., McCaughrean, M.J., Moore, A.M., Pennypacker, C., Qin, W., Riddle, R., Shang, Z., Storey, J.W.V., Sun, B., Suntzeff, N., Tothill, N.F.H., Travouillon, T., Walker, C.K., Wang, L., Yan, J., Yang, J., York, D., Yuan, X., Zhang, X., Zhang, Z., Zhou, X., & Zhu, Z. 2009. The PLATO Dome A Site-Testing Instrumentation and First Results. *Publications of the Astronomical Society of Pacific*, **121**, 174–184.
- Yang, H., Kulesa, C. A., Walker, C. K., Tothill, N. F. H., Yang, J., Ashley, M. C. B., Cui, X., Feng, L., Lawrence, J. S., Luong-van, D. M., McCaughrean, M. J., Storey, J. W. V., Wang, L., Zhou, X., & Zhu, Z. 2010. Exceptional Terahertz Transparency and Stability above Dome A, Antarctica. *Publications of the Astronomical Society of the Pacific*, **122**, 490–494.
- Yuan, X., Cui, X., Xia, L., Hu, J., Lawrence, J.S., Yan, J., Storey, J.W.V., Wang, L., Feng, L., Ashley, M.C.B., Zhou, X., Jiang, Z., & Zhu, Z. 2008. Chinese Small Telescope Array (CSTAR) for Antarctic Dome A. *Proc. of SPIE*, **7012**(7012G-8).
- Zou, H., Zhou, X., Jiang, Z., Ashley, M. C. B., Cui, X., Feng, L., Gong, X., Hu, J., Kulesa, C. A., Lawrence, J. S., Liu, G., Luong-Van, D. M., Ma, J., Moore, A. M., Pennypacker, C. R., Qin, W., Shang, Z., Storey, J. W. V., Sun, B., Travouillon, T., Walker, C. K., Wang, J., Wang, L., Wu, J., Wu, Z., Xia, L., Yan, J., Yang, J., Yang, H., Yao, Y., Yuan, X., York, D. G., Zhang, Z., & Zhu, Z. 2010. Sky Brightness and Transparency in the i-band at Dome A, Antarctica. *The Astronomical Journal*, **140**(2), 602–611.